Tesi di Dottorato

Environmental and Physiological Parameters Measurement in Images and Video

Yuriy Kurylyak

UNIVERSITÀ DELLA CALABRIA

Dipartimento di Elettronica,
Informatica e Sistemistica

Dottorato di Ricerca in
Ingegneria dei Sistemi e Informatica
XXV ciclo

Tesi di Dottorato

Environmental and Physiological
Parameters Measurement
in Images and Video

Yuriy Kurylyak

Coordinatore
Prof. Luigi Palopoli

Supervisore
Prof. Domenico Grimaldi

DEIS

To my parents.

Abstract

Measurement in images and video is a new challenging research direction. Up to now, cameras are mostly used as interaction devices. Computer vision technologies, however, can turn an ordinary video camera to a powerful tool for counting, measuring and inspecting. Using the camera as a measuring sensor is very interesting as allows creating a "universal" measurement instrument, where new type of measurements can be added just by changing the software.

Appearance of smartphones brings measurements in image and video to the new level, introducing a small, portable, autonomous measurement device. A lot of efforts have been made to convert smartphones to mobile tools for measuring the object length, width, size, angles, area, dimensions etc.

This Ph.D. thesis investigates novel image and video processing techniques and shows how they can be used for non-invasive measurement of various environmental and physiological parameters. The three logical steps describe the possible types of measurements: in static image, in video and using smartphones.

First, the case with a single image affected by a motion blur is considered and appropriate techniques for locating the regions with motion blur and parameters extraction are presented. A new method to detect the locally motion blurred regions from the image with complex still background is introduced. Analysis in the frequency domain, statistical analysis and windowing techniques are used to find blurred object, and the Fourier and Radon transformations are used to compute its motion characteristics.

Analysis of video allows measuring additional characteristics of the objects that change over time. Monitoring of the human fatigue level is done by eyelid blinks detection and analysis. Two solutions are proposed: the non-invasive blink detection system based on infrared camera and webcam. The usage of infrared camera with switching light is used for fast and easy pupil detection in each frame, while the webcam is used to create a very cheap but still effective system. The problem of eyes detection is solved by using a cascade of boosted classifiers based on Haar-like features. The algorithm is proposed to detect

closure and opening of the eyes and to distinguish voluntary blinks from the involuntary ones.

Finally, the smartphone is used for photoplethysmogram acquisition and measurement of vital parameters. The proposed approach utilizes a concept of image acquisition similar to the one of a pulse oximeter. The problem of finger detection in video as well as verification of the proper usage of the system is solved by using colour segmentation in each colour channel. Then, the pulse rate is evaluated based on adaptive and statistical analysis. Moreover, the blood pressure is estimated by means of artificial neural network. A set of parameters are proposed to be extracted from the photoplethysmographic signal and used as the input of the neural network. For wide representation of training data the Multiparameter Intelligent Monitoring in Intensive Care waveform dataset is used.

Acknowledgements

First and foremost, I would like to express my thorough gratitude to my supervisor, Prof. Domenico Grimaldi for his guidance, suggestions and encouragement. I appreciate his support and assistance which have helped me to present this work.

Special thanks to my friends Dr. Francesco Lamonaca and Dr. Domenico Luca Carnì with whom I spent many time in the laboratory. Thank you for your suggestions, persistent inspiration and extraordinary kindness.

I would like to express my deep gratitude to everyone else at the Department of Electronics, Computer and System Sciences for providing a great environment.

I have had the pleasure of meeting many good people while at the University of Calabria who were a part of my life during the last three years. I would like to thank all my friends and especially Gaetano, Yuliya, Iryna, Paolo, Andrea and Stefano who have made my time there enjoyable.

Finally, this thesis is dedicated to my parents, who always give me inspiration, support, and encouragement.

Contents

List of Figures

List of Tables

1

Introduction

1.1 Motivations

A modern home is equipped with a multitude of technical devices. A closer examination of things we do in our life can give an idea how many measurements are made and how many measuring instruments we use for that. We use measurements in medicine, sport, building, transportation, to tell the time and make estimations, etc. [1, 2]. The number of measurements and measuring instruments rises dramatically from year to year. We use measurement devices at home, in the office, in a hospital, in a car, on the street and so on. Sometime we use very expensive instruments for doing only one type of measurements. So, is it possible to reduce somehow their number and the total cost?

1.1.1 The role of computers in measurements

Over the last few years computer-based signal and image analysis received great attention from researches. Using the processing power of computers and the advances in mathematical algorithms it is now possible to generate a wealth of information from an image once it has been digitized [3]. Special interest is in computer vision area as both the cameras and the processing algorithms are very powerful. Although the tasks are quite easy for humans, it causes many difficulties for developing of automated systems. However, it introduces a new concept of measurements - they become automatic, and contactless or even telemetric.

Photogrammetry is the science of making measurements from photographs. In particular, the goal is to determine the geometric properties of objects from photographic images, like the distance between two points that lie on a plane parallel to the photographic image plane. The fields of application of such technique are very wide and include topographic mapping, architecture, engineering, manufacturing, quality control, police investigation, geology. It is also used to combine live action with computer-generated imagery in movie post-production, in biomedicine, etc [4].

There are some commercial products on the market that try to use image analysis for getting some measurement information. As an example of such photo measuring system that turns a digital camera and computer into an electronic tape measure is Sticky Yard Digital Photo Measuring System [5]. By sticking a reference model on the object and taking a picture it allows to perform different measurements directly from the photo (Fig. 1.1).

Fig. 1.1. Measurements, provided by the Sticky Yard Digital Photo Measuring System.

Although this system requires some reference and allows taking measurements only of one plane without doing any actual analysis of the object, there are more developments that try to use a scene geometry for more advanced measurements.

Another example of such systems is the CentreCam [6] - a development, based on the usage of low cost webcams for the model engineer. It gives a possibility of centring, edge finding and micro measurements on the model engineer's milling machine or lathe (Fig. 1.2).

Typical image and video analysis applications include security and surveillance, medical imaging, traffic monitoring, manufacturing, quality control, machine vision, industrial measurements, remote or non-contact video inspection, etc [7].
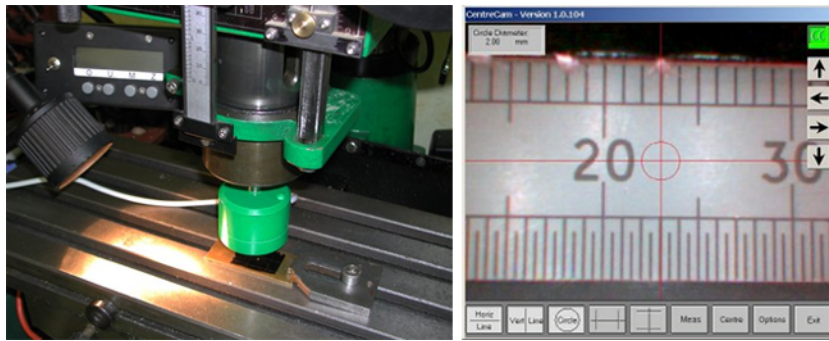
Fig. 1.2. CentreCam: a webcam-based system to improve the technical process accuracy.

1.1.2 Smartphones effect on image processing

Smartphone is a type of mobile device that provides advanced communication and performance possibilities beyond a typical phone. Many of smartphones are equipped by high-resolution touch screens, cameras, processors and light-emitting diode flashes. They run a complete mobile operating system that provides advanced computing capability. Together with the high-speed Internet access and Wi-Fi capabilities they become very interesting alternative to personal computers and laptops.

Indeed, as depicted in Fig. 1.3, the world smartphone sales increase rapidly and reached 169,2 millions of units in the 3rd quarter of 2012 [8].
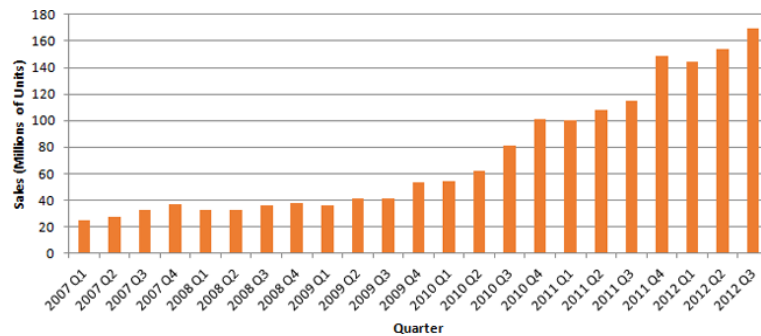
Fig. 1.3. Worldwide smartphone sales to end users from 1st quarter 2009 to 3rd quarter 2012 (in million units).

According to the Imaging Confluence Study by leading market research company "The NPD Group's", the percent of photos taken with a smartphone reached 27 percent while the share of photos taken on any camera dropped to

44 percent [9]. That means that for many people smartphones have replaced cameras.

Moreover, besides making just photos and videos, nowadays smartphone cameras are often used as input devices in numerous research projects and commercial applications. In addition to the usual back camera, most of the current smartphones are equipped with a front camera enabling the possibility of video conferencing.

Indeed, there are a number of initiatives that make use of a built-in camera to create applications for object recognition, face detection, navigation, user interaction, games, etc. There are also many projects that try to convert the smartphone to a mobile telemeter measure tool for object length, width, size, angles, area and dimensions measurements that can be used as a ruler, tape measure or planimeter. Moreover, the usage of additional sensors like accelerometer together with application of geometrical projections allow estimating even the distance to the object.

1.1.3 Specific character of measurement in images and video

Measurements using images and video is a new challenging research direction. As it was mentioned already, computer vision technologies can turn an ordinary video camera to a powerful tool for counting, measuring and inspecting. For example, it's possible to measure automatically object dimensions from a single picture, indicating some reference or even to analyse the object behaviour in a time as video is a unique multimedia data type that contains many spatio-temporal information.

However, measuring in images or video is not as usual as with normal instruments. Instead of direct access to the measuring object and its characteristic, there are just digital images or videos.

In general, still digital image is a numeric representation of the visual perception that has a similar appearance to some physical object or a person. Normally they are raster, two-dimensional images and can be captured by optical devices such as cameras, telescopes, microscopes, etc. Raster images have a finite set of digital values, called pixels and allocated into rows and columns. They are the smallest individual elements of the image, representing the brightness of a given colour at any specific point.

Digital video is a series of bitmap digital images displayed in rapid succession at a constant rate and representing scenes in motion. Such images are called frames and the rate at which frames are displayed are called frames per second (FPS).

Thus, considering a single image or a frame, all information that we have are pixel values. There is no information about objects, their shapes, features, etc. Definitely, that's not what can give directly information about real-world objects. Therefore, the image processing techniques must be applied in order to extract additional information about objects in the scene [10, 11, 12].

1.1.4 Using camera as a measuring device

Up to now, cameras are used mostly as interaction devices. Meanwhile, using the camera as a measuring sensor is very interesting, giving the possibility to create a "universal" measurement instrument. Indeed, just changing the software and the way how the captured information is processed it's possible to perform different measurements.

Any imaging device can be used to acquire information about measuring object: a static camera, digital camera, video camera, webcam, smartphone camera and so on. Then, a specific algorithm installed on computer, smartphone, or even on reprogrammable integrated circuit can provide appropriate measurement results (Fig. 1.4).
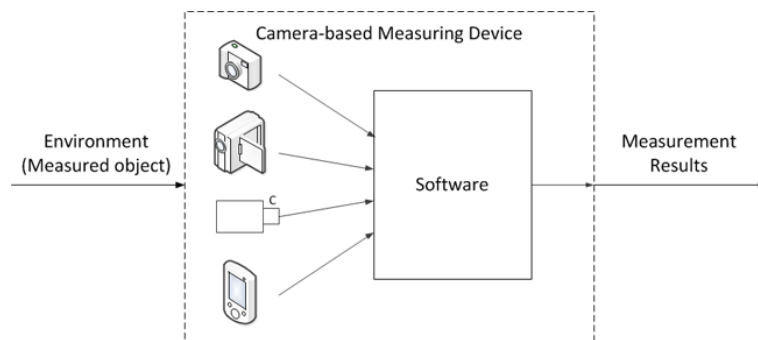
Fig. 1.4. General structure of camera-based measuring instrument.

Normally, the following steps should be performed in order to obtain measurement results from a camera-based system (Fig. 1.5):

- acquire image or video;
- verify the correct usage of the system;
- find the object of interest;
- track the object between frames in order to obtain information over time;
- analyse obtained information and perform measurement.

1.2 Goals

The main goal of the research is to use image processing techniques to extract information from images and video for different kind of applications: video surveillance systems, human-computer interaction, and biomedicine. The common task for all such applications is to obtain information about contours and geometrical shapes of the objects based on pixel examination,
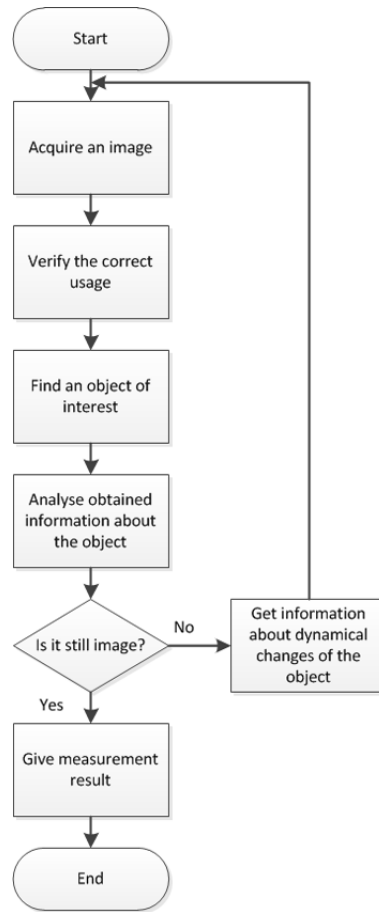
Fig. 1.5. Measuring algorithm using the camera.

and proceed with it in a time to extract different measurement information concerning environment and physiological parameters.

Therefore, the first objective of this thesis is to use a single image affected by a motion blur and extract dynamical parameters of objects in it. Motion blur is the alteration that appears on the image due to the relatively large difference in velocity between the objects in a scene in comparison to the camera exposure time. It is usually considered as an extra noise that affects the quality of the image. However, if detected properly it can be also used to obtain some characteristics about the object movement. In particular, the technique is to find affected by local motion blur regions in the image in order to estimate the direction and the length for each moving objects. If the length and the orientation can be identified it is possible to recover the speed of the object.

Passing from the static image to video, the next objective is to monitor the human fatigue level using analysis of the eyelids blinks. It is well known that the eye blink rate is a significant indicator of the fatigue and can be used to evaluate the human sleepiness. It's expected to use both an infrared camera and a webcam in order to create a non-invasive blink detection and analysis system. It will be also investigated how to distinguish the voluntary blinks from the involuntary ones, as only the last are correlated with the fatigue.

Finally, the last objective is to investigate the possibility of smartphone usage to acquire the photoplethysmogram signal and monitor vital parameters, such as pulse rate and blood pressure. Monitoring of vital parameters was always an important task and many research efforts have been done to make it easier, faster and more accurate. A particular attention is given to make the measurements non-invasive. One of such ways to obtain temporal variation in the blood volume is to use a pulse oximeter. A smartphone, with its computational power, high-resolution cameras and light-emitting diode flashes, is very similar to the pulse oximeter and can be used as a part of health monitoring system measuring vital characteristics.

Therefore, the overall research is dedicated to provide the novel image and video processing techniques and to show how they can be used for measurement of various environmental and physiological parameters.

1.3 Structure of the Ph.D. Thesis

The content of the thesis is organised as follow:

Chapter 2 describes a new approach to detect moving objects affected by motion blur. An overview of the motion blur detection techniques is given. The proposed method of local motion blur detection, based on calculation of the local standard deviation of the image and scanning of all sub-images using the partitioning algorithm with dynamic window size is described. The usage of Fourier and Radon transformations to compute the motion characteristics for each detected region is explained and the experimental results are given.

Chapter 3 presents the infrared camera-based contact-less system used to estimate the fatigue level. The existing blink detection and fatigue analysis techniques are discussed. The infrared camera-based contact-less system is proposed to estimate the fatigue level. The switching infrared light is used to detect the pupil in each frame and, as a result, the blink event. The camera frames processing algorithm is pointed out in order to distinguish involuntary blinks from the voluntary ones. The experimental tests are shown to validate the proposed hardware and software system.

Chapter 4 introduces a non-invasive vision-based system for eye blinks detection and fatigue level monitoring using a webcam, positioned in front of the face. An introduction to the problem is given and the improved system is proposed. The cascade of boosted classifiers based on Haar-like features is presented for fast detection of the eyes region. The algorithm of frames

differencing in combination with the thresholding are shown to detect the eyes closure and opening. The frame processing algorithm is pointed out in order to distinguish the involuntary blinks from the voluntary ones and experimental results that validate the proposed system are given.

Chapter 5 shows the next step for measurements in image and video by involving mobile devices. The analysis of techniques to control heart activity is presented and the possible solutions are discussed. Several smartphones are tested in order to define the common characteristics of the captured video, and establish proper criteria for PPG extraction. The appropriate algorithms are proposed and validated to verify the correct device usage, the system calibration, and the PPG acquisition. The experimental results are presented to confirm the correctness and suitability of the proposed method with respect to the oximeter measurements.

Chapter 6 presents the robust and reliable method for pulse rate evaluation using a smartphone. The usage of the smartphone camera to evaluate volumetric variations of blood by monitoring the change of light absorption in the tissue is discussed. The algorithm of pulse rate evaluation is presented and explained. To validate the pointed out method, the evaluated by smartphone pulse rate is compared with the results of the Spacelabs 90207 Ambulatory Blood Pressure monitor. The experimental tests are performed and discussed to confirm the correctness and suitability of the proposed method.

Chapter 7 deals with the continuous blood pressure estimation. An overview of the current blood pressure measurement devises is given and the new trends of non-invasive measurement are presented. In order to overcome the drawbacks of existent solutions, the usage of artificial neural networks is described. The structure of the training data, obtained from the Multiparameter Intelligent Monitoring in Intensive Care waveform database, are presented and parameters extraction is discussed. The experimental results are given as well.

Last chapter contains the conclusions and summaries of this thesis. Possible avenues of further work are also discussed.

Part I

Measurements in Static Images

2

Detection and Parameters Estimation of Locally Motion Blurred Objects

This chapter presents a new approach to detect moving objects affected by motion blur. The direction and the length of the blur reflect the original motion of the object during a time of picture acquiring by the camera (shutter speed). The image analysis in the spectrum domain using Discrete Cosign or Fourier Transforms allows detecting the motion blur direction and speed. However, such techniques do not work when there are few objects on the image with different blur, or complex background. The proposed method of local motion blur detection is based on image partitioning and allows locating only the regions affected by the motion blur and, therefore, correct measuring the motion parameters of multiple objects.

2.1 Introduction

Motion blur is an alteration that appears on the image due to relatively large difference in the velocity between objects in a scene and the camera exposure time [13]. Motion blur is usually considered as an extra noise that affects the quality of the image. However, if detected properly it can be also used to obtain some characteristics about the object movement. In particular, for any fixed shutter speed of the camera, the moving length of the object is proportional to the amount of blur caused by the imaging process. Thus, if the length and the orientation of the motion blur can be identified it is possible to recover the speed of the moving object [13].

Methods of blur detection can be divided into two groups: methods of the first group intend to analyse the spatial domain while the ones of the second group use different techniques, like Fourier Transform, to analyse the frequency spectrum [14]. Generally, the methods operating in frequency domain are more powerful for motion blur detection.

In [15] was proposed an approach that is based on the theory of Fourier Transformation to detect the vehicle speed from a single motion blurred image.

In particular, the parallel lines appear on the 2D spectrum of the motion-blurred imaged. The distance and orientation of these lines are directly related with the motion length and direction [16] (Fig. 2.1).
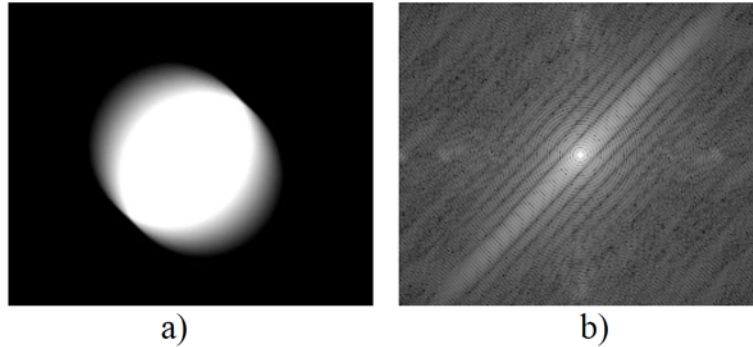
Fig. 2.1. Example of motion blurred circular image (a) and its Fourier spectrum (b).

However, the authors reported the problem of partial motion blur detection, i.e. when only the foreground object is moving and the background does not change. The improved approach was presented in [17], where authors proposed to use an image matting technique. But it still requires to mark the foreground and background regions manually, that does not allow developing of the automatic procedure.

In [18] was proposed to use the fuzzy sets for motion parameters detection. The Radon Transform was used to detect motion orientation, using the angle of the dark parallel lines on the Fourier spectrum. For the noised images, such lines are not visible clearly and the detection of white bound in the centre of image was used. The motion length was estimated as the distance between the first valleys (minimum peaks) using the fuzzy sets.

In [19] proposed a method to estimate the motion by calculating the difference of the spectra of two different images: with motion blur and without. In this way, spectrum, caused by motion blur, can be distinguished using the Fourier Transform theory. The motion orientation is computed then by detecting the spectrum peak in the polar coordinates, while the motion length is calculated as the distance between the first negative peaks of the cepstrum signal, starting from the centre. However, the disadvantage is that it is necessary to acquire two images, and only one of them must contain the motion blur.

Another approach that uses Wavelet transformation to detect the motion blur was proposed in [20]. It was applied to remove the noise, but not to detect the motion length. Moreover, only the cases, where the motion blur affects the entire image were considered.

The above methods of motion blur detection in the frequency domain are powerful but not suitable in case of (i) complex still background, (ii) small size of the moving object in comparison to the image dimensions, or (iii) more than one object is moving with different speed and/or in different directions. In such cases so usual for the real-world situations the Fourier Transform does not show the clear picture. Moving of several objects affects the entire Fourier spectrum and makes impossible distinguishing of the proper orientation and motion length (Fig. 2.2a-b), even if the objects move in the same direction but with different speed (Fig. 2.2c-d). In the case of complex background, the overall noise as well as the sharp boundaries affect the spectrum and motion is not detectable automatically (Fig. 2.2e-f).

To detect regions with the local motion blur in [21] was proposed to go through the image with a fixed-size window and compute the Discrete Cosign Transform (DCT) to each of them. Alternatively, in [22] was proposed a framework that uses a local power spectrum slope, gradient histogram span, and the maximum saturation to detect the local motion blur. However, the first approach deals with the fixed-size window that does not take into account object dimensions and the second one requires a colour image, while very often there is just a greyscale one. Moreover, greyscale images usually are more contrast and, therefore, more details can be extracted.

In [23] the image segmentation was performed using a modified version of the K-means clustering algorithm. Thus, the input image was divided into rectangular sub-regions with assigned uniform Point Spread Function (PSF). The proposed technique is able to detect different motion blur, but does not reject the regions with no blur. Therefore, it can be applied to process images from moving camera, where the entire image is affected by motion blur, but for the static camera with a local motion blur it does not work.

This chapter introduces a new method to detect the locally motion blurred regions in the image with complex background. It is based on calculation of the local standard deviation of the image pixels and scanning of all sub-images using the partitioning algorithm with dynamic window size [24].

The chapter is organized as follows: in Section 2.2 it is described the method of blurred segments detection, in Section 2.3 the motion orientation and the length detection algorithm is presented, Section 2.4 shows the experimental results and in Section 2.5 concluding remarks are given.

2.2 Local Motion Blur Detection

As seen from Fig. 2.2, the spectrum does not give a clear and solid direction of the motion blur. Therefore, it is impossible to obtain the motion parameters of each object just computing the Fourier transform to the entire complex image. Thus, it is necessary to perform the segmentation and extract only the regions with motion blur.
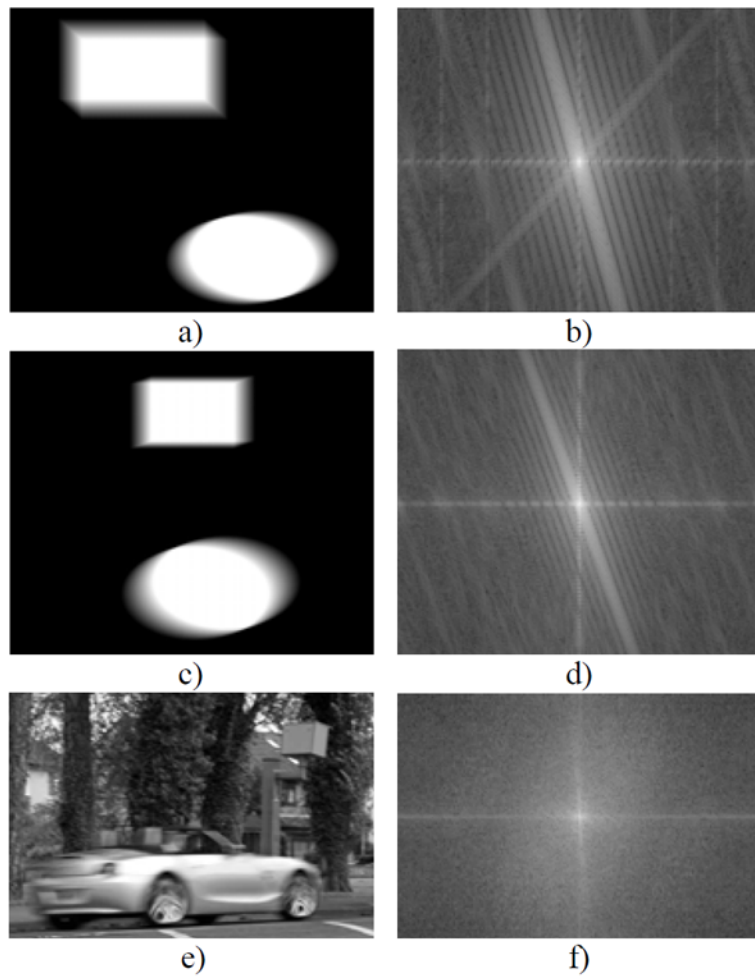
Fig. 2.2. Different images (a, c, and e), and the corresponding spectra (b, d, and f).

The proposed approach is to retrieve information about boundaries, followed by the image partitioning algorithm to check the statistical parameters in each of sub-images and reject the ones that doesn't contain motion blur. The block scheme of the complete procedure to detect the local motion blur is shown on Fig. 2.3.

Obviously, the boundaries of the regions that contain motion are smooth and the regions without motion blur are sharper.

Thus, for each pixel of the input image the standard deviation value of the 3-by-3 neighbourhood is computed as
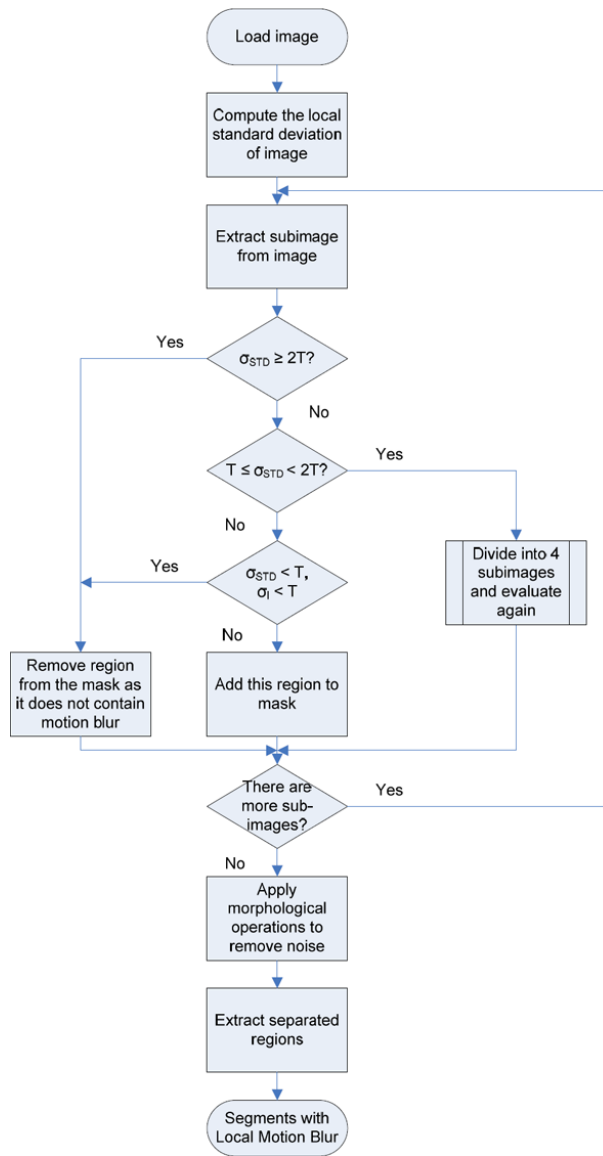
Fig. 2.3. Block scheme of the procedure to detect the regions with a local motion blur.

$$\sigma(x,y) = \sqrt{\frac{1}{N}\sum_{i=1}^{N}(I(x,y)_i - \mu(x,y))^2}, \qquad (2.1)$$

where the N is the size of the neighbourhood window and $\mu(x,y)$ - mean value of the neighbour pixels for pixel $I(x,y)$.

Fig. 2.4 shows an example of such computation. The different motion blur was added manually to the two objects, while the rest background remained sharp. As it can be seen, the boundaries of the objects with motion blur are not so strong and, therefore, easily detectable.

a)   b)

Fig. 2.4. Original image (a) and the result of local standard deviation computation (b).

To detect a local region it was used the method of image partitioning into sub-images (windows). The default window size was defined as 16x16 pixels and it changes depending on the standard deviation value in the current window, computed for the local standard deviation on image σ_{STD} and for original image σ_I. Comparing the values of the standard deviation for each window with the threshold T, established as the maximum value for the images with no motion blur, the following situations are possible (Fig. 2.5):

1. $\sigma_{STD} \geq 2 * T$ means that there are strong boundaries in this window and no motion blur. Therefore the window is rejected (Fig. 2.5c).
2. $T \leq \sigma_{STD} < 2 * T$ means that only some part of the sub-image contains strong boundaries and the rest is smooth. In this case the current window is divided into 4 smaller ones and the decision is made for each of them.
3. $\sigma_{STD} < T, \sigma_I < T$ means that there are no strong boundaries in this window and the values of the original image have very small deviation, i.e. have similar texture which is not a case of the motion blur (Fig. 2.5d).
4. $\sigma_{STD} < T, \sigma_I > T$ means that there are no strong boundaries on the image, but also the texture is not similar. This is the case of motion blur (Fig. 2.5e).
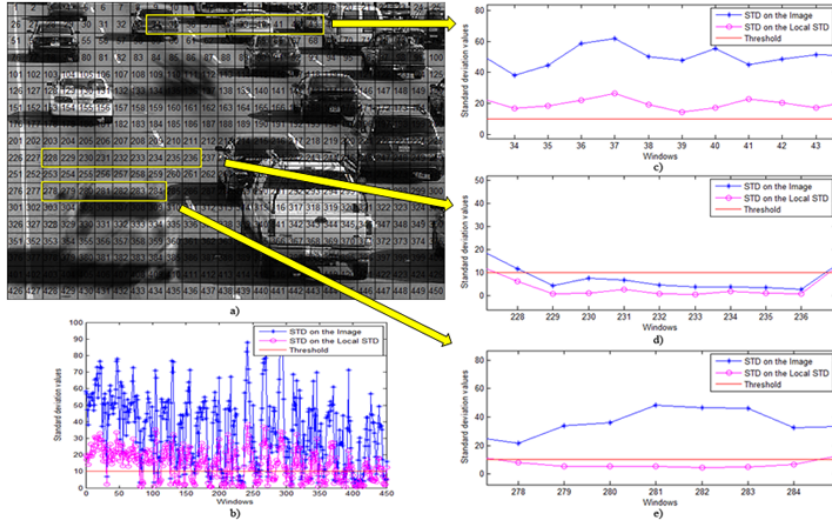
Fig. 2.5. Result of image partitioning (a), trend of sigma values in each window (b), extracted sigma values in windows with no motion blur and sharp edges (c), simple texture with no motion (d), and motion blurred ones (e).

Thus, considering the above cases it is possible to reject background and leave only the regions with the motion blur. After performing such image partition, the binary mask is obtained with "0" at the pixel positions with no motion blur and "1" where it is present. Then the series of morphological operations is applied to remove the isolated pixels.

Finally, each of the detected regions is extracted and considered as a separate one.

2.3 Estimation of the Motion Blur Parameters

The model of the blurred image can be considered as

$$g(x, y) = f(x, y) * h(x, y) + n(x, y), \tag{2.2}$$

where $g(x, y)$ is the observed image, $f(x, y)$ is the original image, $n(x, y)$ is the noise function, and $h(x, y)$ is the PSF causing the motion blur. The symbol $*$ stands for the convolution operation.

To establish the nature of the motion blur, it was used the technique from [25] that allows distinguishing of the motion blur from the out-of-focus blur as well as the case without blur.

The algorithm to determine motion parameters was used as in [18]. Considering the case with the linear motion and uniform velocity, the blur can be specified by the motion length R and the direction θ. The PSF $h(x, y)$ can be written then as [15]

$$h(x,y) = \begin{cases} \frac{1}{R}, & |x| \leq \frac{R}{2}\cos\theta, y = x\tan\theta \\ 0, & otherwise \end{cases}. \tag{2.3}$$

The Fourier transform of (2.2) is

$$G(x,y) = F(x,y) * H(x,y) + N(x,y), \tag{2.4}$$

The Fourier transformation of the function $h(x,y)$, defined in (2.3), is a SINC function, oriented in the direction of the blur. To estimate the blur angle and the blur length it is necessary to identify the ripples in $G(x,y)$. The shape of the SINC function does not depend from the image or its dimension, but only from the parameters of the motion blur.

The direction of the motion blur was determined by computing the Radon transform from Fourier spectrum $G(x,y)$ as [26]

$$R(t,\theta) = \int\limits_{-\infty}^{+\infty} f(t\cos\theta - u\sin\theta, t\sin\theta + u\cos\theta)du. \tag{2.5}$$

Finally, the motion length can be estimated using [18]:

$$L = \frac{N}{d}, \tag{2.6}$$

where d is the distance between the first two valleys from centre of the Fourier spectrum, and N is image dimension.

2.4 Experimental Results

The different motion blur was added manually to real pictures in order to estimate the accuracy of blurred objects detection. Fig. 2.6a) shows the Fourier spectrum of the picture from Fig. 2.4a) while the Fig. 2.6b) shows the computation of the motion blur orientation using Radon Transform.

a)   b)
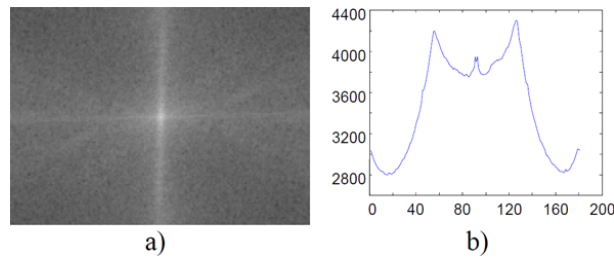
Fig. 2.6. Fourier Transform (a) and maximum values for each angle of the Radon Transform (b) or the original image.

Fig. 2.7 shows the detected regions with the local motion blur. Fig. 2.8 shows the estimation of the motion angle for each detected region and Fig. 2.9 shows the original image without motion blur as well as their detection result. The regions that were found are too small and were rejected.
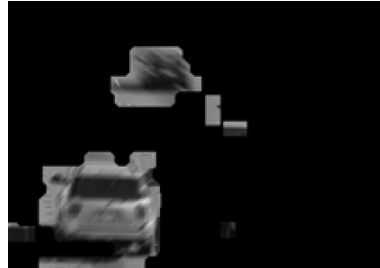
Fig. 2.7. Detection results of the regions with local motion blur.
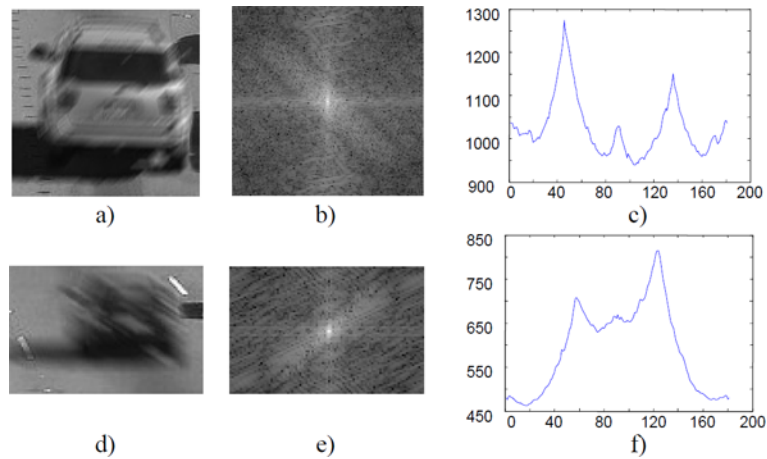
Fig. 2.8. Estimation of the motion blur parameters: a) first extracted region, b) its Fourier spectrum, c) computation of the rotation angle, equal to 45°, d) second extracted region, e) its Fourier spectrum and f)computation of the rotation angle, equal to 128°.

Fig. 2.10 shows another example of motion blur detection on the image with a similar texture of the background and Fig. 2.11 shows a computed mask when the image was affected by the global motion blur.

Fig. 2.9. Detection results on the image without motion blur: a) original image, b) obtained mask.
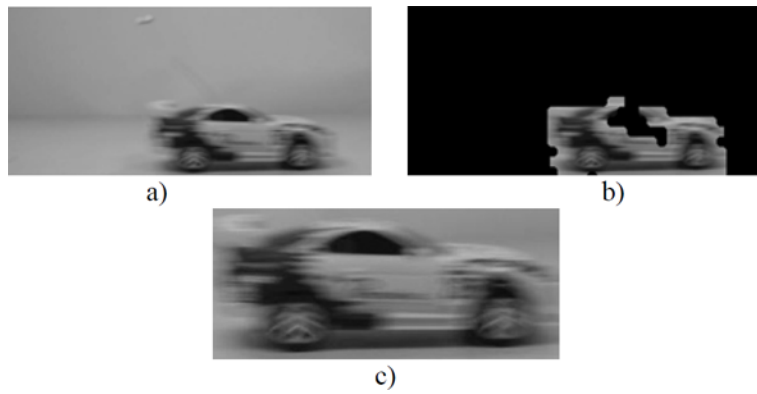
Fig. 2.10. a) Original image, b) computed mask, c) extracted region.
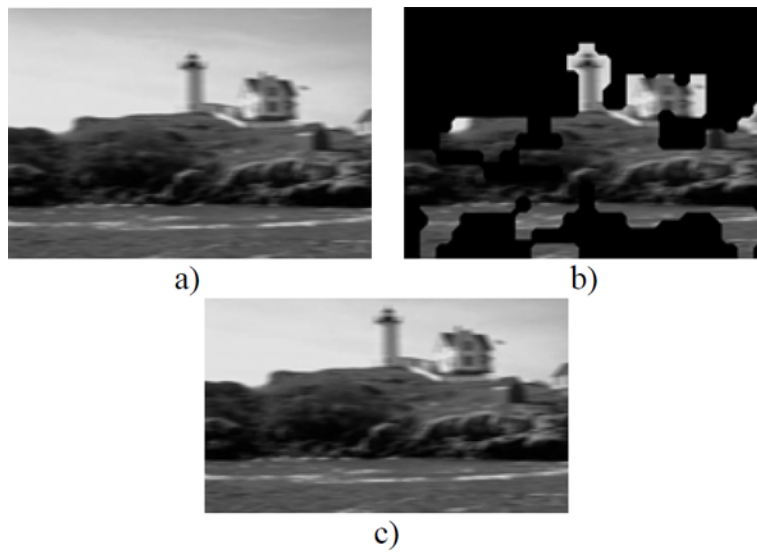
Fig. 2.11. a) globally blurred image, b) computed mask, c) extracted region.

2.5 Conclusions

The chapter is devoted to detection in the image of the regions, affected by local motion blur, in order to estimate the direction and the length for each moving object. Calculation of the image standard deviation allowed rejecting still background and extracting only the blurred regions. The algorithm works also in the case of global motion blur presence or monotonous background.

Part II

Measurements in Video

3

Blink Rate Measurement using Infrared Camera for Non-invasive Fatigue Monitoring

Passing from static images to video allows measuring additional characteristics of the objects that change over time. For example, the eye blinking is a significant indicator of the sleepiness and fatigue, and can be detected by analysing a video frame by frame. The existing systems of blink detection and fatigue analysis usually require fixing the camera on a spectacle frame or on a special helmet, that is not convenient and can affect the obtained results. In this chapter, the infrared camera-based contact-less system is proposed to estimate the fatigue level. The switching infrared light is used to detect the pupil in each frame and, as result, the blink event. The camera frames processing algorithm is pointed out in order to distinguish involuntary blinks from the voluntary ones. The experimental tests are shown to validate the proposed hardware and software system.

3.1 Introduction

Sleepiness is the physiological state of near-sleep or a strong desire for sleep. It is correlated with fatigue level, that is a transition period between wake and sleep state, and, if not interrupted, causes falling asleep [27]. Sleepiness, a tendency to fall asleep or even decrement of the attention, cause a series of negative consequences that are reflected on the everyday life.

Sleepiness and fatigue are terms commonly used in both clinical practice and research literature. Both sleepiness and fatigue are ubiquitous phenomena. They negatively affect the daily functioning and patients who have these feelings are distressed [28].

Advances in computer vision area in the last years allow to automate many everyday tasks in order to make the life safer and easier. Therefore, development of automatic sleepiness and fatigue evaluation techniques that could prevent accidents is very interesting.

3.1.1 Sleepiness

Sleepiness is an ubiquitous phenomenon, experienced not only as a symptom in a number of medical, psychiatric and primary sleep disorders, but also as a normal physiological state by most individuals over any given 24 h period [29]. Generally, sleepiness means an increased propensity to doze off or fall asleep; it may be related to a low arousal level. Sleepiness is also defined as a tendency to fall asleep. It may be affected by different conditions, such as medical problems, psychiatric diseases and primary sleep disorders [28].

The sleepiness can be measured both subjectively and objectively [29].

Subjective measurement of sleepiness

Sleepiness rating scales broadly include two categories. Methods of the first category measure short term changes in sleepiness and include the Stanford Sleepiness Scale (SSS), Karolinska Sleepiness Scale (KSS), and Visual Analogue Scales. Methods of the second category measure a global level of sleepiness and include Epworth Sleepiness Scale (ESS) and Sleep Wake Activity Inventory (SWAI) [28, 30].

Table 3.1 shows the Stanford Sleepiness Scale, that is one of the most widely used measures of subjective sleepiness [29, 31]. It consists of seven statements with different degrees of sleepiness and the subject should select one of them that describe better his/her current state.

Table 3.1. Stanford Sleepiness Scale.

Degree of Sleepiness	Scale
Feel active and vital; alert, wide awake	1
Functioning at a high level, but not at peak, able to concentrate	2
Relaxed; awake; not at full alertness, responsive	3
A little foggy, not at peak; let down	4
Fogginess; beginning to lose interest in remaining awake; slowed down	5
Sleepiness; prefer to be lying down; fighting sleep; woozy	6
Almost in reverie; sleep onset soon; lost struggle to remain awake	7

Objective measurement of sleepiness

Besides the subjective measurement of sleepiness, also objective methods exist. Most popular are Multiple Sleep Latency Test (MSLT) and Maintenance of Wakefulness Test (MWT) [28, 29]. Generally, besides the objective evaluation of the sleepiness, such test require from subjects to stay for some time in a dark room in order their state is been fixed. Because of complicated procedure, these methods can't be done automatically.

3.1.2 Fatigue

Fatigue, like sleepiness, is a highly prevalent phenomenon, associated with a significant level of physical and psychosocial morbidity. It is a commonly reported chief complaint in medicine and it is the primary symptom of chronic fatigue syndrome [29]. Symptoms of fatigue are commonly reported in patients with depression, chronic fatigue syndrome, cancer, etc. Fatigue may be also a side effect of a number of medication treatments [28]. It has been identified as major debilitating and even life-threatening factor in working populations [32].

Subjective measurement of fatigue

While the sleepiness, as it was described above, can be measured both subjectively and objectively, there are no techniques to measure fatigue level objectively. Nevertheless, there are many subjective rating scales which have been developed to measure fatigue. These scales provide a wide range of tools which are of interest both in the mental health field and in the somatic domain [28].

The Fatigue Severity Scale is a nine-item scale and is one of the best known and most used (see table 3.2) [29, 33]. Subjects are asked to respond the questions giving a mark between "1" (Completely disagree) and "7" (Completely agree).

Table 3.2. Fatigue Severity Scale.

During the past week, I have found that:	Value
1. My motivation is lower when I am fatigued	1-7
2. Exercise brings on my fatigue	1-7
3. I am easily fatigued	1-7
4. Fatigue interferes with my physical functioning	1-7
5. Fatigue causes frequent problems for me	1-7
6. My fatigue prevents sustained physical functioning	1-7
7. Fatigue interferes with carrying out certain duties and responsibilities	1-7
8. Fatigue is among my three most disabling symptoms	1-7
9. Fatigue interferes with my work, family, or social life	1-7

Unfortunately, this technique can't be used for automatic fatigue evaluation, so more advanced solutions mush be found.

3.1.3 Relation between blink frequency and behavioural factors

The eyelid is a skin-membranous organ that covers the eye and plays an important protection work, contributing to the distribution of the tear fluid. There is an upper eyelid (larger) and a lower eyelid, both with lachrymal glands and eyelashes. They have a function of protecting from excessive light and from dust as well.

As it was mentioned before, the blink occurs when the upper eyelid and the lower part are joined and the eye is temporarily closed [34].

Initially it was thought that the spontaneous beat of the eyelids was just a random phenomenon which has the purpose to lubricate and clean the eye from dust and external agents. Ponder and Kennedy (1927) were the first to be interested in this phenomenon. They initially agreed that the only purpose of the blink was to lubricate the cornea and that the blinking of the eyes was only a natural reflex of the eye. One of the experiments they carried out was to confirm such theory. Indeed, the eye reaction on the cigarette smoke was subjected. This condition caused significantly increase of the blink frequency. Later it was demonstrated as a result of numerous experiments, that there is a psychological reason why there is certain behaviour of the eyes. Ponder and Kennedy noticed that in all experiments carried out by them, the frequency of the blink did not change as long as the conditions of the experiment did not change. For example, if a person was intent on reading the blink frequency remained constant. But when the subject began to speak, the blink frequency changed. In addition, they found that this parameter mostly depends on the degree of subject attention and the mood during the test. However, the scientific demonstration wasn't provided as it was difficult to make that test on different subjects with the same state of mind. The correlation between the central nervous system and the movement of the blinking of the eyes, however, was evident. Ponder and Kennedy then came to the conclusion that the blink is not only a natural reflex of the eye, but this phenomenon occurs under the control of the central nervous system [35].

A recent study showed that the pupil dilation and the blink are indices of information processing by the brain. The results of this experiment show that the blink occurs during the early stages sensory processing and, consequently, during information processing, while the dilation of the pupil reflects better the acquisition phase of the information by central nervous system. It was also observed that immediately before the central nervous system process information, the blinking suspends. On the other hand, it occurs immediately after information processing and is interpreted as a rapid blink if the information is associated to a cognitive error. A further point that emphasizes the direct modulation between the blink and the nervous system, is represented by the transition between the interoceptive state of mind (sensitivity from outside of the body) and a state in which the exteroceptive information comes from external factors. During the interoceptive state has been observed a tendency to keep eyes closed, and, contrariwise, in a exteroceptive state the subject is tending to keep eyes open [36].

Other studies report the relationship between the reading and the blink frequency. One of the first studies was conducted by Katz using himself as subject. He used a Marey capsule (first instrument designed for heartbeat measurements) connected to the orbital muscle and recorded in this way the number of beats of the eyelids. He made 3 successive measurements each time under different intensity of the light. It was noticed that after the first 5 min-

utes of reading, especially when reading with a low light intensity, the number of the eyelids blinks increased. Therefore, as the result it was concluded that the blink frequency is a reasonable parameter to measure eye fatigue [37].

Table 3.3 lists factors that cause increment of the blink frequency while in the Table 3.4 are listed factors that decrement such frequency [38].

Table 3.3. Factors that increment the blink frequency.

- Conversation
- Anxiety
- Fatigue
- Irritant environment conditions (air conditioning, heating, smoke)
- Poor stability of tears

Table 3.4. Factors that decrement the blink frequency.

- Reading
- Difficulties with visual functions
- Computer usage
- Cornea anaesthesia

Since the eyes blinking depends on several factors, both physical and psychological, is difficult to associate fixed frequency, at which it occurs. However, several studies, carried out in the last years, have shown some correlation between the blink parameters and the level of fatigue.

In particular, the literature has demonstrated that the blink frequency depends on emotional and physical state of the person [39]. In particular, the eye blink is a significant indicator of the fatigue and can be used to measure the fatigue [40]. In [41] was demonstrated that the daily pattern of spontaneous eye-blink rate is a non-invasive peripheral measure of central dopamine activity.

3.1.4 Blink parameters as fatigue measure

Psychologists and physiologists are interested in the psychological and behavioural factors, responsible for the blink. Fatigue is one of them. While some studies report the relationship between mental fatigue that is referred to as effects on the time-on-task (TOT), others show how the transition between the state of awake (no fatigue) and sleepy is characterized by a particular behaviour of the eye parameters, such as duration and frequency of the blink.

In [42], the 11 subjects underwent a driving simulation dividing the drowsiness in 4 stages: awake, reduced alertness, drowsy and sleepy (Table 3.5). The experiment confirmed that the fatigue (the transition between the states wake up and reduced vigilance) is characterized by an increase in the frequency of blinking.

Table 3.5. The fatigue levels characterized by blink behaviour.

Drowsiness stage	Description
Awake	Long blink intervals and short blink durations.
Low vigilance	Short blink intervals and short blink durations.
Drowsy	Long blink durations.
Sleepy	Very long blink durations and/or single sleep events and/or a low eyelid opening level.

An alert subject has a high blink frequency with a short duration, while a sleepy person is characterized by higher than normal blink duration and has difficulties to open eyes immediately, so it has a higher eyelids opening time.

It should be noted that the spontaneous closure of the eyelids has a duration of 200 ms and the frequency ranging from 10 to 20 beats per minute [38].

3.1.5 Physiological measurement

Recent techniques of fatigue and sleepiness measurement involve sophisticated tools like Electrooculogram (EOG) and Electroencephalogram (EEG). The physiological measurements are used to provide a direct and objective measure of the state of sleepiness and fatigue. The electroencephalogram signal is widely accepted as a good indicator of the state of subject drowsiness. It is done by measuring the electrical activity generated by nerve cells in the brain. In addition, the duration of the eye blink, the frequency, the delay in the eyelids opening, and slow movements of the eyes can be good indicators of the degree of fatigue and sleepiness. These parameters are measured by electrooculogram [27]. Normally, they require placement of electrodes on the subject's face or head. These instruments provide an objective measure of the fatigue level and are widely used in medicine, together with the use of different scales which allow a subjective measure of the phenomenon.

Electroencephalogram

Electroencephalogram is a recording of the electrical activity along the scalp. It measures voltage fluctuations resulting from ionic current flows within the neurons of the brain [43]. To get the EEG measure during a fatigue state, data must be collected during the period from awake to the first sleep occasion.

The signal is classified then according to its frequency and the behaviour in the time changes during the different stages of sleep, or during the performance of cognitive tasks, focusing etc. The electrical activity of the brain is classified according to rhythms, which are defined in terms of frequency bands including [27]:

- Delta activity: these are slow waves between 0.5 and 4 Hz. Delta waves have been shown to be present during transition to drowsiness and during sleep.
- Theta frequency: is an activity within the frequency range of 47 Hz. Theta rhythms are associated with a variety of psychological states including hypnagogic imagery, and low levels of alertness during drowsiness and sleep and as such has been associated with decreased information processing.
- Alfa waves: has a frequency range of 813 Hz and occurs during wakefulness. The alpha rhythms are present during an alert and relaxed state.
- Beta waves: they are fast (1330 Hz) EEG potentials associated with increased alertness. Beta activity has been reported to occur in humans while performing a reaction-time motor task.

The difference of potentials is measured between pairs of electrodes placed on the scalp (bipolar recording) or between each electrode and a reference electrode positioned on ear or nose (monopolar recording). The measurement is done by placing of 20 electrodes according to the so called system "International 10/20". That means that electrodes are positioned at a distance equal to 10% and 20% of the distance between 4 anatomical points: the nasion (nasal), the inion (bone projection of the rear part of the head), and right and left points of periauriculars [44]. Fig. 3.1 shows the positioning of the electrodes.
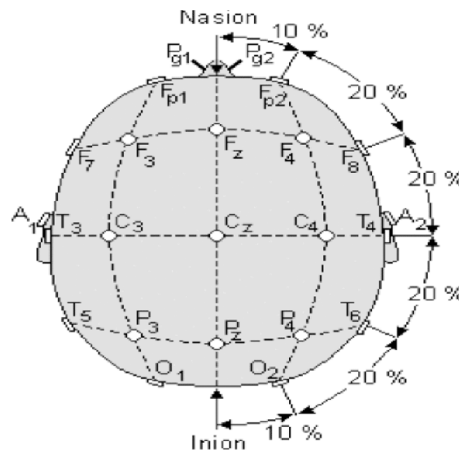
Fig. 3.1. Positioning of the electrodes: F - frontal area, O - occipital area, C - central area, P - parietal area, T - temporal area.

Incrementing of the alpha and theta EEG rhythms and reduction of beta have been interpreted as an indication of fatigue [45].

Electrooculogram

Electrooculogram is an instrument that allows detecting eye movements. It is used to measure the difference of potentials between the cornea and the retina. The eye in this way behaves as a dipole and the movements cause its rotation that gives rise to potential differences oscillating, superficially detectable. These signals are used as a measure of eye movement. In order to acquire a EOG, the electrodes are fixes of the subject's face as shown in Fig.3.2. To reduce the impedance between the electrodes and the skin, a special solution should be used on electrodes before making a measurement.
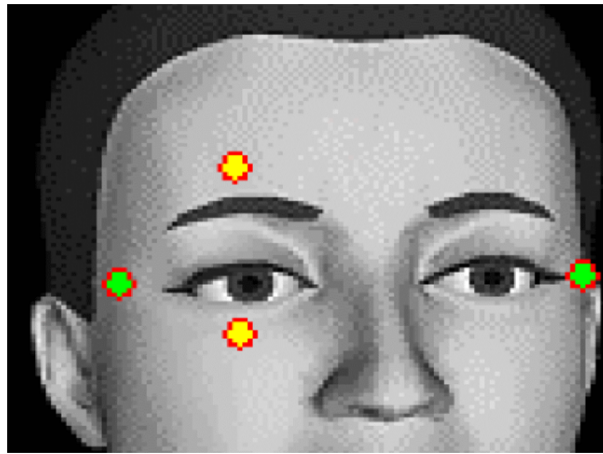
Fig. 3.2. Correct positioning of the electrodes for EOG measurements.

The two type of measurements can be done: the vertical one (also called monocular), when the electrodes are positioned on a single eye (yellow dots in Fig. 3.2), and the horizontal one (biocular), when the electrodes are positioned on the corners of the eyes (green dots in Fig. 3.2).

The blink duration is evaluated from electrooculogram as shown in Fig. 3.3 and means the distance between the point at which the rise time and the fall time reaches 50% of its amplitude. The need to identify a duration of a blink in the following way lies in the fact that it is difficult in the measured EOG signal to detect the precise point at which the blink starts [44]. It is also possible to measure the number of blinks per minute (frequency).

Fig. 3.4 shows the different variation pattern in the EOG signal depending on the subject's fatigue.

In the everyday life, however, it would be useful to have a non-invasive system to monitor fatigue.
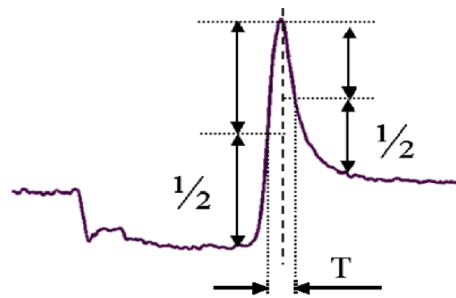
Fig. 3.3. Definition of the blink duration, measured from EOG signal.
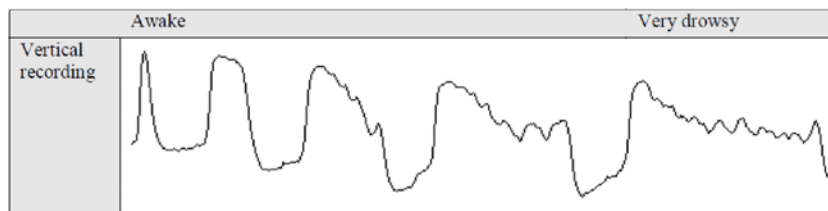
Fig. 3.4. Changes of the EOG signal in awake and drowsy conditions.

3.1.6 Non-invasive blink detection techniques

There are several techniques for non-invasive eye blink detection. Many of them are based on contact lenses, electrodes, specialized hardware, and infrared (IR) emitters. Such systems could easily be separated into three groups, according to the approach used: methods using the electric potential of the human skin [46], methods involving contact lenses [47], and methods involving image analysis [48]. For blink detection, the image analysis is preferred as it is a non-contact method of analysis and it does not affect the human behaviour [49].

In [50] the contact free system based on IR camera fixed on a spectacle frame is proposed, while in [51] a special helmet is used to fix the IR camera. Wearing of the camera allows locating the eye position in a very easy way. However, it is not convenient and is uncomfortably because the camera must be worn during the test. Then, it influences the person also on psychological level, changing the normal behaviour of the eyes.

This chapter presents a non-invasive system to monitor the human fatigue [52]. It is based on a IR camera that can be located in front of the user on the monitor or on the table. The person, therefore, can work as usual forgiving the camera and not concentrating on the test. This allows analysing the results obtained in a normal and usual environment and person's behaviour. Moreover, the algorithm is pointed out to process camera frames in order to distinguish the involuntary blinks from voluntary ones. Such system allows monitoring the people's sleepiness (fatigue) during their work with a computer

as well as to use it in many other places where the attentiveness is important, like driving a car, working with the machines etc.

The chapter is organized as follows. In Section 3.2 the approach is described for human eye segmentation which relies on pupil detection. In Section 3.3 the algorithm for blinks detection is described. In Section 3.4 the experimental results are presented, while in Section 3.5 concluding remarks are given.

3.2 Pupil Segmentation on Image

The IR camera is used to detect a pupil in the image. The working light spectrum is in the near-visible IR domain (860 nm), and the visible light is cut by the IR-pass filter. The examination object is illuminated by the IR LED lightning. In this way, noise coming from the surrounding visible light sources is eliminated and the contrast of the pupil increases. All the images taken from the camera are in the greyscale space. To achieve higher resolution of the eye image with low-resolution cameras as well as increase the accuracy of tracking, only one eye in the frame is detected.

Pupil segmentation is implemented according to the method described in [53] and [54]. It uses the ability of the eyes retina to reflect the penetrated light beam exactly in the same direction as it comes. Hence, if two light sources are used, one on and another off the camera optical axis, the pupil is bright in frame when the on-axis light is on. Respectively, in the frame-shot during the off-axis light is on, the pupil is dark. The rest of the image has almost the same intensity in frames because the lights are close enough to the camera and object.

Thus, subtracting the pixel values of those two frames and finding the region with the greatest difference between pixels allows detecting the pupil.

The proposed algorithm in [53] uses two consequent frames to detect one blink. It means that the pupil detection rate for the camera with 30 fps is only 15 fps. To overcome this limitation, the frame sequence is compared. Thus, the odd frame is compared with the even one, and the even one is compared with the next odd, and so on (Fig. 3.5). That allows detecting the pupil with the same speed as the camera works.

After binarization of the difference image with optimal threshold according with the Otsu algorithm [55], some white dots remain, which can be assumed as noise. As can be seen in Fig. 3.5, by using combination of morphological operators erosion and dilation, the noise can be suppressed. Therefore, the white spot in the final image shows where exactly the pupil is in the image.

This way of finding the position of the pupil in the image is very fast and does not require complex tracking algorithms. As a result, the centre and the size of the white spot are estimated.
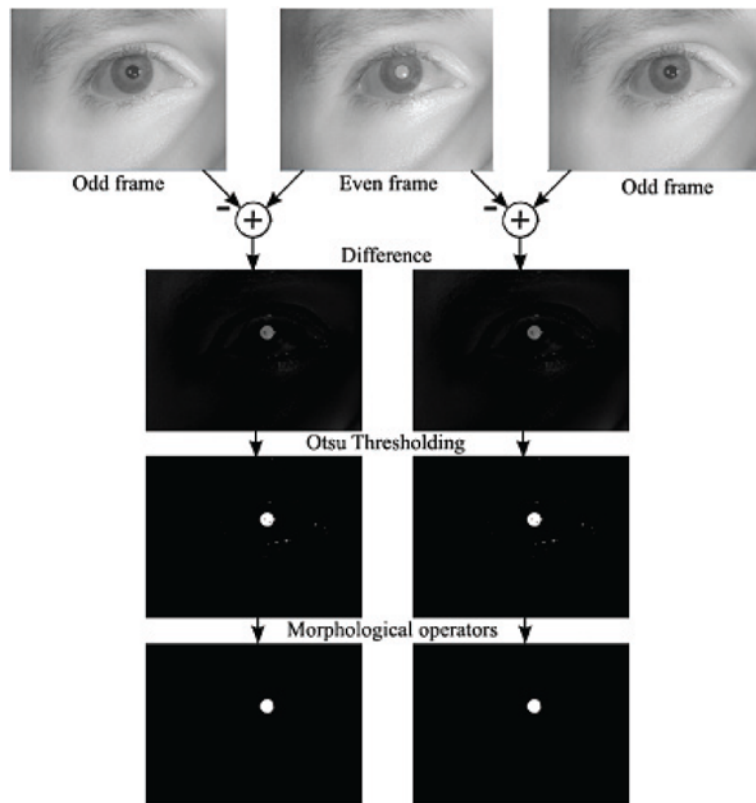
Fig. 3.5. Pupil segmentation procedure.

3.3 Proposed Algorithm of Blinks Detection

The detection of the blinks is performed by considering the size of detected pupil. The blink is detected when the pupil disappears or becomes very small. However, the data referred to the detected blink must be pre-processed in order to distinguish the voluntary and involuntary blinks.

Indeed, only the involuntary blinks are correlated to the emotional-physical state of the person. The count of the voluntary ones alters the measure of the observed parameters, i.e. frequency and duration. Moreover, the blinks can have different durations and may repeat after a very short time, both in the case of voluntary or involuntary blink.

Based on the previous considerations, the proper correction (normalization) of the detected blinks is performed according to the following considerations:

1. Detecting closed eye for few consequent frames. Since the average blink duration is 200-250ms [50], such blink should be considered as one for a

period of time that is less than the average. Moreover, it can also overcome that period. Therefore, only blink with duration less than 1s is taken into account (impulse i in Fig. 3.6a and b). Such threshold is established on the basis of the maximum delay in the close and open eyes [56].
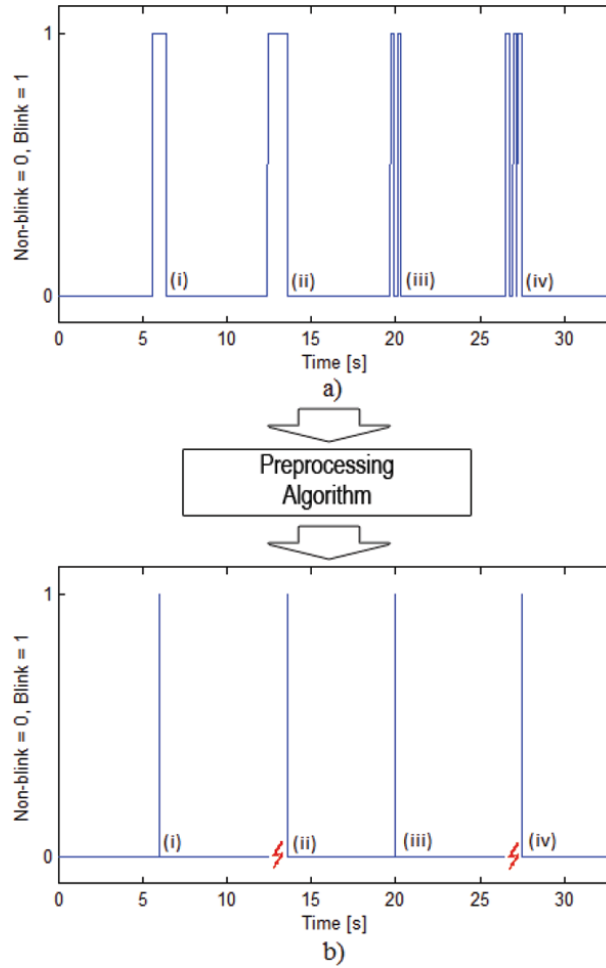
Fig. 3.6. The detected (a) and the corrected (b) results of blink detection.

2. Detecting the eyes closing that is more than 1s. It means that the eye was closed not spontaneously. In this case, the detection of blinking rate should be stopped and restarted as soon as the pupil is detected again in the image (impulse ii in Fig. 3.6a and b).

3. Detecting two blinks with short reopening time within 1s. Such situation is considered as a single blink since it's similar to an involuntary blink [57] (impulse *iii* in Fig. 3.6a and b).

4. Detecting more than 2 consequent closing and reopening eyes means that abnormal behaviour occurs and it is caused by voluntary blink or some disease. They shouldn't be considered during the blinking rate detection. Once the normal behaviour is detected, the count starts again (impulse *iv* in Fig. 3.6a and b).

3.4 Experimental Results

The experimental tests were executed during watching a video for 30 minutes (1800 seconds), at 10:00 in alert state, and at 00:00 (midnight) in drowsy state. In total, for each test there were acquired 54000 frames by the system described above, with the frequency equal to 30 fps.

According to the literature [58], the average duration of the blink in a fresh state is 200-250ms, while the proposed system allows frames capturing with the frequency of 30 fps (each 33.3ms) that is enough to detect the blink.

Fig. 3.7 shows the detected blinks and the elapsed time from the previous one.
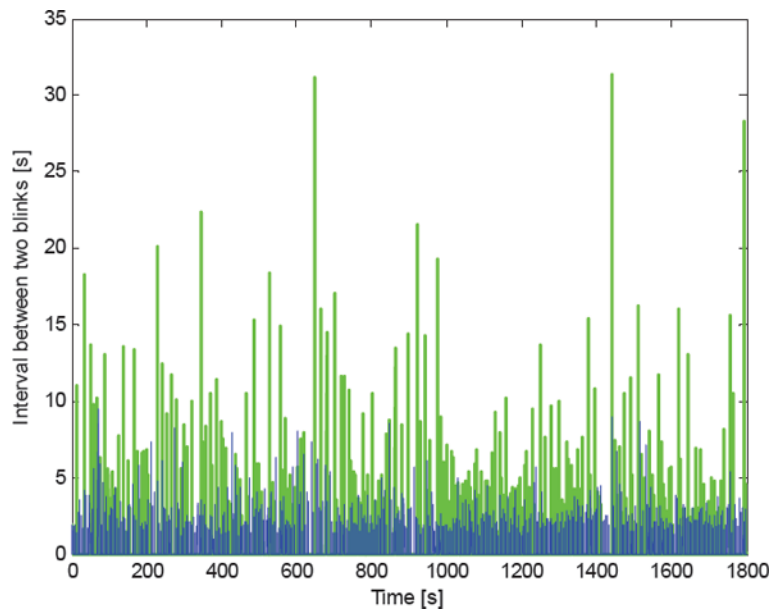
Fig. 3.7. Detected blinks and time interval between them for alert (green) and drowsy (blue) states.

Fig. 3.8 shows the mean interval between the two successive blinks, evaluated as mean value of the time elapsed between each consequent detected blink in previous 2 minutes [41].
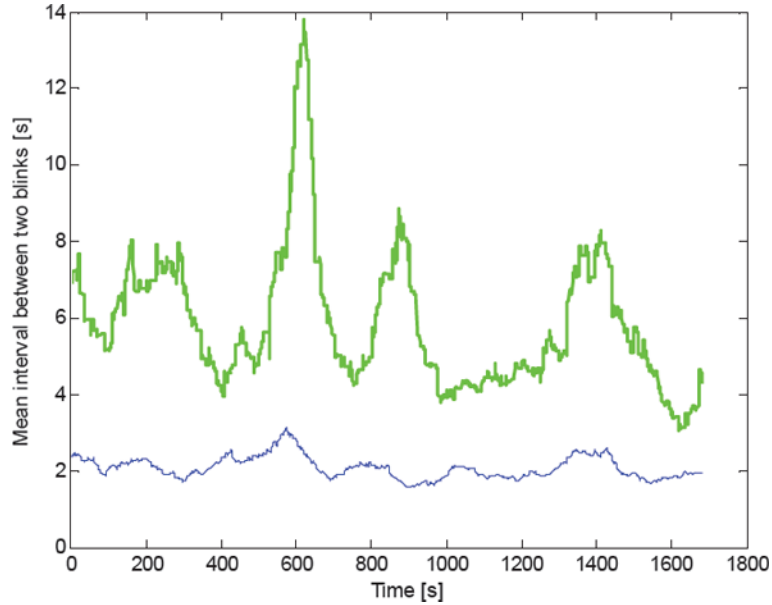
Fig. 3.8. Calculated mean interval between two blinks for alert (green) and drowsy (blue) states.

The blink frequency rate per minute is showed in Fig. 3.9. It is obtained from Fig. 3.8 by multiplying the reciprocal mean interval between two blinks by 60s.

Fig. 3.10 shows the distribution of the number of blinks detected at each frame. It shows that the blinks on the histogram for alert state are located at the very beginning of the scale, while for the drowsy state they are distributed wider and non-uniformly.

Thus, as can be seen from the figure above, the blink frequency for alert and drowsy states are grouped in two regions. The mean value of the blink frequency for alert state is 11.05, with standard deviation $\sigma = 2.89$, while for the drowsy state it is 29.34, with $\sigma = 3.89$. The fatigue level can be estimated by computing the blinking rate for any period of time during an experiment with the typical regions for alert and drowsy states (Fig. 3.10).
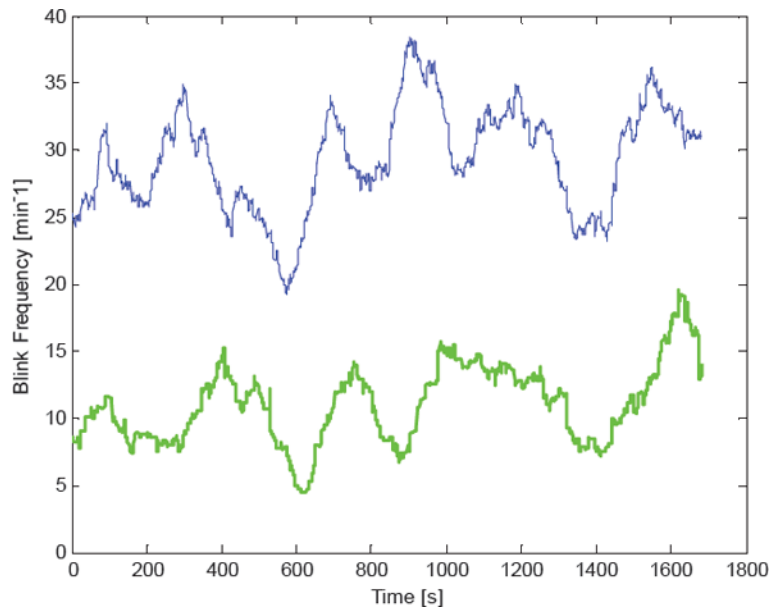
Fig. 3.9. Detected blink frequency for alert (green) and drowsy (blue) states.
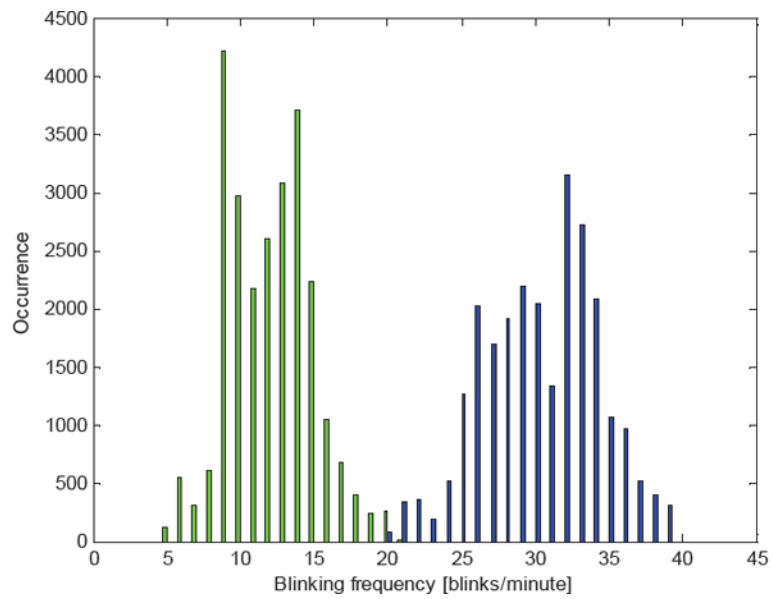
Fig. 3.10. Distribution of detected blink frequency for alert (green) and drowsy (blue) states.

3.5 Conclusions

The chapter is devoted to monitor the human fatigue by detection of the blinks. The eye blink rate was evaluated by detecting the pupil by IR camera and processing the frame according proposed algorithm.

The IR camera allows fast and easy detection of the pupil presence and, therefore, the blink event without analysing the pupil form and shape. The non-invasive nature allows user to feel free during the experiment and to eliminate the concentration on the camera in order to compute the correct blinking rate. Moreover, the developed system does not require expensive high-speed IR cameras as the other solutions do and, therefore, can be used widely.

The pointed out algorithm permits to distinguish the involuntary blinks from voluntary ones, and to estimate the fatigue level.

4

Eyes Blink Detection with Webcam for Human Fatigue Monitoring

In the previous chapter it was introduced the infrared camera-based system for fatigue level monitoring. This chapter presents a non-invasive vision based system for eye blinks detection using a webcam, positioned in front of the face. A cascade of boosted classifiers based on Haar-like features is used for fast detection of the eyes region. The frames differencing in combination with the thresholding are applied to detect the eyes closure and opening. A special algorithm is pointed out to distinguish the involuntary blinks from the voluntary ones. Experimental tests are shown that validate the proposed system.

4.1 Introduction

The eyelids blink is a significant indicator of fatigue and can be used to evaluate the sleepiness in humans [40]. Its frequency depends from the emotional and physical state of the human body [39]. Therefore, estimation of the blink is very interesting part of human-computer interaction and a lot of efforts are made making computers see when, how, and how often we blink [59].

An easy way to detect the pupil and, thereafter, blink appearance is to analyse images acquired by IR cameras with two light sources [52]. The pupil is detected as a white circle due to reflection of IR rays on the retina. In [50] the contact free system is proposed, where the IR camera was fixed on a spectacle frame, while in [51] a special helmet is used to fix the camera. Wearing the camera makes easy eyes localization but it is not comfortable as well as influences the person on psychological level changing the normal behaviour. IR cameras are more expensive than usual webcam, after all.

A number of methods that analyse captured from a webcam frames were presented. They include borders detection and wavelet analysis [60], colour-based eye sclera detection [61], frames difference and template matching [56, 62], eyes tracking using particle filters [63] and active appearance models [64]. One of the best results show the appearance-based object detection methods based on Haar-like features [65, 66, 67, 68, 69].

This chapter extends the approach, presented in [52] and discussed before in Chapter 3. The extension consists in replacing of the expensive hardware composed by the IR camera with a cheap and wide used webcam, available for most users. In order to achieve the same functionality and accuracy, the software architecture is improved by using a tracking algorithm for eyes detection and software optimization to perform the whole process in a real time [70]. A cascade of boosted classifiers based on Haar-like features is used for fast detection of the eyes region, while the frame differencing in combination with image thresholding are applied for blink detection.

Usually, a face is identified before detecting the eyes, as in [67]. Since the face has much more features it slows down the system performance. Moreover, such kind of occlusions as yawing, closing the part of the face with a hand can fail its detection. In this chapter it is considered detection only of the eyes pair that is faster and more precise. Localization of both eyes allows distinguishing the involuntary blinks from the voluntary ones more accurate. Thus, the user can work as usual forgiving the camera and not concentrating on the system. Such solution permits the fatigue level monitoring in a natural environment and usual person's behaviour.

The rest of the chapter is organized as follows: in Section 4.2 the eye detection approach based on cascade of boosted classifiers and Haar-like features is described, Section 4.3 shows the eye tracking algorithm, while Section 4.4 deals with the blink detection procedure. Section 4.5 shows experimental results and Section 4.6 gives concluding remarks.

4.2 Eyes Detection on the Image

The proposed blink detection procedure includes the following steps: i) eyes detection on a new frame or after significant movement, ii) eyes tracking, iii) eye closure detection and evaluation of the blinking rate (Fig. 4.1).

Initially, the goal for each new frame is to localize all regions that contain a pair of eyes. Such a task is challenging because the eyes have different sizes, positions, rotation angles, colour, shapes, etc. Moreover, they are not rigid objects as the person closes and reopens them from time to time, so the shape changes making the detection process more complicated [71].

The eyes detection is done by means of the Viola-Jones algorithm [65, 66] that is commonly used for fast appearance-based detection of different kind of objects [67] and consists of the cascade of weak classifiers. The Haar-like features are the input to the weak classifier and are specified by: (i) their shapes, (ii) positions within the region of interest, and (iii) the scale (Fig. 4.2) [66]. They are represented by "white" and "black" regions of rectangular form and can be computed very fast using an intermediate representation for the image called the integral image [65].

The integral image at location (x, y) contains the sum of the pixels above and to the left of (x, y), inclusive:
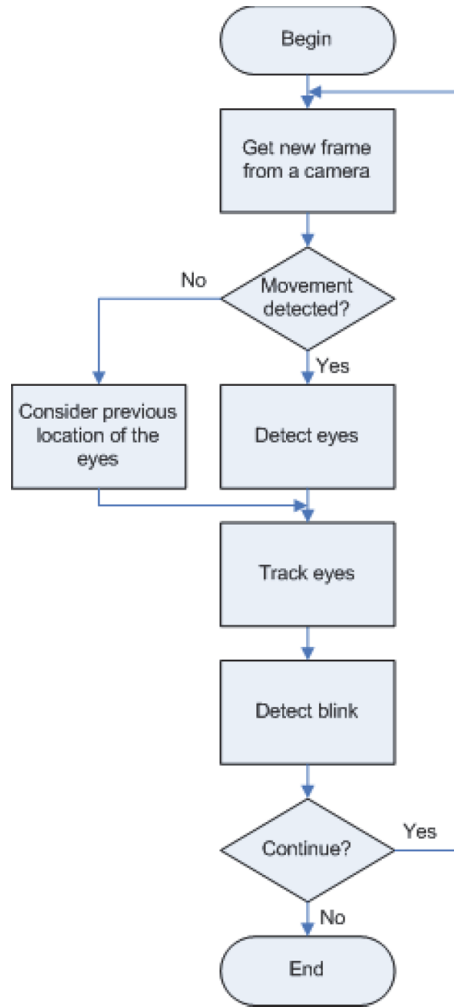
Fig. 4.1. Block diagram of the blink detection.

$$ii(x, y) = \sum_{x' \leq x, y' \leq y} i(x', y'), \qquad (4.1)$$

where $ii(x, y)$ is the integral image and $i(x, y)$ is the original image.

The integral image can be computed in one pass over the original image using the following pair of recurrences [65]:

$$s(x, y) = s(x, y - 1) + i(x, y), \qquad (4.2)$$

$$ii(x, y) = ii(x - 1, y) + s(x, y), \qquad (4.3)$$
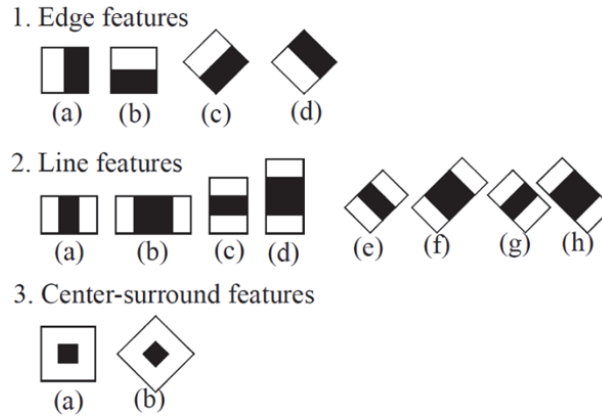
Fig. 4.2. Example of Haar-like features used for cascade training.

where $s(x, y))$ is the cumulative row sum, $s(x, -1) = 0$, and $ii(-1, y) = 0$.

Before applying a classifier to the input image, it should be trained with a number of positive examples (i.e. sample views of a particular object, like a face or a car) and negative examples - arbitrary images of the same size. It is used the AdaBoost algorithm [72] both to select features and to train a classifier [73].

The cascade consists of several simpler (weak) classifiers, applied one after another until all the stages passes and the object is accepted giving "1" in the output or at some stage the candidate is rejected giving "0" in the output (Fig. 4.3) [65]. A positive result from one classifier triggers the next classifier, and a negative outcome at any point leads to the immediate rejection of the sub-window.
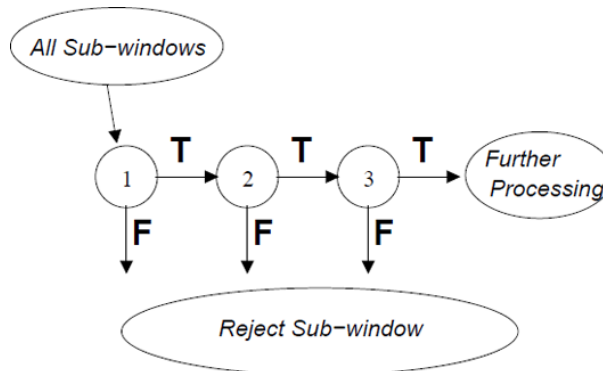
Fig. 4.3. Cascaded structure of the detection cascade. A series of classifiers are applied to every sub-window eliminating a large number of negative examples with very little processing and only very few negatives require additional computation.

In order to increase the accuracy of blink detection it was used a classifier, trained to detect both eyes. Indeed, when the blink is involuntary, both eyes close contemporaneously. On the other hand, only the involuntary blinks are correlated to the emotional-physical state of the person [57]. Thus, if the system detects closing of one eye only, while the second remains open, it means the voluntary blink occurred and it should be eliminated from further consideration.

Since the eyes position is known on the face, the coordinates of each eye can be extracted easily. Fig. 4.4 shows the result of such eye pair detection (red rectangles) as well as pointed out regions of right and left eyes (green rectangles).

Fig. 4.4. Detected regions (red) with indicated pair of eyes (green rectangles).

Considering that the camera is fixed on the table or is built-in into the laptop and the typical acquisition speed is about 30 fps, the difference between each consequent frame is small enough. Therefore, the image processing can be limited to a small region of interest where the eyes were detected previously.

4.3 Eyes Tracking

Assuming that the person during the work does not move frequently and rapidly as well as the background remains mostly static, the two consequent frames do not differ too much. Therefore, the eye tracking allows increasing the system performance. In this case, the detection of the eyes region in each new frame is avoided, doing it only when the significant change occurs in the frame.

Thus, the following algorithm is proposed. Once the eye pair is detected successfully, for each new frame that does not have significant difference with the previous one, the further processing performs only in the region of eyes. If those two areas are the same, the cascade of classifiers is not applied.

Moreover, in the case of small movement, instead of using a whole frame it is proposed to consider only the enlarged region around the previously found (Fig. 4.5). In such case, the possible position of the eyes fits the extended area.

Fig. 4.5. A frame during eyes detection in the case of head movement: the large blue rectangle shows the region where to search and the small red one shows the detected eyes region.

4.4 Blink Detection

As it was mentioned before, the involuntary blink occurs by both eyes at the same time. First, the difference between current and previous frames for each of the eyes is computed separately. Then, the current frame is considered as the one, where the blink occurs if the number of different pixels exceeds the established threshold. $F(t)$ is defined as Boolean value that specifies if the blink is detected in the frame t or not:

$$F(t) = \begin{cases} 1, & (\frac{\sum mask_r(t)}{CARD(mask_r(t))} > T \ and \ \frac{\sum mask_l(t)}{CARD(mask_l(t))}) > \frac{T}{2}) \\ & or \ (\frac{\sum mask_r(t)}{CARD(mask_r(t))} > \frac{T}{2} \ and \ \frac{\sum mask_l(t)}{CARD(mask_l(t))}) > T) \ , \\ 0, & otherwise \end{cases} \quad (4.4)$$

where $mask_r(t)$ and $mask_l(t)$ are the difference masks between current and previous frames for right and left eyes, respectively, $CARD()$ gives the cardinality of the input mask, T is the predefined threshold, computed as a minimal number of pixels that should differ to classify a blink.

The equation (4.4) allows to (i) take into account a non-uniform illumination of the face, i.e. when one of the eyes is darker than another, and to (ii) reject the cases of voluntary blink when just one eye is closed. The threshold T (equal to 0.15) was chosen on the basis of experimental tests performed in different illumination conditions and with different cameras.

Fig. 4.6 shows the frames with detected open and closed eyes (Fig. 4.6a and Fig. 4.6b, respectively) and the resulting binary mask (Fig. 4.6c). Application of a number of morphological operations such as erosion and dilation removes the noise from the computed binary mask. The white spots in the final image refer to the right and left eyes and shows whether the eyelids movement occurred or not.

The frame differencing allows understanding the moments when the eyelids moved. However, it says nothing whether the eye was opened or closed. Thus,
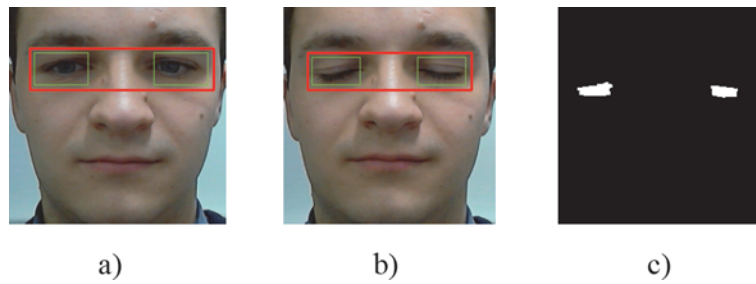
Fig. 4.6. Detected regions when the eye is open (a), closed (b), and the resulting difference mask (c).

a combination of the frames differencing with analysis of the vertical and horizontal projections in binary image is used.

The detected eye region is converted to a greyscale and then thresholded to a binary image (Fig. 4.7) using the Otsu algorithm [55]. Then, the maximal value of the vertical projection is used to detect the openness degree of the eye.
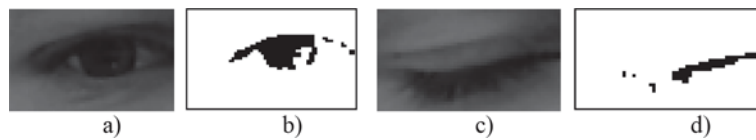
Fig. 4.7. Greyscale (a) and binary images of opened eye (b), Greyscale (c) and binary images of closed eye (d).

As it was mentioned in [52], the data referred to the detected blink must be further processed in order to distinguish involuntary blinks from the voluntary ones. The average blink duration is 200-250ms but can vary if the person is tired [50]. Moreover, blinks can have different duration and may repeat after a very short time, both in the voluntary and involuntary case. There can be a few consequent blinks as well.

Based on these considerations, the following correction of the detected blinks is performed:

i) detection of the closed eye for more than 1s means not spontaneous closure [56]. Thus, the alarm should be given and the detection of the blinking rate should be stopped and restarted as soon as the opened eye is detected again;

ii) detection of two blinks with a short reopening time within 1s should be considered as a single blink since it is similar to the voluntary blink [57]. It is caused by the features of the body and happens without human control;

iii) detection of more than 2 consequent closing and reopening eyes means abnormal behaviour, caused by voluntary blink or some other disease, and it should be eliminated from the blink rate detection. Once the normal behaviour is detected again, the count restarts.

Having the information about involuntary blinks and their duration, the fatigue level can be measured then by calculation of the blink rate (see Chapter 3) or using a PERCLOS method [64], i.e. calculation of the percentage of frames when the eyes are detected closed in a given period of time.

4.5 Experimental Results

The system was implemented and tested in Microsoft Visual Studio 2010 in Windows 7 working on PC with Intel Core 2 Duo 2.2GHz CPU and 4 GB RAM. Video was captured both from the built-in HP webcam and Logitech QuickCam Messenger, and processed using OpenCV library [74]. To find the eyes position it was used the 22x5 Eye pair detector composed by the 7000 positive samples [75]. The system allows eyes localization and blinks recognition when a user is within 1m from the camera and permits horizontal rotations up to $\pm 30°$.

Fig. 4.8a shows the time intervals when there was detected closing and opening of both eyes in a test video for 60s. Such moments are shown as peaks. During the video capturing there were done 9 blinks, one of which between 34s and 42s was a voluntary blink lasted 6s.

The sharp valleys in Fig. 4.8b represent the time instances when the eyes were closed. The value for each analysed frame shows the percentage between the maximum value of the vertical projection and the eye region height.

As it can be seen from Fig. 4.8a and Fig. 4.8b, the charts for both left and right eyes are similar. The detected movements and valleys match perfectly, that means the blinks have been done involuntary (besides the one long blink for 6s). The final result of blink detection is shown in Fig. 4.8c, where high value represents the time interval when the eyes were detected closed and the low when they were opened. The duration of the blinks can be calculated as well.

Videos of 5 persons were captured at 10:00 o'clock in an alert state and at midnight in a drowsy state, and then analysed. Table 4.1 shows the summary of blink detection results in different conditions.

4.6 Conclusions

This chapter is devoted to detect eye blinks in order to monitor the level of fatigue. It is an active topic for research since can be used in many areas where attentiveness of the operator or driver is an important factor.
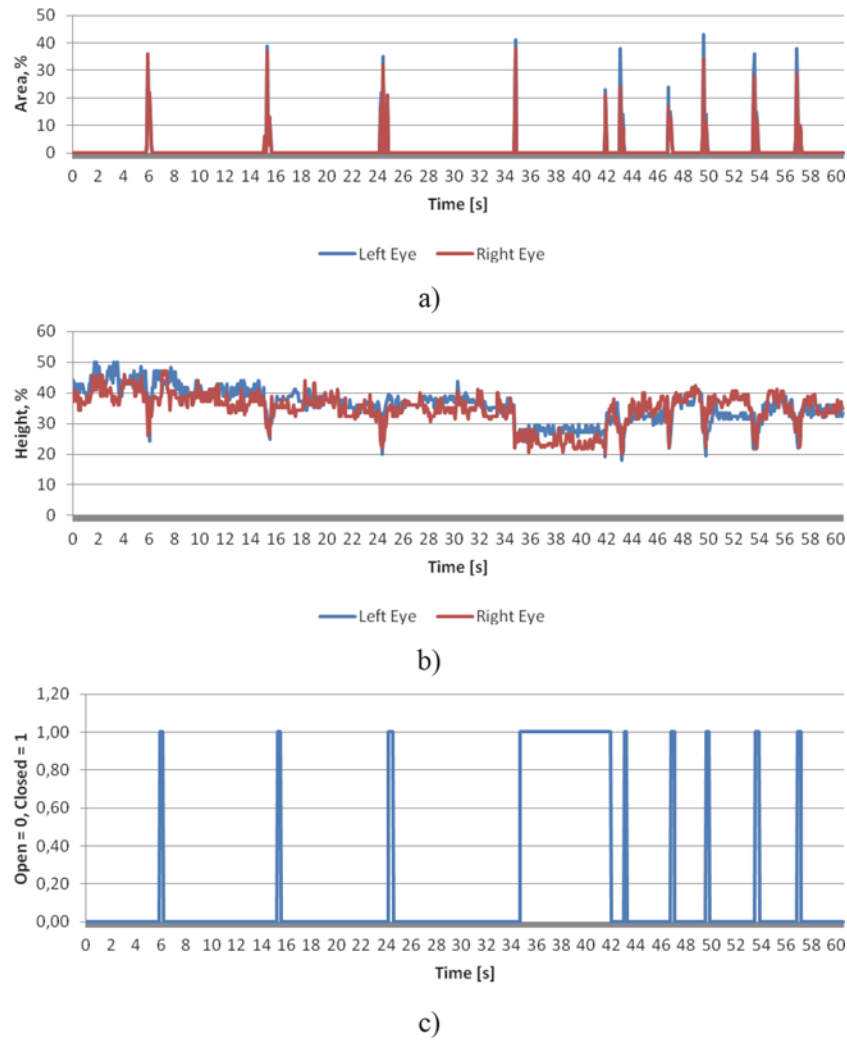
Fig. 4.8. a) closures and openings, the area value represents the percentage of pixels that were detected as changed; b) percentage of the maximum values of the vertical projections of the eyes regions respect to the region height; c) detected blinks.

A webcam based system that uses a set of Haar-like features for fast detection of the eyes region and the frames differencing to detect the eyes closure is proposed. The pointed out algorithm permits to distinguish the involuntary blinks from the voluntary ones, and to monitor the changes of the fatigue level over the time. The experimental results shows reliable results for different persons and illumination conditions.

Table 4.1. Summary of blink detection results

Video condition	Total blinks analysed	No. of missed blinks	No. of false positive	Average accuracy
Daytime video	869	12	17	96.67%
Night-time video	1756	71	86	91.06%
Daytime video, wearing glasses	910	21	18	95.71%
Total	**3535**	**104**	**121**	**94.48%**

Part III

Measurements using Mobile Devices

5

Smartphone-based Photoplethysmogram Acquisition

This chapter introduces the next step for measurements in image and video by involving mobile devices. Smartphones have become one of the widest and often used devices that people bring almost every time and everywhere. Their computational capacities allow their application for many every-day tasks. One of them is health state monitoring.

A smartphone-based photoplethysmogram (PPG) acquisition and pulse rate evaluation system is presented in this chapter. The proposal is designed for different smartphone models, equipped with a LED or not. Different cameras represent the same acquired information in different ways: changes may occur in colour saturation, resolution, frame rate, etc. Therefore, several smartphones are used to define the common characteristics of the captured video, and establish proper criteria for PPG extraction. Moreover, the appropriate algorithms are proposed and validated to verify the correct device usage, the system calibration, and the PPG acquisition. The experimental results confirm the correctness and suitability of the proposed method with respect to the oximeter measurements.

5.1 Introduction

Monitoring of vital parameters is very important for timely detection and prevention of any health diseases. The blood pressure, heart rate and their changes are ones of the most important parameters to control.

There are different techniques to control heart activity: electrocardiography, ambulatory blood pressure monitoring, photoplethysmography, etc. When patients are asked to measure their heart rate, usually the palpation technique is used, however it is not precise. Therefore, individuals should be properly trained on how to measure their own heart rate accurately [76]. To overcome the human factor automatic systems have been proposed.

5.1.1 Electrocardiography

Electrocardiography (ECG) allows evaluating the performance of the cardio-vascular system with high accuracy, and it is "a gold standard" for beat-to-beat heart rate (HR) measurements [77]. It is an interpretation of the electrical activity of the heart, detected by the electrodes attached to the skin, and recorded by an ECG machine over a time interval [78]. Each heart beat is represented by a regular sequence of wave patterns (Fig. 5.1).

Fig. 5.1. ECG wave with detected heart beats.

However, the ECG requires attaching and correctly placing multiple electrodes on the body. That limits the device usage to a clinical environment with trained personnel and makes such approach impractical for most individuals interested in monitoring their HR in natural environments [77].

Moreover, many patients are subjects to a so-called "white coat effect". In particular, several studies of white coat effect have confirmed that it occurs in 20% or more of the hypertensive population [79]. The white coat hypertension is defined as the presence of increased blood pressure due to nervousness when undergoing a clinical examination, while at home it remains normal. Indeed, according to a recent research by Kaiser Permanente Colorado in collaboration with the American Heart Association and Microsoft Corp., patients performing self-monitoring of their vital parameters are 50% more likely to have their blood pressure under control [80]. Therefore, there is a need for low-cost physiological monitoring solutions that are easy to use, accurate, and can be used at home or in ambulatory conditions [81].

There are alternative portable ECG devices such as Holter monitors that allow continuous monitoring of the cardiovascular system. Once the electrodes are attached to the chest, the patient can continue normal activities for 24 hours or more. Then, the cardiologist analyses the recorded ECG and diagnoses. The main drawback of such solution is that there is no immediate feedback to the user, so there is no possibility to help the patient when the incident occurs [82].

5.1.2 Ambulatory blood pressure monitoring

In a similar way, Ambulatory Blood Pressure (ABP) monitoring devices are used for non-invasive examination of heart activity. They provide continuous 24 hour measurements of the blood pressure and HR at regular time intervals.

Having been developed mostly to identify patients with white coat hypertension, they become very useful for the determination of hypertensive end-organ damage risk [83]. For example, a Spacelabs 90207 ABP Monitor (Fig. 5.2) [84] is a clinically validated medical device [85, 86, 87] tested according to the protocols of the Association for the Advancement of Medical Instruments [88], the American Heart Association [89], and the British Hypertension Society [90].
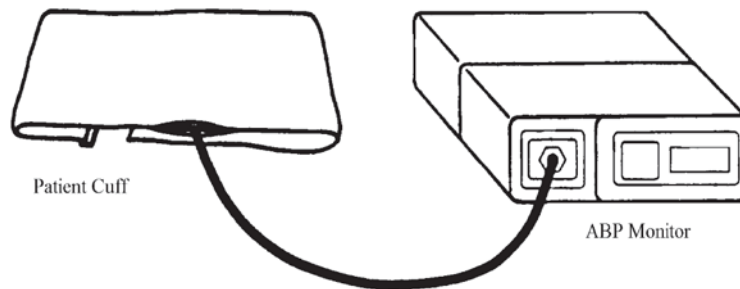
Fig. 5.2. Spacelabs 90207 ABP Monitor.

However, as in the case of portable ECG devices, the ABP monitoring devices are expensive and do not provide the real time measurement results. Patients should visit their doctors for viewing and analysing the measurements.

5.1.3 Photoplethysmography

An alternative non-invasive technique for the detection of blood volume changes during a cardiac cycle is photoplethysmography (PPG). It is a simple and low-cost optical technique that can be used to detect blood volume changes in the microvascular bed of tissue [91]. The technique assumes skin illumination with penetrating optical radiation, usually from a light emitting diode, with a subsequent detection of the signal by a photodetector [92]. Most often the PPG operates at a red or a near infrared wavelength [91].

The PPG has considerable potential for telemedicine including home or remote patient health monitoring. Miniaturization, ease-of-use and robustness are key design requirements for such systems [91]. Clinical PPG applications include monitoring of heart and respiration rate, blood oxygen saturation, pressure as well as detection of peripheral vascular diseases [92].

The PPG waveform consists of a pulsatile ("AC") physiological waveform attributed to cardiac synchronous changes in the blood volume, and a slowly varying ("DC") baseline. The "AC" component has its fundamental frequency typically around 1 Hz, depending on the heart rate. The "DC" component

is influenced by respiration, sympathetic nervous system activity and thermoregulation [91]. Fig. 5.3 shows the pulsatile component of an acquired PPG waveform and the corresponding electrocardiogram.

Fig. 5.3. The pulsatile (AC) component of the PPG signal and the corresponding electrocardiogram.

As was mentioned, the "AC" component corresponds to the heart beats and can be used for heart activity monitoring. The PPG probe should be held securely in place to minimize the probe-tissue movement artefacts [91].

There are two possible PPG operational modes: (1) transmission, when the tissue sample (e.g. fingertip) is placed between the source and detector (Fig. 5.4a), and (2) reflection when the LED is placed next to the detector (Fig. 5.4b) [93]. The transmission mode imposes more restrictions than the reflection mode on the body locations available for study [91].
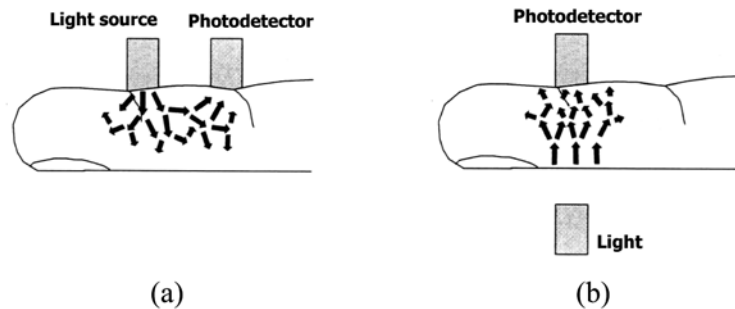
Fig. 5.4. Reflection (a), and transmission (b) modes for video acquisition.

Such photometric-based plethysmogram is normally obtained by using a pulse oximeter (Fig. 5.5) [94, 95]. The device is placed on a thin part of the subject's body, usually a fingertip or earlobe. The light with red and infrared wavelengths sequentially passes through the subject to a photo-detector that measures the changes in light absorption [96].

Fig. 5.5. CMS50DL finger pulse oximeter SpO2 monitor.

In addition to the PPG waveform, an oximeter evaluates the level of oxygen in blood and computes a pulse rate (PR). Fig. 5.6 shows typical information obtained by the CMS50DL oximeter and displayed by the SpO2 software, which comes with the device.
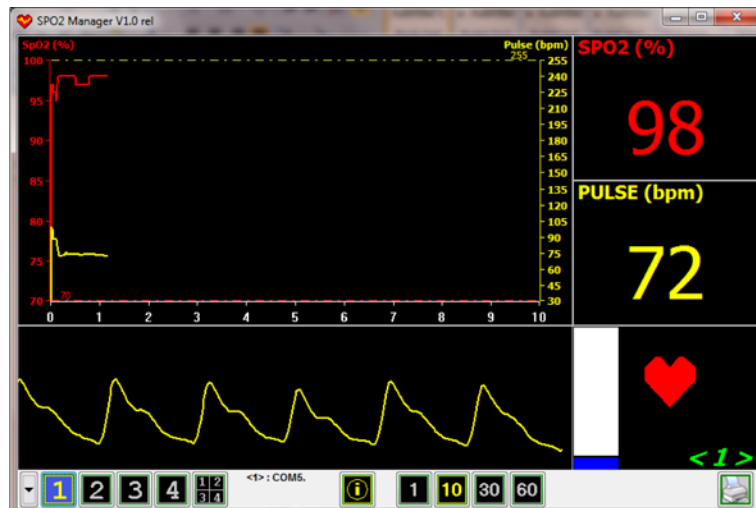
Fig. 5.6. Measurement results showed in SpO2 Manager.

The PPG signal obtained in this way is familiar to clinicians [95]. It clearly shows the pulsatile waveform caused by the pressure wave from the cardiac cycle, and the respiratory sinus arrhythmia induced by breathing [96].

Since the pulse oximeter is non-invasive and relatively inexpensive, in addition to the PR and level of oxygen in blood provided by such devices, much research has been carried out in extracting additional biometric information from the waveform. Linder et al. [96] extracted the following parameters from the obtained PPG: the pulse height, peak threshold, cardiac period, full width half max, and peak width (Fig. 5.7), and used them to detect changes in posture.
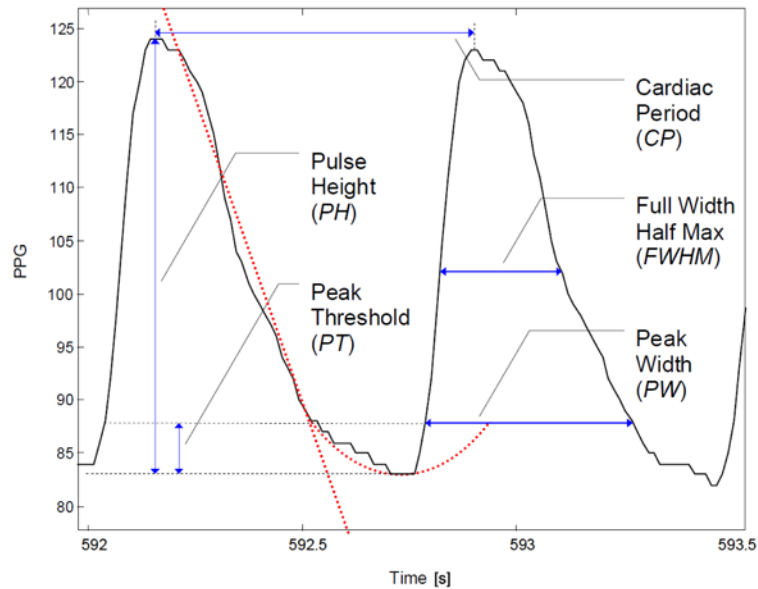
Fig. 5.7. The features of the PPG pulsatile component: Pulse Height, Peak Threshold, Cardiac Period, Full Width Half Max, and Peak Width.

Analysis of the blood volume pulse contour has become important because it contains much information about cardiovascular activity [97]. The final goal is to use the pulse oximeter as a primary sensor in an affordable, wearable health monitoring system [96].

5.1.4 Photoplethysmographic imaging

Replacing the photodetector, used in pulse oximeters, by a video camera enables photoplethysmographic imaging. It is an emerging area for research that provides advantages in terms of improved sensitivity, and real-time large surface area measurement [98]. Optical video monitoring of the skin by a digital camera provides information related to the subtle colour changes caused by the cardiac signal, and the pulsatile signal [81].

A preliminary CCD camera-based imaging photoplethysmographic system was described in [98, 99]. Fast digital cameras allow the development of PPG imaging, a totally contactless technique for monitoring a larger field of view and different depths of tissue by applying multi-wavelength LEDs. The PPG imaging system can work in both transmission and reflection modes as it is depicted in Fig. 5.8. The light intensity that passes through the finger varies with the pulsing of the blood and its plot against time is referred to a PPG signal.
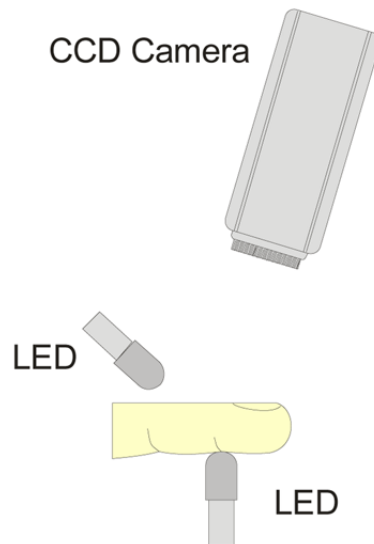
Fig. 5.8. Signal acquisition principle of a PPG imaging system.

5.1.5 Smartphone-based health monitoring systems

Nowadays smartphones have become one of the widest and often used devices that people bring almost everywhere. In addition, their computational power, possibility of wireless communication as well as their multifunctional user interface allows their usage in very wide spheres.

Smartphones are often used in telemonitoring to receive information from portable medical devices (e.g., blood pressure, glucose and pulse oximeter monitors) and mobile sensors (e.g., physical activity, accelerometer counts, heart rate, respiration rate, pulse pressure, and wireless electrodes) [77]. As an example, the iHealth Lab Inc. has announced the iHealth Blood Pressure Monitoring System for the iPhone, iPod Touch and iPad (Fig. 5.9) [100].

It consists of a hardware dock, a blood pressure arm cuff and software, and allows the users to self-monitor their blood pressure at home as well as

Fig. 5.9. The iHealth Blood Pressure Monitoring System.

share results with a doctor. There are also pulse oximeters capable of sending the measured results to smartphones using Bluetooth or Wi-Fi connection.

Such devices can be organized then into personalized health monitoring systems (Fig. 5.10) [82]. The patient fixes sensors (e.g. oximeter) on the body that communicate with a smartphone sending measurement results. The smartphone then processes the received data and monitors the patient's health. In the case of emergency, it automatically calls an ambulance or sends an SMS to the doctor with the location of the patient and the reason [82, 101].
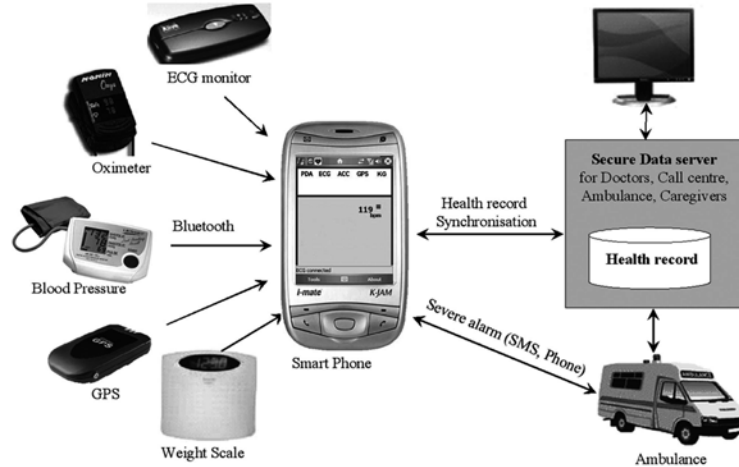
Fig. 5.10. Personalized health monitoring architecture.

There are different health and healthcare smartphone applications already available on the market for Android, Apple iOS, RIM BlackBerry, Symbian, Windows Mobile 6.x and Windows Phone 7. As an example, an EU-funded project for older people with multiple chronic conditions eCAALYX (Enhanced Complete Ambient Assisted Living Experiment) can be cited. The smartphone-based application receives data from the patient-wearable wireless health sensors and communicates over the Internet with a remote server accessible by healthcare professionals who are in charge of the remote monitoring and management of the older patient with multiple chronic conditions [102].

5.1.6 Smartphone-based photoplethysmography

Most of the current generation cellular phones are equipped with high-resolution cameras, processors and light-emitting diode flashes (LEDs). This is very similar to the PPG imaging technology and, therefore, instead of using a smartphone just as a device for storing and visualizing measured data, they can directly measure some vital characteristics. Smartphones can be used for the express-measurement of such vital characteristics as pulse rate [77, 81, 92, 103], breathing rate [104], as well as providing deeper analysis of the PPG waveform in order to extract additional data [105].

Nowadays, there are smartphone-based commercial applications such as Instant Heart Rate [106], Heart Rate Tester [107], Pulse Rate Monitor [108], Cardiograph [109], etc. that allow evaluating HR. However, while they provide a PPG-like waveform in the ideal usage conditions, they often fail when something goes wrong. Moreover, there is no comparison to the medical devices and, as reported by developers, such applications should be used for reference only but not as a medical tool.

Pelegris et al. proposed a novel method to detect heart beat rate using a mobile phone [103]. In particular, they proposed to analyse brightness information of the greyscale portion of every captured frame, while the user keeps his/her finger on the lens. To ensure reliability of acquisition, the input signal is matched to a crude heart beat pattern of alternating peaks and troughs. The results were based on the Nokia N95 smartphone, and the authors reported a performance problem of the Android-based smartphone.

Jonathan and Leahy used a Nokia E63 smartphone for pulse rate measurement, and they assessed that the green channel provides a stronger PPG signal than the red one [92, 110]. A central region of interest measuring 10×10 pixels was selected in order to compute the mean intensity value, and a Fourier transform spectral analyses was applied to evaluate the heart rate. The authors reported a possibility to detect changes in HR from rest to after exercise using their approach.

Later, in [77] an Android application was developed and the experimental tests were performed on a Motorola Droid smartphone with a comparison to medical instruments (BioZ ECG and Nonin Onyx II model 9560BT am-

bulatory finger pulse oximeter). As a result, the validity of HR smartphone measurements was confirmed.

Scully et al. [81] developed a system for physiological parameter monitoring from optical recordings with a mobile phone. The videos were obtained by a Motorola Droid smartphone, and the PPG value was computed at each frame as the 50×50 pixel average of the green channel region. The results for the heart rate were compared to the HP 78354A acquisition system using a standard 5-lead electrode configuration, and the respiration rate was compared with the metronome. In addition, the blue and red channels were used to detect the oxygen saturation and compared to the Masimo Radical SET™. The high correlation of the results was reported as well.

It is well known that PPG measurements are very sensitive to patient and/or tissue movement artefacts. The automatic detection of such motion artefacts and their separation from good quality signal is a non-trivial task [91].

However, the above research works are based on testing the specific smartphone model for each case and do not refer to the problem of movement artefacts. On the other hand, as was already noted in [111], our tests show that the distribution of the pixels in either green or blue channels is not uniform for different smartphone models, such as HTC, iPhone4, Nokia, or Samsung. The only channel that has similar characteristics is the red one, while the rest can be used to distinguish a normal usage of the system from the abnormal one, when the finger is not located properly or there is no finger at all. Moreover, we noted that the red channel information remains similar even when the smartphone was used without LED, but in a well-illuminated environment.

Therefore, the aim of this research is to develop a method that would address these two problems. In this chapter, we describe a new method, as presented in [112], to acquire the PPG waveform from a video captured by a smartphone camera. The main emphasis is placed on the development of robust algorithms suitable for different smartphone models.

The rest of the chapter is organized as follows: in Section 5.2 we show a general system overview and the acquisition scheme, Section 5.3 deals with the correct usage assessment procedure, in Section 5.4 we explain the initial system calibration, the PPG evaluation algorithm and pulse computation procedure are described in Section 5.5, while in Section 5.6 the experimental results are presented and we conclude with Section 5.7.

5.2 System Work Overview

The proposed approach utilizes an image acquisition concept similar to the one of a pulse oximeter and PPG imaging. A subject covers with his fingertip a smartphone camera lens, trying to hold the finger steady and pressing without additional force (Fig. 5.11). In this case the volumetric variation of blood

changes the light absorption that passes through a finger. Such variation of light absorption is registered by a camera, and is used for PPG evaluation.
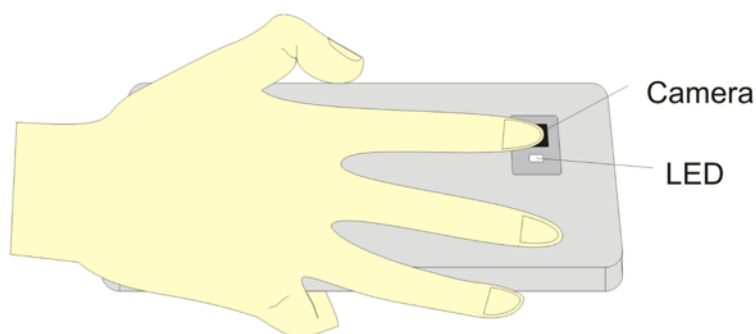
Fig. 5.11. General video capturing scheme with a smartphone equipped by LED.

The measurements are performed continuously and for each new acquired frame the change of colour values is computed. The feature of the proposed approach is that both reflection and transition modes of the system usage are possible. Therefore, to evaluate pulsations it is possible to use smartphones with a LED as well as without it in the case of good lighting conditions.

After obtaining a new frame it is verified for correctness, as shown in the flow chart of the algorithm shown in Fig. 5.12. Such verification procedure checks if the system is used in a proper mode: there is a finger in front of the camera and the illumination conditions are sufficient.

Then, there are two stages in the operation of the system: calibration and measurement. In the calibration stage the threshold value is established and the system parameters are updated while in the measurement stage the pulse rate is evaluated based on thresholding results and binary mask analysis. These two stages are explained in detail later in the appropriate sections of this chapter.

5.3 Assessment of Correct Use

When health monitoring is performed in a clinical environment, the medical staff can supervise the whole procedure and detect when it goes wrong. However, when doing self-monitoring, only the person itself can control the correctness of this process. For example, the wrong position of the fingertip on the smartphone optical sensor or its absence, finger movement during the measurement or even changing the force with which fingertip presses the lens may cause wrong results and, as a result, the program gives false alarms or misses a dangerous situation. To prevent wrong health parameter measurement, the
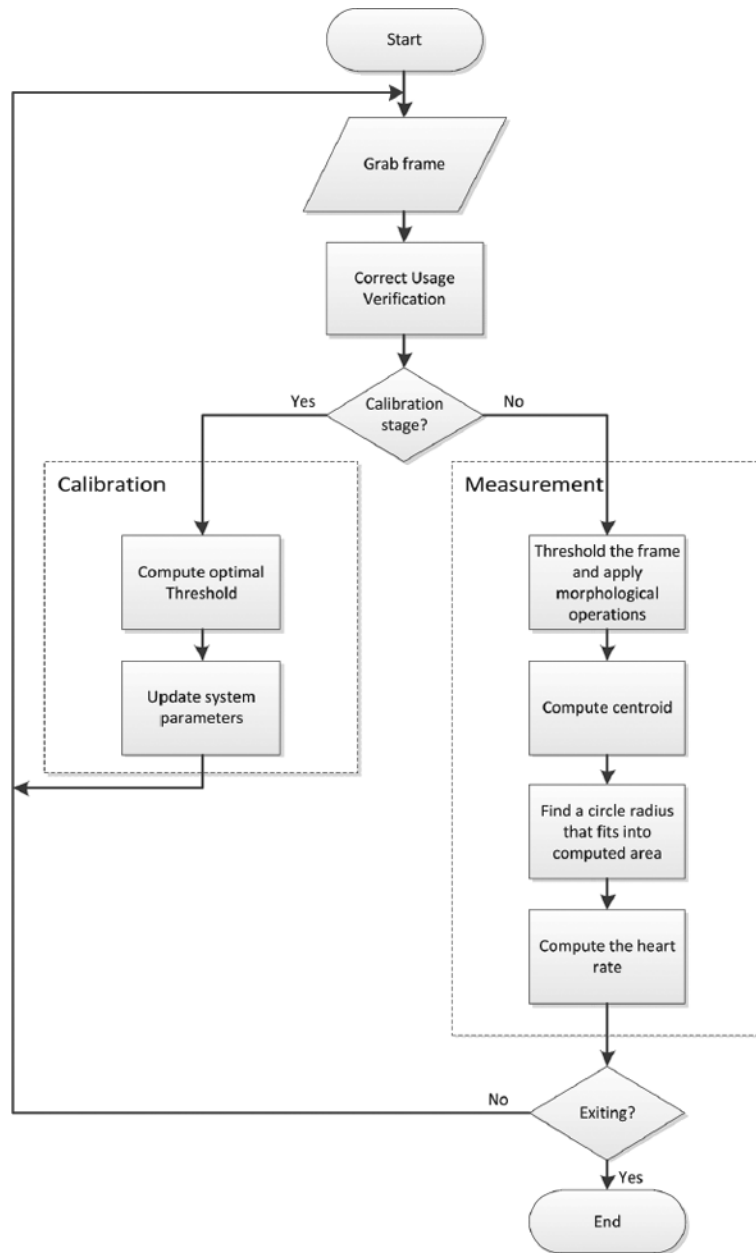
Fig. 5.12. The PPG acquisition algorithm includes: correct usage verification, calibration and measurement stages.

program automatically detects all cases of improper usage and instructs the person properly.

As it was stated previously, colour saturation of the frames, acquired from different smartphones and in different illumination conditions, varies. Fig. 5.13 shows the frames as well as the histograms of each colour channel, obtained by HTC HD2, Nokia 5800, iPhone4, HTC HD2 without LED and Samsung Galaxy S i9000 smartphones, respectively.

It was also assessed experimentally that the values of the red and green colour channels are much higher when the LED is used (i.e. in the light reflection mode) with respect to the case of light transmission. Thus, taking into account this value it is possible to automatically identify the usage mode and select appropriate system parameters.

In order to define the typical colour model of the finger image a number of experiments with different smartphone models were carried out in different conditions. Some of the results obtained are illustrated in Fig. 5.14.

The analysis of the results obtained (Fig. 5.14) permits the following conclusions:

- when the LED is used:
  - pixel values in the green and blue colour channels are concentrated in the lower half of their value range;
  - the red component values are concentrated in the top of the 0 to 255 range, and tend to the value 255.
- without using LED:
  - values of the green colour channel are very low and are close the value 0;
  - the red component values in this case has no typical range. They vary for different phone models and depend on the patient finger's tissue and the amount of light that passes through it. However, they should be higher than some minimum value $R_{NOLED_{min}}$ as will be specified later. Otherwise, the small variation of the values, which happens when the illumination is not sufficient, makes further analysis impossible;
  - the values of the blue component vary depending on the smartphone model, but in general they tend to the value 0.

Hence, taking into account the above considerations, the state of the LED can be detected by the amount of green colour in the frame.

In order to distinguish a proper usage of the system from an improper one, the following scheme was applied to each captured frame:
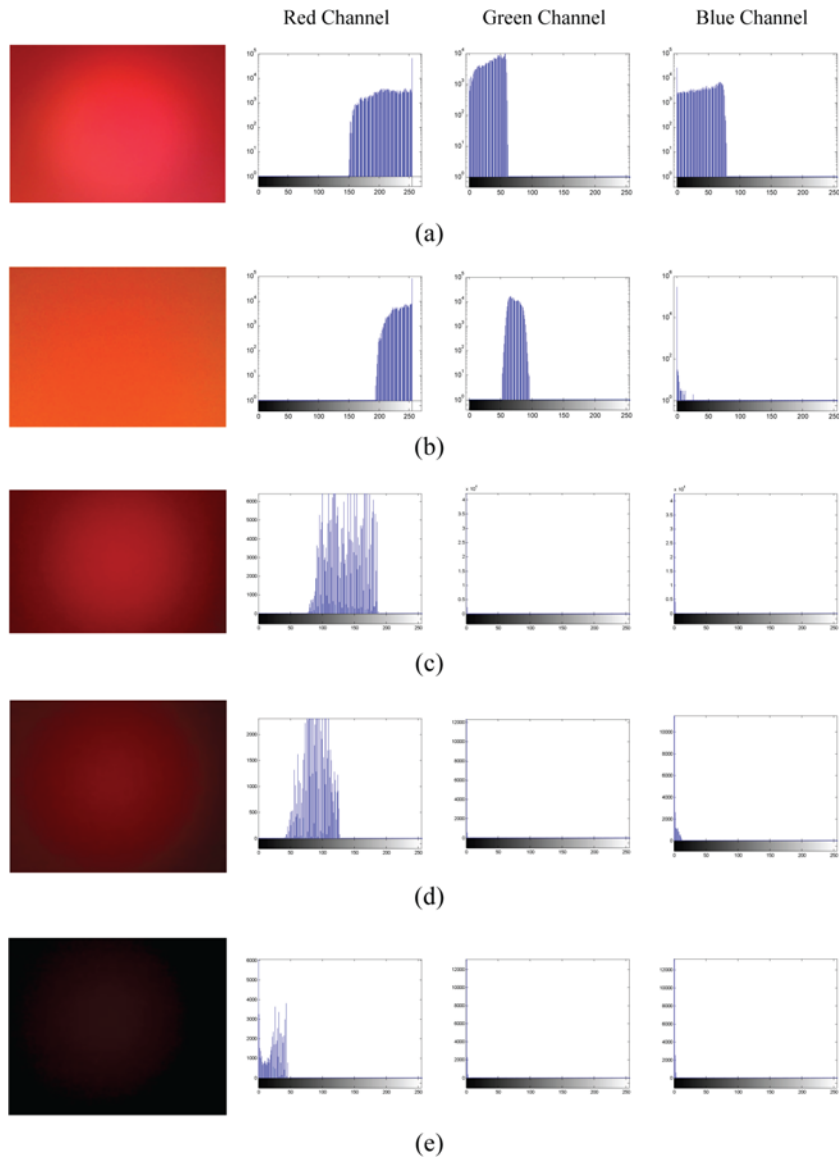
Fig. 5.13. Acquired frames and their histograms of the red, green and blue channels for different smartphones and in different lighting conditions: (a) HTC HD2 with LED, (b) Nokia 5800 with LED, (c) iPhone4 with LED, (d) HTC HD2 without LED and (e) Samsung Galaxy S i9000 without LED.
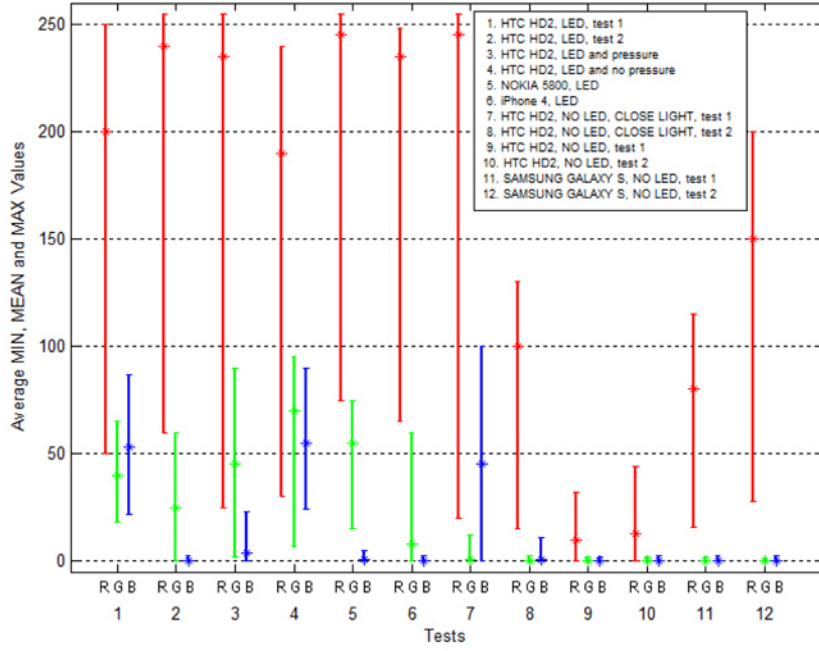
Fig. 5.14. Distribution of the MIN, MEAN and MAX values of the pixels in RGB colour space for videos captured using different smartphone cameras and under different lighting conditions.

$$
\begin{aligned}
&\% \ Colour\ ranges\ when\ using\ LED: \\
&\quad mean(G) + \sigma_G \geq G_{LED_{min}} \ AND \ \% \ Green\ must\ not\ be\ small \\
&\quad mean(R) - \sigma_R \geq R_{LED_{min}} \ AND \ \% \ Red\ should\ be\ mostly\ high \\
&\quad mean(G) + \sigma_G \geq G_{max} \ AND \\
&\quad mean(B) + \sigma_B < B_{max} \ AND \ \% \ Green\ and\ Blue\ are\ mostly\ low \\
&\quad\quad \sigma_R, \sigma_G, \sigma_B < \sigma_{max} \ \% \ Values\ should\ not\ be\ distributed \\
&\quad\quad\quad\quad \% \ too\ much
\end{aligned}
\tag{5.1}
$$

OR

$\%$ *Colour ranges without LED usage* :

$$mean(G) + \sigma_G < G_{NOLED_{max}} \ AND \ \% \ Green \ must \ be \ very \ small$$
$$mean(B) + \sigma_B < B_{max} \ AND \ \% \ Blue \ should \ be \ mostly \ low$$
$$mean(R) > R_{NOLED_{min}} \ AND \ \% \ Red \ must \ not \ be \ small$$
$$\sigma_R, \sigma_G, \sigma_B < \sigma_{max} \ \% \ Values \ should \ not \ be$$
$$\% \ distributed \ too \ much$$

$$(5.2)$$

where mean(R), mean(G) and mean(B) are the mean values of the red, green and blue components, respectively, computed for each captured frame, σ_R, σ_G, σ_B are the standard deviation values, computed for each frame and each colour channel, $G_{LED_{min}}$ and $R_{LED_{min}}$ are the minimum values of the green and red channel, correspondingly, in the case the LED is used, G_{max} and B_{max} are the maximum values of the green and blue channels, respectively, σ_{max} is the maximum standard deviation among all colour channels, $G_{NOLED_{max}}$ is the maximum value of the green channel in the case the LED is not used, $R_{NOLED_{min}}$ is the minimum value of the red channel in the case the LED is not used.

The above scheme describes a proper colour cluster in the RBG colour space of the finger image. For the calibration stage the threshold values in (5.1) and (5.2) are defined based on the analysis of the preliminary experimental results. Thus, they are: $G_{LED_{min}} = 10$, $R_{LED_{min}} = 128$, $G_{max} = 128$, $B_{max} = 128$, $\sigma_{max} = 40$, $G_{NOLED_{max}} = 10$, $R_{NOLED_{min}} = 10$, and are used to make sure that the finger is placed on the camera correctly. Such thresholds are valid for different models and used to define if initially the smartphone was used correctly. For the measurement phase, however, the threshold values are updated on the basis of the chromatic parameters of the acquired frames during the calibration stage. This is done to limit the possible colour cluster to the characteristics of the current smartphone model, person's tissue and lighting conditions.

The validation step of the correct use is essential for further algorithm execution and quality assessment of the results, especially in the case of health monitoring systems. For the frames with no finger or with a finger in the wrong position, the colour distribution in the channels does not fit defined rules, but it is spread out over the whole value range. Therefore, the proposed model allows considering only the case of finger presence, and, as a result, permits validating the correct use.

5.4 Initial System Calibration

As mentioned earlier, the system calibration step is used to adapt the system configuration to the particular smartphone camera and lighting conditions, as well as to the personal characteristics of the finger tissue (skin colour, opacity, etc.). There are a few factors that must be taken into account to do that:

  (i) different smartphone models lead to different colour saturation in the cap-
       tured frames;
 (ii) different fingertip pressure force on the camera lens as well as different
       features of the tissue change the level of light absorption when it passes
       through the finger and, therefore, cause different colour ratios;
(iii) shifting the finger with respect to the camera lens creates motion artefacts
       and, as a result, causes wrong segmentation.

Considering the above cases it is clear that a fixed threshold value is not
suitable. To compute the PPG signal it is possible to threshold the red compo-
nents for each frame obtained and compute the number of pixels that surpass
the threshold, as was proposed in [111]. The threshold T was established as
95% of the range between the min and max values during the first 5s of
system operation. That is:

$$T = \overline{max}(I) - \frac{1}{20}(\overline{max}(I) - \overline{min}(I)), \tag{5.3}$$

where $\overline{max}(I)$ and $\overline{min}(I)$ are the mean maximum and minimum values,
respectively, of the red component for the acquired frames during the first 5s.

It was confirmed also that acquiring at least three full pulsations is enough,
and the number of captured frames is suitable to perform statistical analy-
sis. Such algorithm is reliable and works fine in the case the LED is used.
However, if the system works without the LED the range between the min
and max values is small and the number of computed pixels is not enough
to make robust measurements. Moreover, it may occur that for some frames
the maximum pixel value is lower than the established threshold, and the
segmentation does not provide the expected result.

Hence, it was proposed to calculate the T as a mean of such values T_i,
computed during the calibration step, at which the number of pixels in the
corresponding thresholded image occupy more than $\theta\%$ of the frame:

$$T = mean(T_i), T_i : \frac{\|val(P_i) \geq T_i\|}{\|P_i\|} = \theta\%, i = 1, ..., N, \tag{5.4}$$

where T_i is the computed threshold for frame i, P_i is the array of red com-
ponent pixels of the frame i, $val(P_i)$ is the value of each pixel in P_i, $\|\ldots\|$
is the number of pixels in the array, and N is the number of frames for the
calibration stage.

Since the finger is not fixed on the camera lens, it can shift during the mea-
surement changing its position as well as its pressure on the lens. Therefore,
it is necessary to ensure that the area, which surpasses the established thresh-
old, always fits the image boundaries. Otherwise, the measurement would be
incorrect. It was noted also that the pulsating dynamics (i.e. the difference
between smallest and largest radiuses) is more for the pixels with high colour
values. It means that the final result is better if the threshold is high (closer
to the max value of the pixels). In this work a value of $\theta = 20$ is used.

Fig. 5.15 shows examples of the thresholded image according to (5.4), captured from different smartphones and in different lighting conditions.
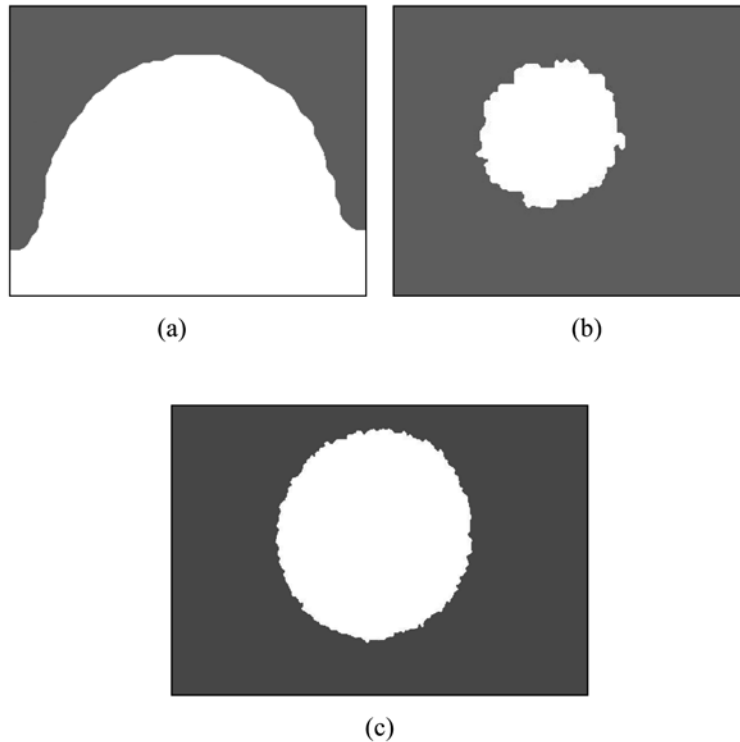
Fig. 5.15. Computed masks that satisfy the threshold on the frames, captured (a) from HTC HD2 with LED, (b) HTC HD2 without LED, and (c) Samsung Galaxy S i9000 without LED.

As can be seen from Fig. 5.15a, the thresholded area contains some artefacts, caused by the close position of the LED and, as a result, high illumination of the pixels. The next section explains how to eliminate such artefacts and extract the proper PPG value.

5.5 PPG Evaluation Algorithm

As discussed previously, only the red component is suitable for PPG measurement since the figure shape remains similar for any smartphone model and any lighting conditions. Normally it has the shape of a paraboloid (Fig. 5.16) with the maximum pixel value in the centre.

The shape of the thresholded binary mask depends on how the smartphone is used. Using a smartphone with a LED or specific finger position on
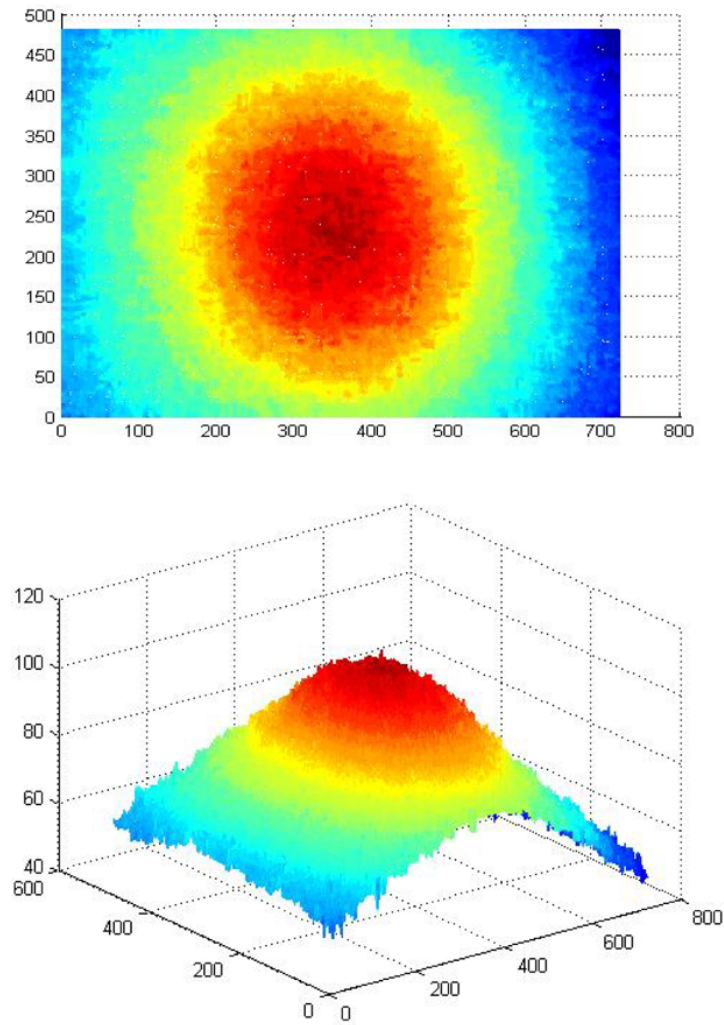
Fig. 5.16. The pixels intensity and the surface of the red component for the frame captured from the Samsung Galaxy S i9000 smartphone.

the camera this shape can change. As was already mentioned, the mask in Fig. 5.15a does not have a circular shape because the frame is acquired with the LED on, and some parts of the finger are better illuminated. Thus, a simple calculation of the number of pixels, as proposed in [111], cannot take into account the above factors.

To overcome this limit, we propose finding the circle that better fits the thresholded image, and use its radius as the PPG value. In particular, for each captured frame, we first calculate the coordinates C_x and C_y of a centroid of

the binary mask as:

$$C_x = \frac{\sum\limits_{n} x_n}{n}, C_y = \frac{\sum\limits_{n} y_n}{n}, \tag{5.5}$$

where x_n and y_n are the coordinates of each pixel with a value 1 on a binary mask, and n is the total number of such values.

Then, the radius of the circle with the centre in the centroid is considered as a photoplethysmogram value (Fig. 5.17).
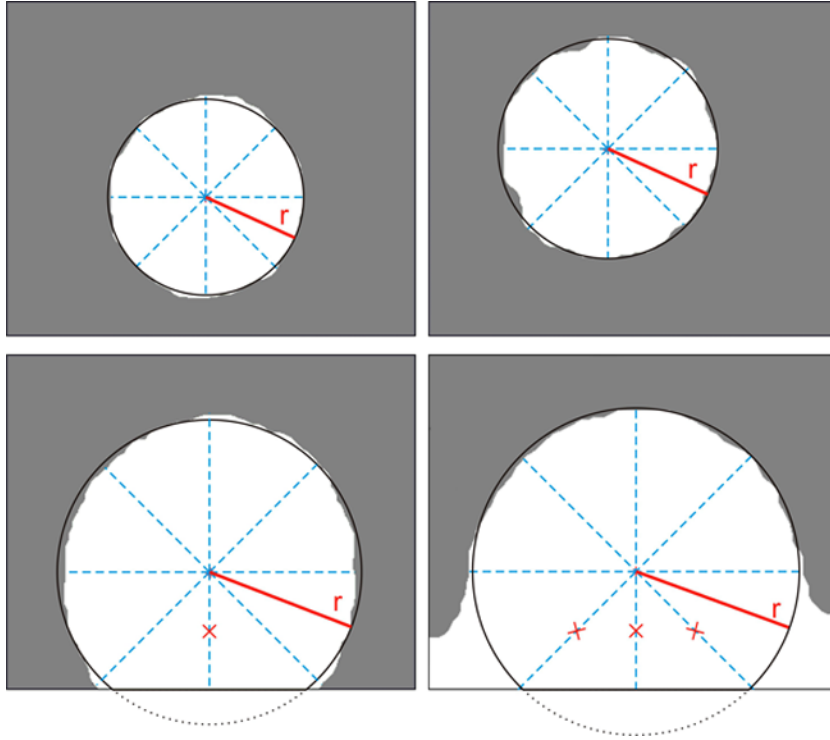
Fig. 5.17. Computing the PPG value: white is a thresholded area; dashed lines are the distances from the centroid to the boundaries; crossed out lines are the lines that do not have a boundary on the image and should be skipped; solid bold lines are the radiuses, computed as average values of the above distances, solid lines - circles inscribed into the figures with radiuses r; dotted lines are the parts of the circle that do not fit the picture.

Normally, the Hough transform can be applied to find the circles. However, such approach requires significant computational resources and also does not work well in the case of non-smooth boundaries. Since the computational complexity is important, it was proposed to compute the radius as follows (Fig. 5.17):

1. find distance from the centroid to the boundary at positions 0°, 45°, 90°, 135°, 180°, 225°, 270°, 315°;
2. if the length exceeds the distance to the image boundaries, ignore this value;
3. find the mean value for all the remaining distances, and use it as the radius of a circle.

In this case, even if the circle does not fit the image completely because of shifted centre, the radius will still be computed properly.

Computing the radius as described above for a sequence of captured frames gives a photoplethysmogram, where each cardiac cycle appears as a peak. Such waveform is generally referred to as the inverted PPG (Fig. 5.18) [113], as the camera corresponds to the received rather than absorbed light intensity [99]. Thus, the final PPG signal is inverted vertically to be used for further processing.
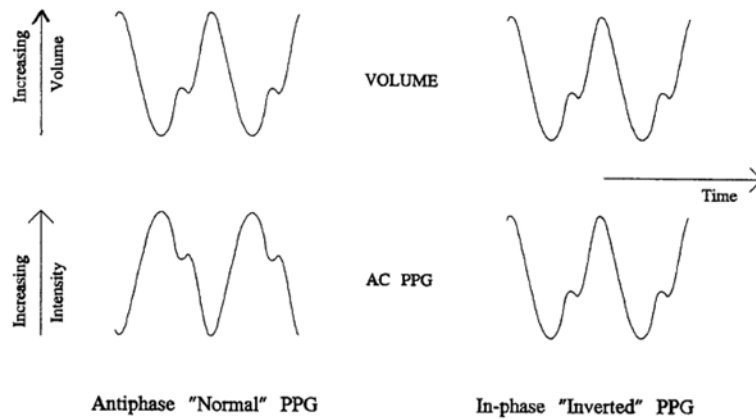
Fig. 5.18. "Normal" and "inverted" PPG waveforms.

Recovering the PR from such a PPG signal can be done by passing the computed waveform with a 10s moving window and applying the Fourier transformation to each of the windows. The maximal peak on the spectrum near the frequency of 1Hz corresponds to the pulse rate frequency [104].

Fig. 5.19 shows an example of computed PPG, inverted and normalized from 0 to 100, and the corresponding Fourier spectrum. The PPG signal itself is unfiltered. As it can be seen from Fig. 5.19b, the evaluated PR is equal to 1.081 Hz and corresponds to about 65 beats per minute (bpm).
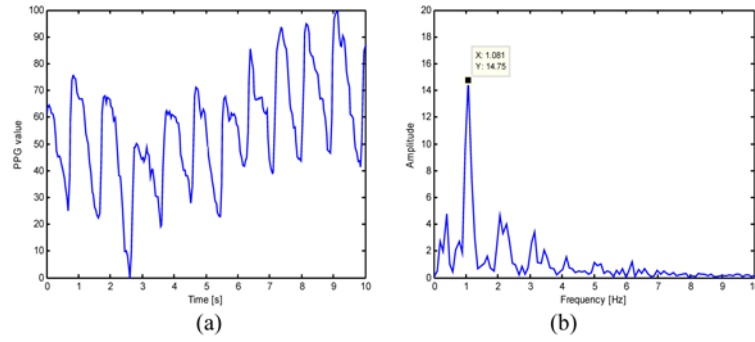
Fig. 5.19. Measured PPG during a time interval of 10s (a), and a corresponding Fourier spectrum. The evaluated value of PR is equal to 1.081 Hz (about 65 bpm) (b).

5.6 Experimental Results

The experimental tests were carried out using different smartphone models, in particular HTC HD2, iPhone4, Nokia 5800, Samsung Galaxy S i9000. Table 5.1 shows their specifications such as version of the operating system, presence of the LED, frames resolution and capturing frequency.

Videos from the smartphones were transferred to a computer, processed and compared to the data obtained from an oximeter. Further processing was done in Visual Studio C++ using the OpenCV library.

Table 5.1. Specification of the smartphones used for experiments

Device name	Operating System	LED	Video resolution (pixels)	Frequency (fps)
HTC HD2	Windows Mobile 6.5	yes	352×288	25
Nokia 5800	Symbian OS v9.4	yes	640×480	29
Apple iPhone 4	iOS 4	yes	480×272	30
Samsung Galaxy S	Android OS, v2.3	no	720×480	30

First, the system was tested to recognize the wrong usage cases. Therefore, a number of videos were captured with a finger positioned properly, and in a wrong mode. In particular, Fig. 5.20a and 5.20b show examples and statistical values of the colour components when the finger was positioned properly, while Fig. 5.20c and 5.20d show the cases with no full contact between the finger and the phone camera.

Other examples of wrong usage, when the finger did not cover the entire camera lens or even was not on the camera at all are shown in Fig. 5.20e and 5.20f, respectively. In general, the proposed verification scheme allowed proper recognition of more than 98% wrong usage cases.
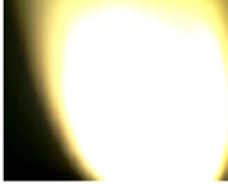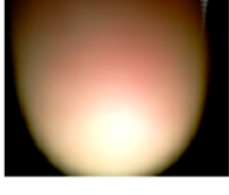
Image	Statistical Data	Accepted
(a)	$mean(R) = 244.72,$ $\sigma_R = 16.65,$ $mean(G) = 26.51,$ $\sigma_G = 4.54,$ $mean(B) = 6.00,$ $\sigma_B = 9.52$	YES
(b)	$mean(R) = 144.35,$ $\sigma_R = 27.37,$ $mean(G) = 0.27,$ $\sigma_R = 0.46,$ $mean(B) = 0.25,$ $\sigma_R = 0.46$	YES
(c)	$mean(R) = 167.53,$ $\sigma_R = 50.08,$ $mean(G) = 49.14,$ $\sigma_G = 29.64,$ $mean(B) = 11.03,$ $\sigma_B = 15.79$	NO
(d)	$mean(R) = 242.34,$ $\sigma_R = 27.18,$ $mean(G) = 166.09,$ $\sigma_R = 47.01,$ $mean(B) = 114.41,$ $\sigma_R = 35.98$	NO
(e)	$mean(R) = 207.04,$ $\sigma_R = 90.07,$ $mean(G) = 205.01,$ $\sigma_R = 89.02,$ $mean(B) = 184.03,$ $\sigma_R = 97.12$	NO
(f)	$mean(R) = 134.04,$ $\sigma_R = 90.38,$ $mean(G) = 109.25,$ $\sigma_G = 80.13,$ $mean(B) = 77.11,$ $\sigma_B = 74.22$	NO

Fig. 5.20. Accepted frames (a) and (b), frames recognized by the system as wrong because of not enough pressure of the finger (c), (d), wrong position on the camera (e), and missing of the contact between finger and camera (f).

Then, to evaluate the accuracy of pulse measurements, the PPG waveforms were obtained simultaneously by the smartphone and the CMS50DL Finger Pulse Oximeter SPO2 Monitor using two fingers of the left hand. Ten subjects participated in the test, going from 26 to 60 years of age. The PPG waveforms obtained by the smartphone were then inverted and normalized from 0 to 100 as explained before for further comparison.

As can be seen from Fig. 5.21, which shows the two signals obtained by the smartphone and the oximeter in the normal subject state in the same time period, the peaks and the valleys correspond on both PPGs.
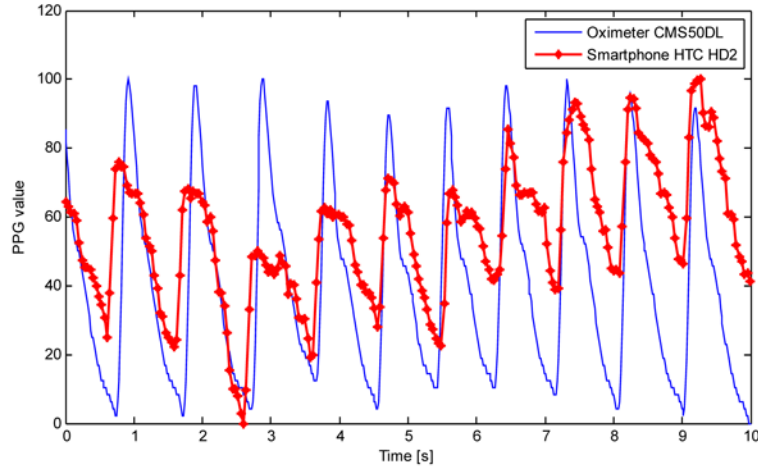
Fig. 5.21. Comparison between the photoplethysmograms obtained by the HTC HD2 smartphone and the oximeter. The peaks and the valleys of both signals correspond.

To prove the suitability and the correctness of the proposed method, the above test was repeated again just after squatting for 60s. In this case the pulse rate changed because of the physical activity. As it is shown in Fig. 5.22, the PPG evaluated by the smartphone shows more rapid pulsations and also corresponds to the one from oximeter.

Table 5.2 shows the summary of the tests where the mean PR and standard deviation value were computed for several measurements, performed with the HTC HD2 smartphone using LED and the CMS50DL Finger Pulse Oximeter SPO2 Monitor at respective time periods. The signals were acquired for 60 s and the number of pulsations per minute was computed by applying the Fourier transform to a previous 10 s period.

Then, the mean and standard deviation values were computed. The same tests were performed using other smartphones and the results are shown in Fig. 5.23. They confirm that the PPGs obtained from the smartphones are
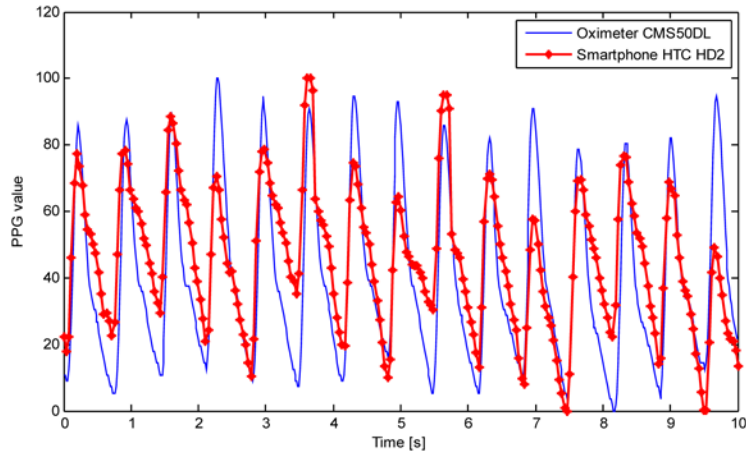
Fig. 5.22. Comparison between the photoplethysmograms obtained by the HTC HD2 smartphone and the oximeter after squatting for 60 s. Also in this case the peaks and the valleys of both signals are highly correlated.

Table 5.2. Comparison between the PR evaluated from the HTC HD2 using LED and the CMS50DL Finger Pulse Oximeter SPO2 Monitor

Test No.	Mean PR from smartphone (bpm)	Mean PR from oximeter (bpm)	Error (%)
Video 1, before squatting	61.46 ± 1.48	62.07 ± 1.34	0.98
Video 2, after squatting	790.15 ± 4.6	91.58 ± 3.29	1.56
Video 3, before squatting	79.42 ± 3.23	79.80 ± 3.14	0.48
Video 4, after squatting	98.86 ± 12.15	97.79 ± 11.17	1.09
Average Error			**1.03**

highly correlated to those obtained by a finger pulse oximeter and, therefore, can be used for PR measurements.

5.7 Conclusions

This chapter is devoted to the photoplethysmogram measurement by means of a smartphone and integrated camera. Prior work has reported the possibility of smartphone usage for pulse rate measurement. The successful application of the green colour component for PPG signal computing was reported.

However, such reports involved a limited number of smartphones and further research has shown that the typical colour range varies from model to model. In particular, it has been shown in this chapter that only the red channel has similar characteristics for different models of smartphones while the green and blue may vary dramatically. Although the last two components do
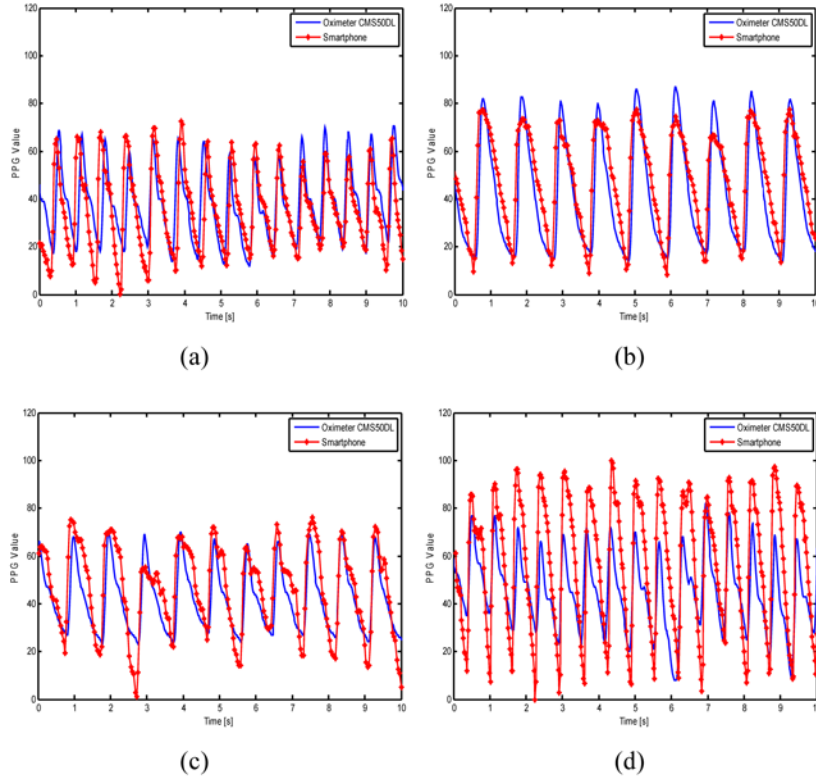
Fig. 5.23. PPG waveforms obtained from (a) Nokia 5800 with the LED enabled, (b) iPhone4 with LED, (c) HTC HD2 without LED, (d) Samsung Galaxy S i9000 without LED, and the corresponding waveform, acquired from a CMS50DL Finger Pulse Oximeter SPO2 Monitor.

not have a fixed colour range, they can be used to detect a wrong usage of the system.

The proposed PPG evaluation method is suitable to work in both reflection and transmission modes, and allows evaluating the PPG when the LED is not used. The appropriate algorithms for the correct usage verification procedure and the initial system calibration were proposed and tested. In addition, an improved PPG value calculation algorithm was proposed.

The experimental tests were carried out with smartphone models such as the HTC HD2, iPhone4, Samsung Galaxy S i9000 and Nokia 5800. Devices, equipped with LED were tested in two modes: when the LED was enabled and disabled. A total of 10 persons aged between 26 and 60 years took part in the experiments. The obtained results were compared to the CMS50DL Finger Pulse Oximeter SPO2 Monitor. The pulse rates obtained as well as the signals themselves were comparable between all the devices. Thus, it confirms

the correctness and reliability of the proposed PPG calculation technique with respect to medical pulse measurement instruments.

In the next chapter the advanced method of pulse rate evaluation is presented.

6

Reliable Pulse Rate Evaluation

After introducing in the previous chapter the possibility of smartphone usage for acquisition of the photoplethysmographic signal, this chapter presents the robust and reliable method for pulse rate evaluation using a smartphone. The smartphone camera is used to evaluate the volumetric variation of blood by monitoring the change of light absorption in the tissue. Once assessed the correct working operation, the photoplethysmographic signal is detected and the pulse rate is evaluated on the basis of adaptive and statistical analysis. To validate the pointed out method, the evaluated by smartphone pulse rate was compared with the Ambulatory Blood Pressure monitor Spacelabs 90207, which is clinically validated medical device. The experimental results confirm the correctness and suitability of the proposed method.

6.1 Introduction

As stated in Chapter 5, the PR can be evaluated from PPG signal. PPG refers to monitoring of time varying changes in the intensity of light scattered from the tissue in vivo [105, 113]. A smartphone camera was found suitable to acquire the PPG signal in reflection mode, using the LED as light source. A subject fixed his/her finger on the smartphone camera as explained in Section 5.2 (Fig. 5.11) and for each obtained frame the level of light absorption that passes through pulsating capillary tissue is calculated. The volumetric variation of blood changes the light absorption allowing the PPG evaluation.

The PR is usually evaluated by frequency domain analysis of the PPG signal and by detecting the frequency of the tone with maximum amplitude. The reliability of this method depends on the monitoring time: if just a few pulses are acquired the PR evaluation is misstated.

In [77] the problem of the validation of the PR monitoring application was taken into consideration. The results obtained by the Motorola Droid Libertyville were found correlated with the ones derived from electrocardiograph and Nonin 9560BT pulse oximeter.

In [112], the aspects concerning with the experimental conditions that strongly influence the reliability of the results are taken into consideration and the proper method is pointed out to address the inconvenient due to (i) heterogeneous characteristics of different cameras, (ii) changes in chromatic and geometrical features of the frame if the LED is used, and (iii) wrong finger location on the smartphone camera.

In this chapter, other aspects concerning the robust evaluation of the PR are investigated. The new method [114], based on the adaptive analysis of the time intervals between two consecutive pulses and statistical evaluation of the PR final value, is presented. Such analysis allows reducing the alteration effects introduced by variations of (i) the finger strength on the camera, and (ii) light conditions.

The combination of the method pointed out in [112] and the one, proposed in this chapter, overcomes the inconveniences of the solutions available in the literature, and makes complete the investigation about the reliable evaluation of the PR by smartphone. Its validation is performed by comparing the PR obtained by different smartphone models, with the Ambulatory Blood Pressure monitor (ABP) Spacelabs 90207 [84]. This is clinically validated medical device [85, 86, 87] according to the protocols of the Association for the Advancement of Medical Instruments (AAMI) [88], American Heart Association (AHA) [89], and British Hypertension Society (BHS) [90].

The rest of the chapter is organized as follows. Section 6.2 presents the PR evaluation method, Section 6.3 deals with the procedure to validate the proposed method and the experimental results, while Section 6.4 concludes.

6.2 Pulse Rate Evaluation

The PR is evaluated according to the block scheme of Fig. 6.1. Each pulse in the PPG signal is constituted by two physiological peaks (Fig. 6.2): the bigger one due to the heart pulse and the smaller one due to the venous pulse [91].

To evaluate the PR only the heart peaks must be considered [91]. To this aim, a proper threshold (Th) is established. On the basis of preliminary experimental results, it can be assessed that the venous peak is always lower than 1/10 of the heart peak. Nevertheless, in order to adapt the threshold to the variation characteristics of the PPG signal, the Th is established in the adaptive manner, as:

$$Th = \begin{cases} \sigma(PPG), & \sigma(PPG) > 10 \\ 10, & \sigma(PPG) \leq 10 \end{cases}, \qquad (6.1)$$

where $\sigma(PPG)$ is the standard deviation of the PPG signal.

Once established Th, the Peak Detector Algorithm (PDA) is applied [115, 116]. It receives the PPG signal and Th in the input, and works as follows:

(i) fits the quadratic polynomial in the PPG signal;
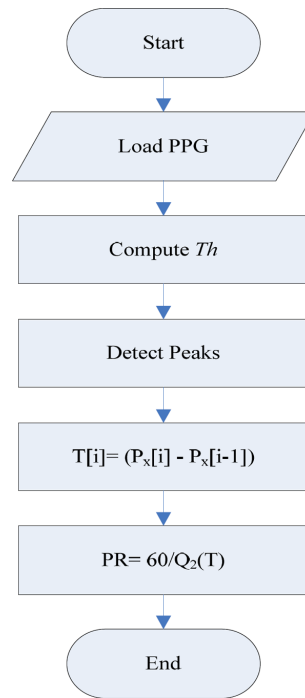
Fig. 6.1. Block scheme of the method to evaluate the PR.
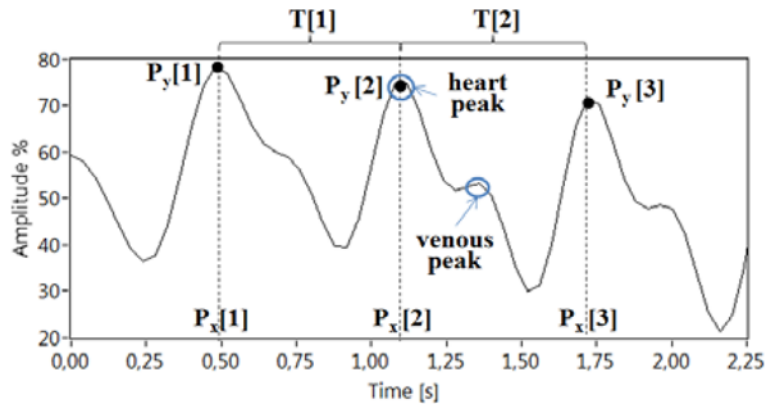
Fig. 6.2. Evaluation of the peak coordinates from to the PPG signal.

(ii) detects the peaks as relative maximum;
(iii) ignores the peak with amplitude lower than Th;
(iv) evaluates the coordinates (x, y) of each peak (Fig. 6.2);
(v)   returns the peak coordinates in two vectors, $P_x[i]$ and $P_y[i]$ respectively.

The collection of the time intervals between two successive peaks, stored in the vector $T[i]$, is evaluated as:

$$T[i] = (P_x[i] - P_x[i-1]). \tag{6.2}$$

The PR is computed as the ratio between the 60 and the 2nd quartile of T:

$$PR = \frac{60}{Q_2(T)}. \tag{6.3}$$

In addition, the $60/Q_1[T]$ and the $60/Q_3[T]$ indicate the variation range of the PR value.

6.3 Experimental Validation of the PR Evaluation Method

In order to validate the proposed method, the PR is evaluated at the same time by smartphone and ABP [84]. Because the ABP monitoring requires to occlude the artery, that changes normal blood flow in fingers, in the tests ABP is used on the left arm, and the smartphone on the right hand, as shown in Fig. 6.3.

Fig. 6.3. Positioning of the ABP and the smartphone for simultaneous PR evaluation.

The smartphones, used in the tests, are equipped by different camera. They are:

- HTC HD2, video resolution 288x352 pixels, sampling frequency 25 fps, equipped by LED.
- Samsung Galaxy S I9000, video resolution 480x720 pixels, sampling frequency 30 fps, not equipped by LED.

In the tests, the video including one or more frames acquired in non-correct working operation were rejected. The automatic video evaluation is performed according to the procedure described in the Chapter 5.

The tests are performed on 10 subjects, from 27 to 60 years old. The monitoring time is equal to 6s.

Table 6.1 shows some experimental results, obtained by different smartphones and different subjects. If the PR is evaluated by frequency domain analysis of the PPG signal, observed for 20s, the values are not compatible with the ones of the ABP. In the case the proposed method is used, the maximum error is equal to 2 pulses per minute. This result is fully compatible with the accuracy ± 2 PR declared by the ABP data sheet [84].

Table 6.1. Comparison among PR evaluated by smartphones and ABP.

No. Exp	Smartphone model	LED	Frequency domain analysis, ppm	Q_1 ppm	Q_2 ppm	Q_3 ppm	ABP ppm
1	HTC HD2	Yes	128	53.5	55.7	58.9	55
2	HTC HD2	No	140	57.4	60.1	64.8	60
3	Samsung Galaxy S I9000	No	135	58.7	60.8	67.7	60
4	Samsung Galaxy S I9000	No	134	61.7	66.3	81.3	67
5	HTC HD2	Yes	168	55.3	66.9	87.4	69
6	HTC HD2	No	143	59.2	65.2	70.2	66
7	Samsung Galaxy S I9000	No	132	47.8	72.4	95.8	72
8	Samsung Galaxy S I9000	No	145	68.7	72.7	76.9	74
9	HTC HD2	Yes	123	57.4	63.8	71.6	63
10	HTC HD2	No	126	54.1	59.2	64.1	59
11	Samsung Galaxy S I9000	No	120	53.0	62.8	81.6	60
12	HTC HD2	Yes	123	59.9	62.6	65.3	64
13	Samsung Galaxy S I9000	No	120	58.1	60.3	63.5	61
14	HTC HD2	Yes	156	51.3	54.7	61.9	54
15	HTC HD2	No	165	53.4	54.9	56.9	55
16	HTC HD2	Yes	170	72.3	77.4	85.4	78
17	HTC HD2	No	150	70.9	74.5	78.4	75

6.4 Conclusions

This chapter describes a new method to evaluate the Pulse Rate using a smartphone camera. The novelties are:

 (i) evaluation of the PR on the basis of the time interval between two consecutive PPG peaks that allows the fast and reliable evaluation of PR;
 (ii) evaluation of the adaptive threshold to detect the peak by taking into account the standard deviation of the PPG that allows to adapt the threshold to the actual characteristics of the PPG;
(iii) statistical analysis of the collected time intervals that allows to reject outliers.

The proposed method makes reliable the evaluation of the PR by different smartphones with respect to the: (i) heterogeneous characteristics of the cameras, (ii) changing of the chromatic and geometrical features of the frame if the LED is used, and (iii) wrong finger position on the smartphone.

The proposed algorithm is validated respect to Ambulatory Blood Pressure Systems Spacelabs 90207. The experimental results confirm the correctness, suitability and reliability of the proposed technique.

7

Continuous Blood Pressure Estimation

Besides acquisition of the photoplethysmographic signal and evaluation of the pulse rate, as described in previous sections, more vital parameters can be extracted from the acquired signal. For example, there is a relation, not always linear, between the blood pressure and the pulse duration, obtained from photoplethysmographic signal. In order to overcome such non-linearity and estimate the blood pressure from the PPG signal, in this chapter the Artificial Neural Networks (ANNs) are used. Training data were extracted from the Multiparameter Intelligent Monitoring in Intensive Care waveform database for better representation of possible pulse and pressure variation. In total there were analysed more than 15000 heartbeats and 21 parameters were extracted from each of them that define the input vector for the ANN. The comparison between estimated and reference values shows better accuracy than the linear regression method and satisfy the American National Standards of the Association for the Advancement of Medical Instrumentation.

7.1 Introduction

Blood pressure is the pressure of the blood flowing through the blood vessels against the vessel walls [117]. It must be monitored regularly to prevent hypertension cases and, as a result, strokes, myocardial infarction or heart failure. As example, the number of persons suffering of cardiovascular problems is very high and is increasing particularly in the most developed countries. In particular, the arterial hypertension does not cause immediate symptoms but it can provoke harms to the cardiovascular system over medium/long-term periods of the human life bringing to ictuses or heartbreaks [118]. The World Heart Organization (WHO) reports that more than 600 millions of people worldwide suffer of hypertension causing 7 millions of deaths a year [119].

Measuring the BP means obtaining the highest (or systolic BP - SBP) and the lowest (or diastolic BP - DBP) pressures during a cardiac cycle. It depends on the quantity of blood flow and the resistance of the blood vessels to this

flow. Each time the heart beats, a surge of blood is pumped from the heart into the arteries increasing the pressure in the arteries. The systolic blood pressure is the pressure of the blood against the artery walls when the heart contracts and the diastolic blood pressure is the pressure against the artery walls when the heart relaxes between beats [117].

The blood pressure may be measured using direct or indirect techniques. Direct measurement is the invasive one and implies the use of catheter. Such method give the best results, however, requires intrusion into aorta. The non-invasive (indirect) methods use different techniques such a Korotkoff-based with the usage of a cuff and stethoscope [120] or oscillometric ones [121].

The BP measurement using a Korotkoff's technique means wrapping a cuff around the upper arm of the patient and inflating the cuff. This cuts off the blood stream through the brachial artery. The physician listens with a stethoscope to the sounds in the brachial artery, which are created by the blood stream that is restored due to the deflation of the cuff (see Fig. 7.1) [122].
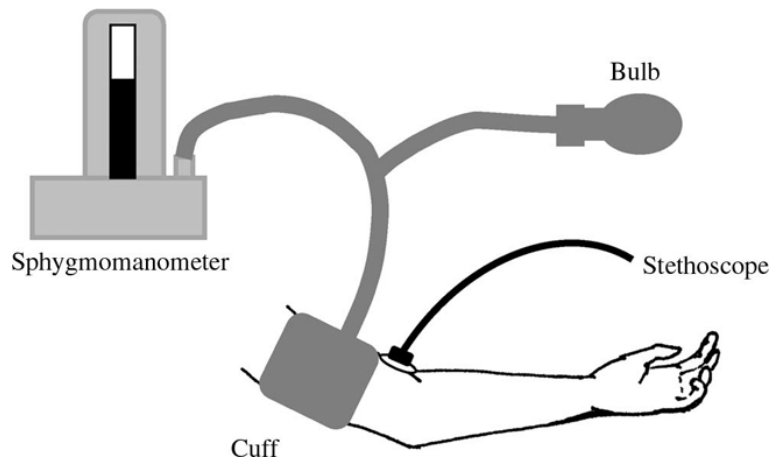
Fig. 7.1. Korotkoff blood-pressure measurement method.

However, the problem of this method is that the physician must be trained to make such a measurement and also the moments when he starts and stops hearing the sounds depend from a lot of factors. The most important one is the physician's hearing.

Alternatively, the Ambulatory Blood Pressure (ABP) monitoring devices (see Fig. 5.2) are used for non-invasive examination of the blood pressure. However, besides they are expensive, the use of the cuff often causes under-estimation of systolic BP, false readings caused by improper cuff size, and patient discomfort [123]. In addition, there are different techniques and algorithms to compute the BP by such ABP that causes criticism [122] and low accuracy.

Previous study has reported that the pulse transit time (PTT) [124, 125, 126, 127], pulse arrival time (PAT) [128] and pulse wave velocity (PWV) [129] can be used for continuous, non-invasive, and cuff-less BP estimation. It is based on the assumption that the pressure waves propagate through the arteries at a certain speed and there is a linear correlation between this speed and the BP [128]. The BP is obtained by measuring the time between the peak in electrocardiogram and a particular point in the photoplethysmogram signal (for PTT, PAT), or between such points in two PPG signals, acquired simultaneously from two sensors fixed on a known distance (PWV). However, besides the usage of two devices, these methods require a calibration stage. Moreover, another problem is that the pressure wave speed in arteries is individual for every person.

The idea to use a single PPG signal for BP estimation was investigated in [130, 131, 118]. In particular, authors also reported a linear correlation between the BP and heartbeat duration, calculated from the PPG signal. As example, the systolic upstroke time, diastolic time as well as width of 2/3 and 1/2 pulse amplitude were considered as the possible parameters and the diastolic time was stated as the more correlated to the BP.

Tests show that the higher BP the shorter is the duration of every heartbeat. However, more tests with different signals show that such correlation is not always linear. For example, the diastolic time doesn't definitely represent the blood pressure and different people with the same diastolic time may have different BP. Moreover, most of the authors [123, 124, 125, 126, 127, 128, 129, 130, 131, 118] provide their own, always different, coefficients that allow estimating the BP with high probability for a specific test set only, normally obtained from healthy people. For another input data such coefficients mush be adjusted.

In order to overcome the above mentioned drawbacks, in this chapter is presented a new approach to non-invasive continuous blood pressure estimation based on Artificial Neural Networks (ANN) [132]. ANN are widely used to model complex relationships between inputs and outputs or to find patterns in data [133, 134]. In [127] was reported better performance of ANNs with respect to the regression analysis for blood pressure estimation using the PTT. In this work, additional input parameters are taken into consideration respect to [127] in order to achieve better performance using only the PPG signal. To get a wide representation of possible PPG signals and correspondent BP, the signal from Multiparameter Intelligent Monitoring in Intensive Care (MIMIC) database [135] were extracted for ANN training.

The rest of the chapter is organized as follows: Section 7.2 explains the parameters extracted from the PPG signal, in Section 7.3 the architecture of the ANN is presented and discussed, Section 7.4 gives the general overview of the MIMIC database, while Section 7.5 shows the experimental results and Section 7.6 concludes.

7.2 Pulse Parameters Extraction from PPG

The PPG signal is characterized by the amplitude of the signal and duration of specific components of the cardiac cycle. Due to the moving artefacts during a PPG signal acquisition, the pulse height may vary significantly and, therefore, cannot be used as a parameter for BP estimation.

On the other hand, the acquisition frequency of oximeters or other devices that provide the PPG signal [112, 114] varies as well as varies the duration of individual heartbeat. That means that every single heartbeat is represented with a different number of sampled values, that can't be the ANN input because the number of input neurons is fixed during the use of the ANN architecture and can't be changed. Therefore, another solution must be found.

Several parameters could be used in order to characterize the PPG pulsatile component. Besides the Systolic upstroke Time (ST), Diastolic Time (DT), width of 2/3 and 1/2 pulse amplitude, mentioned in [130], the pulse height, cardiac period and peak width at 10% of the pulse height are used in [96] (see Fig. 5.7).

In order to extract as much information as possible and then to investigate the best combination of the parameters, additional data are considered. In particular, it is proposed to calculate the width also at 25%, 33% and 75% of the pulse height and extract separate value for the systolic part (i.e. in the interval from minimal to the maximal point) and for diastolic part (from the maximal to the next minimal point).

The following 21 parameters, including the times of systolic, diastolic parts and ratio between them, are extracted according to Fig. 7.2 1 and used to train the ANN:

- CP, SUT, DT;
- At DW10, SW10+DW10, DW10/SW10;
- At 25%: DW25, SW25+DW25, DW25/SW25;
- At 33%: DW33, SW33+DW33, DW33/SW33;
- At 50%: DW50, SW50+DW50, DW50/SW50;
- At 66%: DW66, SW66+DW66, DW66/SW66;
- At 75%: DW75, SW75+DW75, DW75/SW75.

The reference SBP and DBP is calculated as the highest and lowest values, respectively, in the BP waveform within the current cardiac pulse.

Such set of parameters provides a good representation of the cardiac pulsation, suitable for the ANN. The combination of parameters to be passed to the ANN input is discussed in Section 7.5.

7.3 Artificial Neural Network Architecture

There are different ANN architectures such as radial basis function, counter propagation, or learning vector quantization that can be used for fitting the
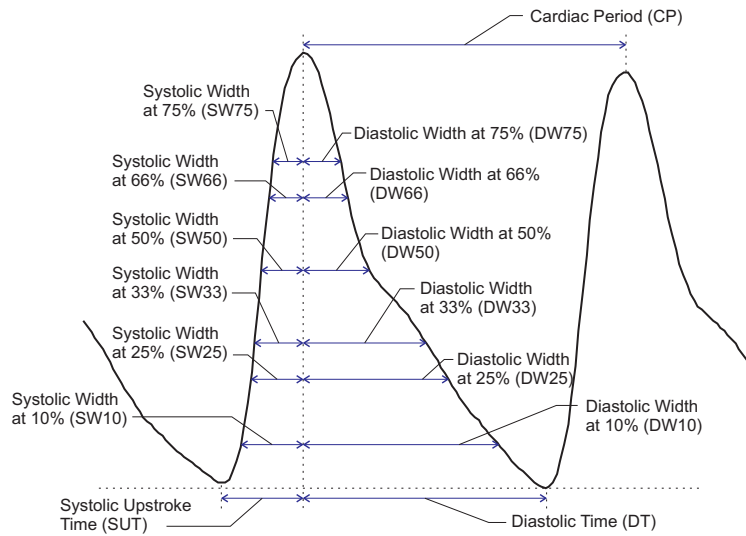
Fig. 7.2. Parameters of the PPG pulsatile component for ANN training and BP estimation.

input data to the output. They are good from performance point of view, but require large number of neurons and, therefore, can't be applied in the case of big training set because of memory lack.

Therefore, it is considered a multilayer feed-forward back propagation ANN with N input neurons (N is the number of used parameters) and two output neurons to simultaneously estimate SBP and DBP (Fig. 7.3).
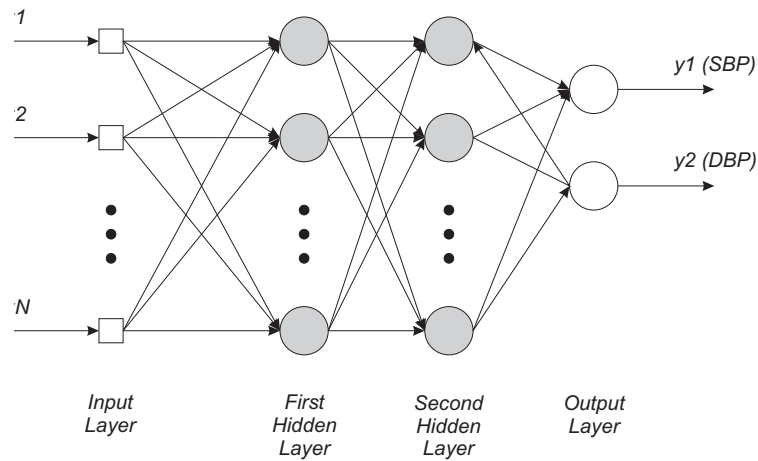
Fig. 7.3. Artificial neural network architecture for SBP and DBP estimation.

The number of hidden layers and hidden neurons is varying in order to obtain best performance. The selection of the optimal number of such neurons is discussed in Section 7.5.

7.4 Data Source

To have a wide representation of PPG signals and correspondent beat-to-beat BP values the distributed freely MIMIC database is used. It includes multiple recordings of physiologic signals and vital signs captured from monitors for tens of thousands of intensive care unit patients. Most of them include ECG, BP, PPG, respiratory signals which were recorded simultaneously with a sampling rate of 125Hz.

From this database only the signals with both ABP and PPG are extracted. An example of such signals is shown in Fig. 7.4.
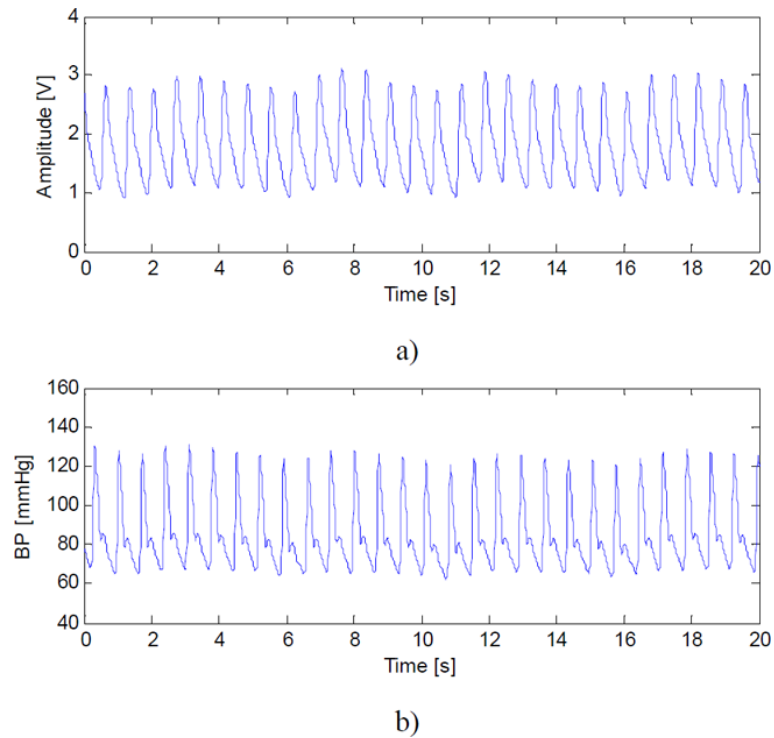
Fig. 7.4. Extracted PPG (a) and the corresponding BP (b) waveforms from MIMIC Database.

In total, there were identified more than 15000 separate PPG heartbeats with corresponding BP values for different persons and different time instances.

7.5 Experimental Results and Discussion

To validate the proposed method, first we investigated how are correlated the data between each other. Fig. 7.5 shows the relation between extracted DT and SBP as well as possible linear regression line. In Fig. 7.6 is depicted the DT vs. measured DBP and the linear regression model.
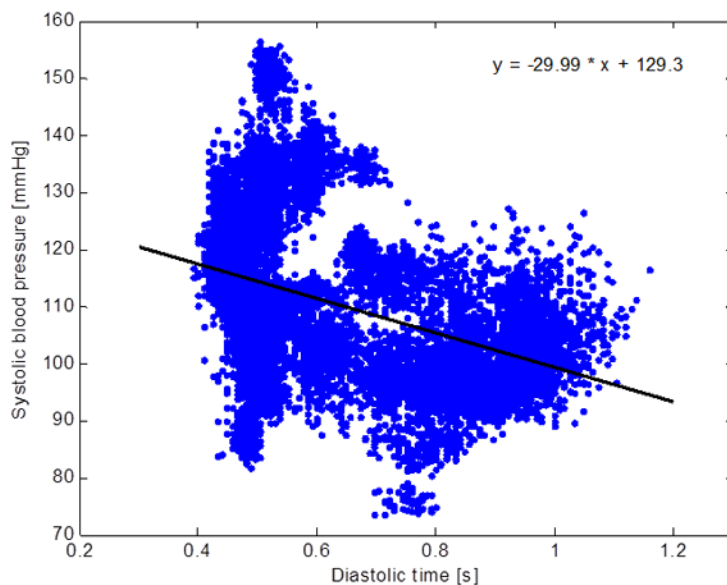
Fig. 7.5. Diastolic time vs. systolic blood pressure and a possible linear regression line.

Both figures confirm a non-linear correlation between the DT and BP. The reason is that besides healthy people, the MIMIC database contains also signals, obtained from elder people, people with hypertension and other diseases. As the result, estimation of the BP using a simple regression method is not possible as the error is too high. Thus, application of the proposed approach based on ANNs is reasonable.

Several ANNs were trained to determine how many neurons of the hidden layer are enough. Fig. 7.7 shows the performance of such ANNs, calculated as the mean squared error. The optimal architecture is {35, 20} with 2 hidden layers 35 neurons on the first hidden layer and 20 on the second one. Even if
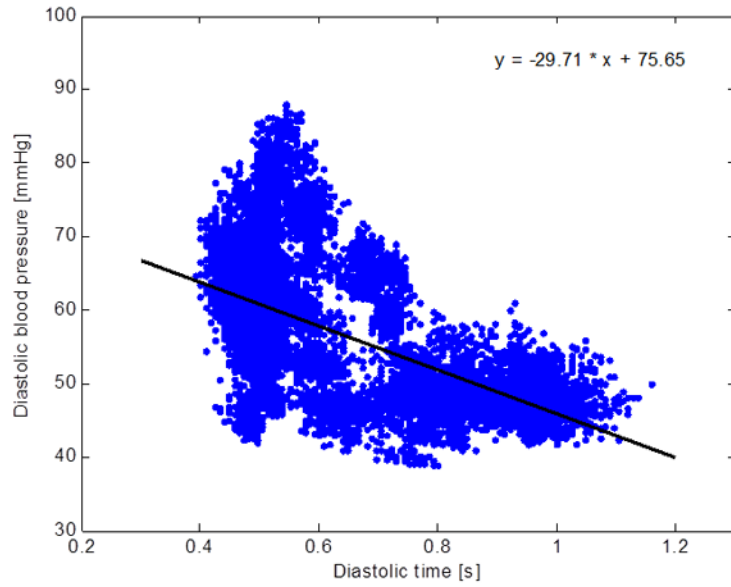
Fig. 7.6. Diastolic time vs. diastolic blood pressure and a possible linear regression line.

the performance of the ANN with {50, 30} of hidden neurons is quite better, the number of calculations in the production phase becomes very high.
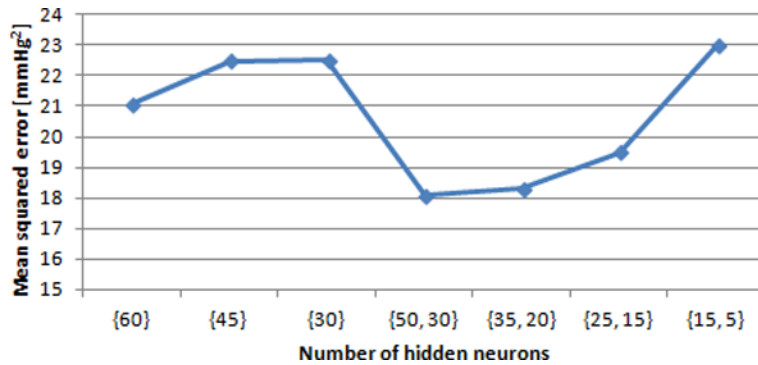
Fig. 7.7. Performance of the ANN vs. number of hidden layers and neurons.

Finally, the tests to determine the optimal number of the input parameters showed that the best results are obtained when all data are used. In particular, Fig. 7.8 shows the histograms of the errors, calculated as the difference between ABP SBP/DBP and the estimated values, for linear regression method,

ANN with 4 inputs, as discussed in [130], and ANN with 21 input parameters, defined in the previous sections.
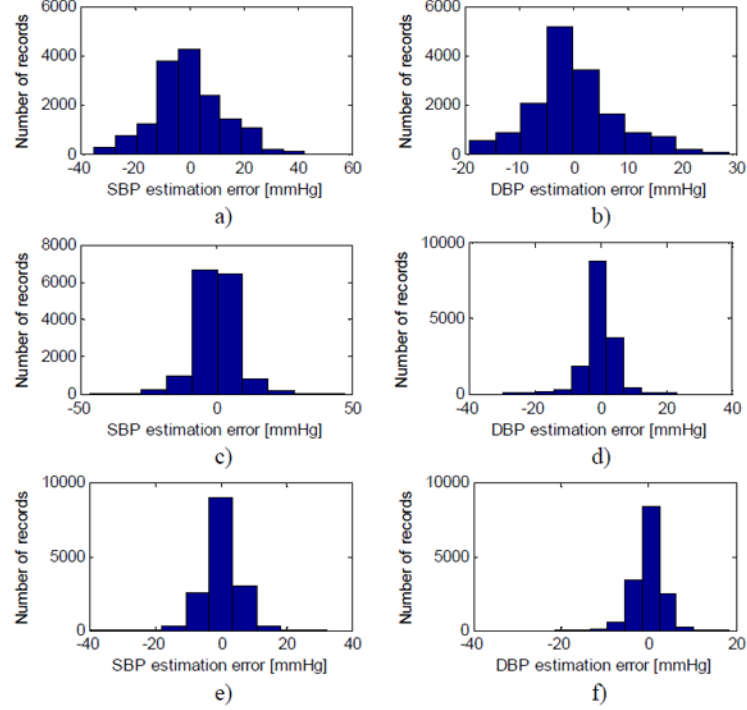
Fig. 7.8. Histograms of absolute errors to estimate: a) SBP using linear regression, b) DBP using linear regression, c) SBP using 4-input ANN, d) DBP using 4-input ANN, e) SBP using 21-input ANN and f) DBP using 21-input ANN.

The absolute error e and relative error e_r are calculated for each heartbeat as

$$e = |BP_{est} - BP|, \ \ e_r = \frac{e}{BP}, \tag{7.1}$$

where BP_{est} is the estimated SBP or DBP using linear regression or ANN, and BP is the reference value, obtained from MIMIC Database.

Table 7.1 shows the performance results of the above tests, presented as mean and standard deviation of errors among reference SBP/DBP and the estimated values.

The experimental results confirm the correctness of the proposed method. According to the American National Standards of the Association for the Advancement of Medical Instrumentation [136], the mean absolute difference between the device and the mercury standard sphygmomanometer must be less than 5 mmHg, and the standard deviation must be less than 8 mmHg. In

Table 7.1. Performance Results of Different Methods, Averaged over All Records (Mean Value ± Standard Deviation).

	SBP $e, mmHg$	SBP $e_r, \%$	DBP $e, mmHg$	DBP $e_r, \%$
Linear Regression	9.80±8.09	8.94±7.57	5.88±5.11	10.26±8.83
Neural Network (4 input neurons)	5.19±5.01	4.73±4.59	2.91±2.92	5.02±4.80
Neural Network (4 input neurons)	3.80±3.46	3.48±3.19	2.21±2.09	3.90±3.51

our tests the mean error is 3.80±3.46 mmHg for systolic and 2.21±2.09 mmHg for diastolic pressure that fulfils the standard requirement. The relative error is less than 4±3.5%.

7.6 Conclusions

In this chapter a new method to continuous and non-invasive blood pressure estimation from the PPG signal is proposed. The blood pressure is estimated by a feed forward ANN with two hidden layers, with the 35 neurons on the first layer and the 20 neurons on the second one. Such configuration shows better results on performance in comparison with other architectures.

The MIMIC database was used for training the ANN, and a total of more than 15000 pulsations were analysed and the 21 parameters were extracted from each of them. The obtained results 3.80±3.46 mmHg for systolic and 2.21±2.09 mmHg for diastolic pressure fulfils with the American National Standards of the Association for the Advancement of Medical Instrumentation, where the maximal accepted errors is 5±8 mmHg.

Conclusions and Future Work

Analysis of images and video received great attention from the scientists in computer vision area in the last years with a large variety of applications. Using the processing power of computers and the advances in mathematical algorithms it is now possible to extract a wealth of information from an image.

Up to now, cameras are mostly used as interaction devices. Computer vision technologies, however, can turn an ordinary video camera to a powerful tool for counting, measuring and inspecting. Therefore, measurement in images and video is a new challenging research direction and introduces a new concept of measurements - they become automatic, and contactless or even telemetric.

However, measuring in images or video is not as usual as with normal instruments. Instead of direct access to the measuring object and its characteristic, there are just digital images or videos. Thus, considering a single image or a frame, all information that we have are pixel values. There is no information about objects, their shapes, features, etc. And, definitely, that's not what can give directly information about real-world objects. Therefore, the image processing must be done in order to extract additional information about objects in the scene.

The goal of this Ph.D. thesis is to develop different information extraction techniques from images and video for environmental and physiological parameters measurement. The measurements in the following cases were considered: in static image, in video and using smartphones. The common task in all these cases is to obtain information about contours and geometrical shapes of the objects based on pixel examination, and proceed with it in time.

Chapter 2 addressed measurements in single images. In particular, a single image, affected by a motion blur, was considered and the method of movement parameters extraction was proposed. It was introduced a new method to detect the locally motion blurred regions from the image with complex still background. The method is based on calculation of the local standard deviation of the image and checking all the sub-images by using the partitioning algorithm with dynamic window size. The following possible cases were anal-

ysed: (i) strong boundaries on the image, (ii) the image with a similar texture as well as (iii) motion blurred image. Finally, the Fourier and Radon transformations were used to compute the motion characteristics for each detected region and extract movement direction. As a result, the proposed method was tested on different images and the proper characteristics were extracted.

Chapters 3 and 4 are dedicated to the problem of measurements in video. The monitoring of the human fatigue level was considered and the non-invasive system, based on eyelid blink detection was proposed. Two solutions are proposed: the blink detection system based on infrared (IR) camera and a webcam.

Chapter 3 presented the usage of the IR camera with switching light for fast and easy pupil and, consequently, the blink event detection without analysing the pupil form and shape. The non-invasive nature allows user to feel free during the experiment and to eliminate the concentration on camera in order to compute the correct blinking rate. Moreover, the developed system does not require the expensive high-speed IR camera as the other solutions do and, therefore, can be used widely.

Chapter 4 discussed a webcam-based system that uses a set of Haar-like features for fast eyes region detection and the frames differencing to detect the eyes closure. The pointed out algorithm permits to distinguish the involuntary blinks from the voluntary ones, and to monitor the changes of the fatigue level over the time. The experimental results showed reliable results for different persons and illumination conditions. As a result, such system can be used in many areas where attentiveness of the operator or driver is an important factor.

The possibility of smartphone usage is discussed in chapters 5, 6 and 7.

Chapter 5 showed how to acquire the photoplethysmographic (PPG) signal by smartphone and integrated camera. Preliminary tests showed that the typical colour range of the captured video varies from model to model. It has been shown that only the red channel has similar characteristics for different models of smartphones, while the green and blue may vary dramatically. Although the last two components do not have a fixed colour range, they can be used to detect a wrong usage of the system. The proposed PPG evaluation method is suitable to work in both reflection and transmission modes, and allows evaluating the PPG when the LED is not used. The appropriate algorithms for the correct usage verification procedure and the initial system calibration were proposed and tested. The experimental tests were carried out on HTC HD2, iPhone4, Samsung Galaxy S i9000 and Nokia 5800 smartphones. Devices, equipped with LED were tested in two modes: when the LED was enabled and disabled. A total of 10 persons aged between 26 and 60 years took part in the experiments. The obtained results were compared to the CMS50DL Finger Pulse Oximeter SPO2 Monitor and the obtained pulse rates as well as the signals themselves were comparable between all the devices. Thus, the comparison confirms the correctness and reliability of the

proposed PPG calculation technique with respect to medical pulse measurement instruments.

Chapter 6 addressed the problem of reliable pulse rate (PR) evaluation from a PPG signal. The proposed method is based on the evaluation of the PR on the basis of the time interval between two consecutive PPG peaks. It uses the adaptive threshold to detect the peak by taking into account the standard deviation of the PPG and statistical analysis of the collected time intervals to reject outliers. The obtained results have been found reliable for different smartphones with respect to the: (i) heterogeneous characteristics of the cameras, (ii) changing of the chromatic and geometrical features of the frame if the LED is used, and (iii) wrong finger position on the smartphone. The proposed method was validated respect to Ambulatory Blood Pressure Systems Spacelabs 90207. The results confirm the correctness, suitability and reliability of the proposed technique. In particular, the proposed method shows the maximum error of PR evaluation equal to 2 pulses per minute (ppm) that is fully compatible with the accuracy ±2 ppm declared in the ABP datasheet.

Chapter 7 described the method for continuous and non-invasive blood pressure estimation from a PPG signal. The blood pressure was estimated by a feed forward artificial neural network with two hidden layers, with 35 neurons on the first layer and 20 neurons on the second one. The two output neurons are used to estimate the systolic and diastolic blood pressure. Such configuration showed better results on performance in comparison with other architectures. In addition, the Multiparameter Intelligent Monitoring in Intensive Care waveform dataset was used for training the neural network, and a total of more than 15000 pulsations were analysed and the 21 parameters were extracted from each of them. The mean error and standard deviation of obtained results was 3.80±3.46 mmHg for systolic and 2.21±2.09 mmHg for diastolic pressure. It fulfils with the American National Standards of the Association for the Advancement of Medical Instrumentation, where the maximal accepted errors is 5±8 mmHg. The mean relative error was less than 4±3.5%.

In conclusion, the research was dedicated to provide the novel image and video processing techniques and to show how they can be used for measurement of various environmental and physiological parameters. Indeed, using the camera as a measuring sensor is very interesting. It permits to create a "universal" measurement instrument, where new type of measurements can be enabled just by changing the software. The advantage of such approach is that any imaging device can be used to acquire information about measuring object: static camera, digital camera, video camera, webcam, smartphone camera etc. Then, a specific algorithm installed on computer, smartphone, or even on reprogrammable integrated circuit can provide appropriate measurement results.

The current work showed just few possible applications of such techniques to prove the concept of measurements in images and video. Further improvement that can be done is adding additional, more advance image and video processing techniques in order to have better results.

Another possible improvement is the data collection procedure. It should be useful to extend the scope of the data available, especially for measurement of the physiological parameters. It is well known that different diseases might influence the activity of the organs and wide representation of such data would supplement the research.

References

1. L.A. Malanichev, "The role of measurements in everyday life," Measurement techniques, Vol. 12, pp. 731-732, 1969.
2. "10 everyday reasons why measurement is important in your life?" http://www.mathworksheetscenter.com/mathtips/whymeasurement.html
3. A. Criminisi, A. Zisserman, L. van Gool, S. Bramble, D. Compton, "A new approach to obtain height measurements from video," In Proceedings of SPIE - The International Society for Optical Engineering, Vol. 3576, 1999, pp. 227-238.
4. P. Patias, "Medical imaging challenges photogrammetry," ISPRS Journal of Photogrammetry and Remote Sensing, Vol. 56, Iss. 5-6, pp. 295-310, August 2002.
5. Sticky Yard Digital Photo Measuring System, http://www.stickyyard.com/
6. CentreCam, http://www.miketreth.mistral.co.uk/centrecam.htm
7. S. Gil, H.D. Reisin, E.E. Rodríguez, "Using a digital camera as a measuring device," American Journal of Physics, Vol. 74, Iss. 9, pp. 768-775, September 2006.
8. "Gartner Says Worldwide Sales of Mobile Phones Declined 3 Percent in Third Quarter of 2012; Smartphone Sales Increased 47 Percent," http://www.gartner.com/it/page.jsp?id=2237315
9. The NPD Group/Imaging Confluence Study 2011, https://www.npd.com/wps/portal/npd/us/news/press-releases/pr_111222/
10. Yu. Kurylyak, A. Sachenko, "Moving objects detection from the video stream based on the background subtraction and hierarchical data structure," Scientific Journal of Chernivtsi National University, Iss. 426, pp. 135-139, 2008. (in Ukrainian)
11. Yu. Kurylyak, "A real-time motion detection for video surveillance system," in Proceedings of 5th IEEE International Workshop on Intelligent Data Acquisition and Advanced Computing Systems: Technology and Applications, 21-23 September 2009, Rende (Cosenza), Italy, pp. 386-389.
12. Yu. Kurylyak, A. Sachenko, D. Grimladi, "System of human detection and tracking for video surveillance," in Proceedings of International Conference "Modern Information and Electronic Technologies" (MIET-2010), Odessa, Ukraine, 2010, p. 129.
13. F. Krahmer, Y. Lin, B. McAdoo, K. Ott, J. Wang, D. Widemannk, B. Wohlberg, "Blind image deconvolution: motion blur estimation," Report, 2006.

14. J. Mohammadi, R. Akbari, M. Keshavarz Ba Haghighat, "Vehicle speed estimation based on the image motion blur using RADON transform," in Proc. of 2nd International Conference on Signal Processing Systems (ICSPS), 2010, pp. 243-247.
15. Huei-Yung Lin, "Vehicle speed detection and identification from a single motion blurred image," Proceedings of the Seventh IEEE Workshop on Applications of Computer Vision (WACV/MOTION'05), 2005, pp. 461-467.
16. H. Pazhoumand-Dar, A.M.T. Abolhassani, E. Saeedi, "Object speed estimation by using fuzzy set," in Journal World Academy of Science, Engineering and Technology, Vol. 64, pp. 241-244, 2010.
17. Xu Ting-Fa, Zhao Peng, "Image motion-blur-based object's speed measurement using an interlaced scan image," in Measurement Science and Technology, Vol.21, No.7, pp 1-9, 2010.
18. M.E. Moghaddam, M. Jamzad, "Motion blur identification in noisy images using fuzzy sets," in Proc. of the Fifth IEEE International Symposium on Signal Processing and Information Technology, 2005, pp. 862-866.
19. S. Kawamura, K. Kondo, Y. Konishi, H. Ishigaki, "Estimation of motion using motion blur for tracking vision system," in Proc. of World Automation Congress, 2002, pp. 371-376.
20. Hanghang Tong, Mingjing Li, Hongjiang Zhang, Changshui Zhang, "Blur detection for digital images using wavelet transform," in Proc. of IEEE International Conference on Multimedia and Expo, ICME'04, Vol.1, 2004, pp.17-20.
21. E. Kalalembang, K. Usman, I.P. Gunawan, "DCT-based local motion blur detection," in Proc. of International Conference on Instrumentation, Communications, Information Technology, and Biomedical Engineering (ICICI-BME), 2009, pp. 1-6.
22. Renting Liu, Zhaorong Li, Jiaya Jia, "Image partial blur detection and classification," in Proc. of IEEE Conference on Computer Vision and Pattern Recognition, CVPR 2008, pp 1-8.
23. A. Pretto, E. Menegatti, M. Bennewitz, W. Burgard, E. Pagello, "A visual odometry framework robust to motion blur," in Proc. of IEEE International Conference on Robotics and Automation, 2009, pp.2250-2257.
24. D. Grimaldi, Yu. Kurylyak, F. Lamonaca, "Detection and parameters estimation of locally motion blurred objects," in Proc. IEEE International Conference on Intelligent Data Acquisition and Advanced Computing Systems: Technology and Applications (IDAACS'2011), Prague, Czech Republic, September 2011, pp. 483-487.
25. D. Grimaldi, F. Lamonaca, "Optimized evaluation of image alteration indexes in IFC," in Proc. of IEEE Workshop on Medical Measurements and Applications, MeMeA 2009, pp. 202-205.
26. Jae S. Lim, Two-Dimensional signal and image processing. Englewood Cliffs, NJ, Prentice Hall, 1989.
27. K.L. Saroj Lal, A. Craig, "A critical review of the psychophysiology of driver fatigue," Biological Psychology, Vol. 55, pp. 173-194, 2001.
28. A. Shahid, J. Shen, C.M. Shapiro, "Measurements of sleepiness and fatigue," Journal of Psychosomatic Research, Vol. 69, Iss. 1, pp. 81-89, July 2010.
29. J. Shen, J. Barbera, C.M. Shapiro, "Distinguishing sleepiness and fatigue: focus on definition and measurement", Sleep Medicine Reviews, Vol. 10, Iss. 1, pp. 63-76, 2006.

30. S. Bailes, E. Libman, M. Baltzan, R. Amsel, R. Schondorf, C.S. Fichten, "Brief and distinct empirical sleepiness and fatigue scales," Journal of Psychosomatic Research, Vol. 60, Iss. 6, pp. 605-613, June 2006.
31. A.W. Maclean, M. Criollo, G.C. Fekken, et al., "The Stanford Sleepiness Scale in a clinical sample: the need for revision," Sleep Res., Vol. 19, p. 249, 1990.
32. D. Dawson, A. Fletcher, "A quantitative model of work-related fatigue: background and definition," Ergonomics, Vol. 44, pp. 144-163, 2001.
33. L.B. Krupp, N.G. LaRocca, J. Muir-Nash, et al., "The fatigue severity scale: application to patients with multiple sclerosis and systemic lupus erythematosus," Arch Neurol, Vol. 46, pp. 1121-1123, 1989.
34. J. Andreassi, Psychophysiology, Human Behavior & Physiological Response, London: Lawrence Erlbaum Associates, Publishers, 2000.
35. E. Ponder, W.P. Kennedy, "On the act of blinking," Quarterly Journal of Physiology, Vol. 18, pp. 89-110, 1927.
36. G.J. Siegle, N. Ichikawa, S. Steinhauer, "Blink before and after you think: Blinks occur prior to and following cognitive load indexed by pupillary responses," Psychophysiology, Vol. 45, pp. 679-687, 2008.
37. R. Katz, "Blinks as a measure of visual fatigue," Klinische Monatblaetter fur Augenheilkunde, pp. 154-157, 1895.
38. K. French, J. Veys, "L'ammiccamento dell'occhio," P.O. Professional Optometry, pp. 132-141, 2008. (in Italian)
39. A. Krolak, P. Strumillo, "Vision-based eye blink monitoring system for human-computer interfacing," Proc. Human System Interactions, 2008, pp. 994-998.
40. A.J. Stern, D. Boyer, D. Schroeder, "Blink rate: a possible measure of fatigue. Human factors," Human Factors: The Journal of the Human Factors and Ergonomics Society, Vol. 36, No. 2, pp. 285-297, June 1994.
41. G. Barbato, G. Ficca, G. Muscettola, M. Fichele, M. Beatrice, F. Rinaldi, "Diurnal variation in spontaneous eye-blink rate", Psychiatry Research, Vol. 93, No. 2, pp. 145-151, 6 March 2000.
42. V. Hargutt, H.P. Krüger, "Eyelid movements and their predictive value for fatigue stages," Würzburg: Psychologisches Institut der Universitt Würzburg, 2000.
43. E. Niedermeyer, F.L. da Silva, "Electroencephalography: basic principles, clinical applications, and related fields," Lippincot Williams & Wilkins, 2004.
44. U. Svensson, "Blink behaviour based drowsiness detection - method development and validation," M.S. thesis, Linkping University, Dept.Biomedical Engineering, 2004.
45. C.D. Harris, "Maintenance of wakefulness test," AARC Times, pp. 50-51, 2001.
46. J. Gips, P. Olivieri, "EagleEyes: an eye control system for persons with disabilities," the Eleventh Intern. Conference on Technology and Persons with Disabilities, 1996, pp. 128-132.
47. L. Young, D. Sheena, "Methods & designs: survey of eye movement recording methods," Behavioural Research Methods & Instrumentation, Vol. 7(5), pp. 397-429, 1975.
48. K. Roy, C.Y. Suen, and P. Bhattacharya, "Segmentation of unideal iris images using game theory", 20th International Conference on Pattern Recognition (ICPR), 2010, pp. 2844-2847.
49. D. Grimaldi, Y. Kurylyak, F. Lamonaca, "Elaborazione dei segnali fisiologici per monitoraggio psicofisico," Atti del XXVIII Congresso Nazionale GMEE'2011, Genova, Italy, Settembre 2011, pp. 291-292. (in Italian)

50. M. Bologna, R. Agostino, B. Gregori, D. Belvisi, D. Ottaviani, C. Colosimo, G. Fabbrini and A. Berardelli, "Voluntary, spontaneous and reflex blinking in patients with clinically probable progressive supranuclear palsy", Brain: Oxford University Press, Vol. 132, No. 2, pp.502-510, 2009.

51. D.A. Usanov, N.M. Romanova, A.V. Skripal, A.Yu. Vagarin, A.P. Rytik, M.A. Samokhina, "A method for assessment of the psycophysiological state", RF Patent No. 2337607, 2008.

52. Yu. Kurylyak, F. Lamonaca, G. Mirabelli, O. Boumbarov, S. Panev, "The infrared camera-based system to evaluate the human sleepiness," in Proc. IEEE International Symposium on Medical Measurements and Applications (MeMeA 2011), Bari, Italy, May 2011, pp. 253-256.

53. S. Panev, O. Boumbarov, P. Petrov, "Single eye gaze tracking with active pantilt camera", XLV International Scientific Conference on Information, Communication and Energy Systems and Technologies (ICEST), 2010, pp.225-228.

54. Y. Ebisawa, "Improved video-based eye-gaze detection method", IEEE Transactions on Instrumentation and Measurement, Vol. 47, No. 4, August 1998.

55. N. Otsu, "A threshold selection method from gray-Level histograms", IEEE Transactions on Systems, Man, and Cybernetics, 9(1), pp. 62-66, 1979.

56. K. Grauman, M. Betke, J. Gips, and G. Bradski, "Communication via eye blinks - detection and duration analysis in real time," in Proc. IEEE Computer Vision and Pattern Recognition Conference (CVPR 2001), Vol. 2, 2001, pp. 1010-1017.

57. G. Calabria, M. Rolando, Il Film Lacrimale, Milan, Italy: Fogliazza Editore, 1997 (in Italian).

58. P.P. Caffier, U. Erdmann, P. Ullsperger, "Experimental evaluation of eye-blink parameters as a drowsiness measure," Eur J Appl Physiol, Vol. 89, No. 3-4, pp. 319-325, 2003.

59. H. Misra, "Users' computer human interface capabilities in information system development life cycle: An organizational perspective", Engineering Management Conference, 2008, pp. 1-5.

60. M. Turkan, M. Pardas, A.E. Cetin, "Human eye localization using edge projections," Proc. Second International Conference on Computer Vision Theory and Applications, 2007, pp. 410-415.

61. M. Betke, W.J. Mullally, J. Magee, "Active detection of eye scleras in real time," Proc. IEEE Work. on Human Mod., Anal. and Synt, 2000.

62. P. Smith, M. Shah, N. da V. Lobo, "Monitoring head/eye motion for driver alertness with one camera," Proc. of 15th IEEE International Conference on Pattern Recognition, vol. 4, 2010, pp. 636-642.

63. J. Wu and M.M. Trivedi, "Simultaneous eye tracking and blink detection with interactive particle filters," EURASIP Journal on Advances in Signal Processing, 2008.

64. I. Saeed, A. Wang, R. Senaratne, S. Halgamuge, "Using the active appearance model to detect driver fatigue," Proc. Information and Automation for Sustainability Conference, 2007, pp. 124-128.

65. P. Viola, M. Jones, "Rapid object detection using a boosted cascade of simple features," Proc. 2001 IEEE Computer Society Conference on Computer Vision and Pattern Recognition, 2001, pp. I511-518.

66. R. Lienhart, J. Maydt, "An extended set of Haar-like features for rapid object detection," Proc. International Conference on Image Processing, vol.1, 2002, pp. I900-903.

67. A. Cristiani, M. Porta, D. Gandini, G.M. Bertolotti, N. Serbedzija, "Driver drowsiness identification by means of passive techniques for eye detection and tracking," Proc. 4th IEEE International Conference on Self-Adaptive and Self-Organizing Systems, 2010, pp.142-146.

68. Yu. Kurylyak, I. Paliy, A. Sachenko, A. Chohra, K. Madani, "Face detection on grayscale and color images using combined cascade of classifiers," International Journal of Computing, Vol. 8, Iss. 1, pp. 61-71, 2009.

69. I. Paliy, V. Dovgan, O. Boumbarov, S. Panev, A. Sachenko, Yu. Kurylyak, D. Zagorodnya, "Fast and robust face detection and tracking framework," in Proc. IEEE International Conference on Intelligent Data Acquisition and Advanced Computing Systems: Technology and Applications (IDAACS'2011), Prague, Czech Republic, September 2011, pp. 430-434.

70. Yu. Kurylyak, F. Lamonaca, G. Mirabelli, "Detection of the eye blinks for human's fatigue monitoring," in Proc. IEEE Int. Symp. Medical Measurements and Applications (MeMeA 2012), Budapest, Hungary, 2012, pp. 91-94.

71. M.H. Yang, D.J. Kriegman, N. Ahuja, "Detecting faces in images: a survey," IEEE Trans. Pattern Analysis and Machine Intelligence, Vol. 24, No. 1, pp. 34-58, 2002.

72. Y. Freund, R. Schepire, "A short introduction to boosting," Journal of Japanese Society for Artificial Intelligence, 14(5), pp. 771-780, 1999.

73. Ognian Boumbarov, Strahil Sokolov, Plamen Petrov, Anatoly Sachenko, Yuriy Kurylyak, "Kernel-based face detection and tracking with adaptive control by Kalman filtering," in Proceedings of 5th IEEE International Workshop on Intelligent Data Acquisition and Advanced Computing Systems: Technology and Applications, 21-23 September 2009, Rende (Cosenza), Italy, pp.434-439.

74. http://opencv.willowgarage.com/wiki/

75. M. Castrillón, O. Déniz, C. Guerra, M. Hernández, "ENCARA2: Real-time detection of multiple faces at different resolutions in video streams," Journal of Visual Communication and Image Representation, ISSN 1047-3203, Vol. 18, No. 2, pp. 130-140, 2007.

76. D.J. Terbizan, B.A. Dolezal, C. Albano, "Validity of seven commercially available heart rate monitors," Measurement in Physical Education and Exercise Science, Vol. 6(4), pp. 243-247, 2009.

77. M.J. Gregoski, M. Mueller, A. Vertegel, et al., "Development and validation of a smartphone heart rate acquisition application for health promotion and wellness telehealth applications," International Journal of Telemedicine and Applications, doi:10.1155/2012/696324, 2012.

78. A. Kumar. ECG - simplified, LifeHugger, November 2010.

79. T.G. Pickering. White coat hypertension. Current Opinion in Nephrology and Hypertension, Vol. 5(2), pp.192-198, March 1996.

80. A. Smith, T. Ferriss, "Home health monitoring may significantly improve blood pressure control," Kaiser Permanente Study Finds, May 2010.

81. C.G. Scully, J. Lee, J. Meyer, A.M. Gorbach, D. Granquist-Fraser, Y. Mendelson, and H. Chon Ki, "Physiological parameter monitoring from optical recordings with a mobile phone," IEEE Transactions on Biomedical Engineering, Vol. 59(2), pp. 303-306, 2012.

82. V. Gay and P. Leijdekkers. "A health monitoring system using smart phones and wearable sensors," International Journal of ARM, Vol. 8(2), pp. 29-35, 2007.

83. M. E. Ernst, G. R. Bergus, "Ambulatory blood pressure monitoring," Southern Medical Journal, Vol. 96(6), pp. 563-568, June 2003.
84. Operations Manual 90207-80/90217-1HABP Monitors, 070-0715-00 Rev. B, Spacelabs Medical, Inc.
85. A. Shennan, A. Halligan, M. Gupta, D. Taylor, M. de Swiet, "Oscillometric blood pressure measurements in severe per-eclampsia: validation of the Space-Labs 90207," BJOG: An International Journal of Obstetrics & Gynaecology, Vol. 103(7), pp. 171-173, 1996.
86. C.W. Belsha, T.G. Wells, H.B. Rice, W.A. Neaville, and P.L. Berry. Accuracy of the SpaceLabs 90207 ambulatory blood pressure monitor in children and adolescents. Blood Pressure Monitoring, Vol. 1, pp. 127-133, 1996.
87. P. Iqbal, M.D. Fotherby, J.F. Potter, "Validation of the SpaceLabs 90207 automatic non-invasive blood pressure monitor in elderly subjects," Blood Pree Monit, Vol. 1, pp. 367-373, 1996.
88. Association for the Advancement of Medical Instrumentation, http://aami.org.
89. American Heart Association, Inc., http://heart.org.
90. British Hypertension Society, http://bhsoc.org.
91. J. Allen, "Photoplethysmography and its application in clinical physiological measurement," Physiological Measurement, 28, pp.1-40, 2007.
92. E. Jonathan, M. Leahy, "Investigating a smartphone imaging unit for photoplethysmography," Physiological Measurement, Vol. 31, No. 11, pp. N79-N83, November 2010.
93. D. Damianou, "The wavelength dependence of the photoplethysmogram and its implication to pulse oximetry," Ph.D. dissertation, University of Nottingham, October 1995.
94. A. Reisner, P. Shaltis, D. McCombie, and H. Asada, "Utility of the photoplethysmogram in circulatory monitoring," Anesthesiology, Vol. 108(5), pp. 950-958, May 2008.
95. P. Leonard, N. Grubb, P. Addison, D. Clifton, J. Watson, "An algorithm for the detection of individual breaths from the pulse oximeter waveform," Journal of Clinical Monitoring and Computing, Vol. 18(5-6), pp. 309-312, 2004.
96. S. Linder, S. Wendelken, E. Wei, S. McGrath, "Using the morphology of photoplethysmogram peaks to detect changes in posture," Journal of Clinical Monitoring and Computing, vol.20(3), pp.151-158, June 2006.
97. U. Rubins, "Finger and ear photoplethysmogram waveform analysis by fitting with Gaussians," Medical and Biological Engineering and Computing, Vol. 46(12), pp. 1271-1276, December 2008.
98. Jia Zheng, Sijung Hu, "The preliminary investigation of imaging photoplethysmographic system," Journal of Physics: Conference Series, 85, doi:10.1088/1742-6596/85/1/012031, 2007.
99. Jia Zheng, Sijung Hu, V. Azorin-Peris, A. Echiadis, V. Chouliaras, R. Summers, "Remote simultaneous dual wavelength imaging photoplethysmography: A further step towards 3-D mapping of skin blood microcirculation," Multimodal Biomedical Imaging III, Proc. of SPIE, 2008.
100. iHealth Blood Pressure Monitoring System, Medisana AG, http://ihealth.medisana.com/en/index.php.
101. D.L. Carnì, G. Fortino, R. Gravina, D. Grimaldi, A. Guerrieri, F. Lamonaca, "Continuous, real-time monitoring of assisted livings through wireless body sensor networks," in Proceedings of the IEEE International Conference Intelligent

Data Acquisition and Advanced Computing Systems IDAACS'2011, September 2011, pp. 872-877.

102. M.N. Kamel Boulos, C. Tavares et al., "How smartphones are changing the face of mobile and participatory healthcare: An overview, with example from eCAALYX," BioMedical Engineering OnLine, 10(24), 2011.

103. P. Pelegris, K. Banitsas, T. Orbach, and K. Marias, "A novel method to detect heart beat rate using a mobile phone," in Proceedings of 32nd IEEE Annual International Conference on Merging Medical Humanism and Technology, 2010, pp. 5488-5491.

104. W. Verkruysse, L.O. Svaasand, J.S. Nelson, "Remote plethysmographic imaging using ambient light," Optics Express, Vol. 16(26), pp. 21434-21445, 2008.

105. S.C. Millasseau, J.M. Ritter, K. Takazawa, and P.J. Chowienczyk, "Contour analysis of the photoplethysmographic pulse measured at the finger," Journal of Hypertension, Vol. 24, Iss. 8, pp. 1449-1456, 2006.

106. Instant HeartRate, https://play.google.com/store/apps/details?id= si.modula.android.instantheartrate

107. Heart Rate Tester, https://play.google.com/store/apps/details?id= cn.menue.heart.activity

108. Pulse Rate Monitor, https://play.google.com/store/apps/details?id= com.sheaimace.android.prm

109. Cardiograph - Heart Rate Meter, http://itunes.apple.com/us/app/ cardiograph/id441079429?mt=8

110. E. Jonathan and M.J. Leahy, "Cellular phone-based photoplethysmographic imaging," Journal on Biophotonics, Vol. 4(5), pp. 293-296, 2011.

111. D. Grimaldi, Yu. Kurylyak, F. Lamonaca, A. Nastro, "Photoplethysmography detection by smartphone's videocamera," in Proc. IEEE International Conference on Intelligent Data Acquisition and Advanced Computing Systems: Technology and Applications (IDAACS'2011), Prague, Czech Republic, September 2011, pp. 488-491.

112. Yu. Kurylyak, F. Lamonaca, D. Grimaldi, "Smartphone-based photoplethysmogram measurement," in Digital Image, Signal and Data Processing for Measurement Systems, R.J. Duro and F. López-Peña Ed. Aalborg, Denmark: River Publishers, 2012, pp. 135-164.

113. J. Nijboer, J. Dorlas, and H. Mahieu, "Photoelectric plethysmography: some fundamental aspects of the reflection and transmission method," Clinical Physics and Physiological Measurement, Vol. 2, No. 3, pp. 205-215, 1981.

114. F. Lamonaca, Y. Kurylyak, D. Grimaldi, V. Spagnuolo, "Reliable pulse rate evaluation by smartphone," in Proc. IEEE Int. Symp. Medical Measurements and Applications (MeMeA 2012), Budapest, Hungary, 2012, pp. 234-237.

115. M.L. Chugani, A.R. Samant, M. Cerna, "LabVIEW Signal Processing," Prentice Hall, 1998.

116. A.V. Oppenheim, R.W. Schafer, "Discrete time signal processing," Prentice Hall, 1999.

117. L. Mason, "Signal processing methods for non-invasive respiration monitoring," Ph.D. dissertation, Trinity College, Michaelmas, 2002.

118. G. Fortino, V. Giampà, "PPG-based methods for non invasive and continuous BP measurement: an overview and development issues in body sensor networks," in Proc. IEEE Int. Workshop on Medical Measur. and Applications (MeMeA'2010), Ottawa, ON, 2010, pp. 10-13.

119. World Health Organization, cardiovascular diseases (CVD), Geneve, Switzer-land, 2005. http://www.who.int/cardiovascular_diseases/en/
120. N. Korotkoff, "To the question of methods of determining the blood pressure," Rep. Imperial Mil. Acad., Vol. 11, pp. 365-367, 1905.
121. A. Sapinski, "Theoretical basis for a proposed standard algorithm of blood pressure measurements by the sphygmo-oscillometric method," J. Clin. Eng., Vol. 22, No. 3, pp. 171-174, 1997.
122. K. Barbé, W. Van Moer, D. Schoors, "Analyzing the windkessel model as a potential candidate for correcting oscillometric blood-pressure measurements," IEEE Trans. on Instrumentations and Measurements, Vol. 61, No. 2, pp. 411-418, Feb. 2012.
123. Y.S. Yan, Y.T. Zhang, "Noninvasive estimation of blood pressure using pho-toplethysmographic signals in the period domain," 27th Annual International Conference of the Engineering in Medicine and Biology Society (IEEE-EMBS 2005), 2005, pp.3583-3584.
124. W.B. Gu, C.C.Y. Poon, Y.T. Zhang, "A novel parameter from PPG dicrotic notch for estimation of systolic blood pressure using pulse transit time," Medical Devices and Biosensors (ISSS-MDBS 2008), pp. 86-88, 2008.
125. K. Meigas, R. Kattai, J. Lass, "Continuous blood pressure monitoring using pulse wave delay," in Proc. 23rd Annu. Int. Conf. of the IEEE Eng. in Medicine and Biology Society, Vol. 4, 2001, pp.3171-3174.
126. M.K. Ali Hassan, M.Y. Mashor, N.F. Mohd Nasir, S. Mohamed, "Measur-ing blood pressure using a photoplethysmography approach," Proc. 4th Kuala Lumpur Int. Conf. on Biom. Eng., Vol. 21, 2008, pp. 591-594.
127. J. Yi Kim, B. Hwan Cho, S. Mi Im, M. Ju Jeon, I. Young Kim, S. I Kim, "Comparative study on artificial neural network with multiple regressions for continuous estimation of blood pressure," 27th Annual Intern. Conf. of the Engin. in Medicine and Biology Soc., 2005, pp. 6942-6945.
128. F.S. Cattivelli, H. Garudadri, "Noninvasive cuffless estimation of blood pres-sure from pulse arrival time and heart rate with adaptive calibration," Sixth International Workshop on Wearable and Implantable Body Sensor Networks (BSN 2009), 2009, pp. 114-119.
129. D.B. McCombie, A.T. Reisner, H. Asada, "Adaptive blood pressure estimation from wearable PPG sensors using peripheral artery pulse wave velocity mea-surements and multi-channel blind identification of local arterial dynamics," 28th Annual International Conference of the IEEE Engineering in Medicine and Biology Society (EMBS'06), 2006, pp. 3521-3524.
130. X.F. Teng and Y.T. Zhang, "Continuous and noninvasive estimation of arterial blood pressure using a photoplethysmographic approach," In Proceedings of the 25th Annual Inter. Conf. of the IEEE Engineering in Medicine and Biology Society, Cancun, Mexico, 2003, pp. 3153-3156.
131. Y. Yoon, G. Yoon, "Nonconstrained blood pressure measurement by photo-plethysmography," Journal of the Optical Society of Korea, Vol. 10, No. 2, pp. 91-95, June 2006.
132. Yu. Kurylyak, F. Lamonaca, D. Grimaldi, "A neural network-based method for continuous blood pressure estimation from a PPG signal," in Proc. 2013 IEEE International Instrumentation and Measurement Technology Conf., Min-neapolis (MN), 2013, submitted.
133. I. Paliy, A. Sachenko, Yu. Kurylyak, "The analysis of neural network's ar-chitectures for face recognition," in Proc. of the 8th International Conference

"Pattern Recognition and Information Processing", May 18-20, 2005, Minsk, Belarus, pp. 442-444.

134. Y. Kurylyak, I. Paliy, A. Sachenko, V. Turchenko, V. Kapura, "Faces detection using combined cascade of classifiers for video-monitoring," Trans. of Brest State Technical University, series: physics, mathematics and informatics, pp.5-8, 2007. (in Russian)

135. A.L. Goldberger, L.A.N. Amaral, L. Glass, J.M. Hausdorff, P.Ch. Ivanov, R.G. Mark, J.E. Mietus, G.B. Moody, C.K. Peng, H.E. Stanley, "PhysioBank, PhysioToolkit, and PhysioNet: components of a new research resource for complex physiologic signals," Circulation 101(23), pp. e215-e220, 2010.

136. American National Standard for Electronic or Automated sphygmomanometers: ANSI/AAMI SP10, Arlington, VA: Association for the Advancement of Medical Instrumentation, 1992.